Functionalization of Carbon Fibers by Atmospheric Pressure Plasma Treatment for Improved Self-Healing Composites

A Thesis Presented for the Degree of

Doctor of Philosophy

Wei-Yu Chen

Department of Materials Science and Engineering

The University of Sheffield

Acknowledgements

The author would like to express his appreciation for the guidance and encouragement given by his supervisors, Professor Allan Matthews, Professor Frank Jones and Dr. Adrian Leyland, in the course of this thesis. The author would also like to express his sincerest gratitude to Dr. Joel Foreman and Ying-Lan Ang for their support for the mechanical tests used in this thesis. The author also wishes to express his sincere thanks to Dr. Alison Beck and Dr. Deborah Hammond for their guidance and support on the XPS analysis and Prof. Claus Rebholz for his helpful input into the final thesis. The author will never forget all his friends who helped and encouraged him during his academic career. Finally, the author would like to attribute honour to his parents, families and relatives.

Abstract

This study aimed towards the investigation of using a novel atmospheric pressure plasma (APP) process to introduce carboxylic acid functional groups on carbon fibers (CFs), so the functionalized CFs can react with an ionomer-modified epoxy resin, which was developed in this study, to prepare a self-healing composite. The APP process, which was performed in a bespoke Pyrex chamber, was comprised of an APP surface activation and a subsequent acrylic acid (AAc) vapour grafting. The effects of various APP functionalization parameters, such as grafting time and working gas, on surface wettability, stability and chemical composition, were first investigated on silicon wafers before applying them to CFs. The healing efficiency of the ionomer-modified epoxy resin network, and functional group reactions between the ionomer healing agent and the functionalized silicon and CF surfaces, were also studied to estimate the self-healing function.

Contact angles of the silicon wafers with water were initially 56.1±0.8° and after APP activation with air and argon 8.2±0.2° and 4.6±0.2°, respectively, and increased to a range between 4.8° to 16.1° after AAc vapour grafting, suggesting the capability of the APP process to control surface wettability and to potentially perform surface deposition.

By observation of the binding energy peak at 289.2 eV in the C1s core level spectrum from XPS, the results indicated the presence of carboxylic acid groups on the surfaces, which was also confirmed by 2,2,2-trifluoroethanol derivatization. A 19.72% atomic percentage of carboxylic acid functional groups was achieved, which is higher than the result from a conventional APP process (13.36% by a 60-second APP treatment with AAc vapour directly being injected into the activating zone during the process), compared with the theoretical percentage of pure AAc (33.3%).

For the investigation of the ionomer healing system, a healing efficiency of 31.07% was observed on the ionomer-modified epoxy resin network. The functional groups on the ionomer healing agent were proved to be able to react with APP/AAc-grafted carboxylic acid functional groups.

In summary, a novel, rapid APP process, which utilizes APP activation and AAc vapour grafting in a bespoke Pyrex chamber, was developed in this study. The APP process was capable of not only tailoring surface wettability but also introducing carboxylic acid functional groups. Combining this novel APP process with the ionomer self-healing system, a self-healing composite material with potentially enhanced load carrying capacity can be envisaged.

Table of Contents

List of Figures

List of Tables

Chapter 1 Aims and Objectives

1.1 Introduction

Over the past fifty years, there has been great interest in carbon fibers (CFs) due to the excellent properties they exhibit, including superior specific strength and modulus, which are larger than for other fibers, including glass, steel and alumina. CFs also have good thermal and electrical conductivity and a low (negative in the axial direction) linear coefficient of thermal expansion in the fiber direction [1].

As an effective reinforcement system, the development of CF-reinforced composite materials have attracted considerable attention. CFs possess properties such as a tensile modulus of 200-600 GPa and a strength of 2.5-7.0 GPa, depending on the precursor and temperature of carbonization and graphitization (400-600 °C for dehydrogenation and 600-1300 °C for denitrogenation (PAN-based CFs)) during their preparation process [2], making them suitable for CF-reinforced composites. Among polymer composites, epoxy systems have the potential to prepare composite materials with high strength, light weight and multifunctionality; therefore, they have played an important role in, for example, aircraft, space shuttles and electrical products.

Creating a strong fiber-matrix composite requires several features, which depend not only on the properties of the fibers and matrices but also on the characteristics of fiber

surface and the quality of the interface, which is formed in the cured composite and responsible for the load transfer mechanism at the interface between the fiber and the matrix. The interface between the fiber and the matrix needs to be optimized because with a low interfacial bond strength, the load bearing capacity is limited by debonding at low loads. With a strong bond, the composite fractures like a monolith, losing the toughness associated with multiple matrix fractures. With optimal interfacial interaction, fiber-matrix composites possess superior efficiency at carrying loads and make it possible for materials to bear weight evenly.

However, due to the crystallized graphitic basal structure of CFs, the non-polar nature makes them difficult to chemically bond with matrices. Furthermore, surface lipophilicity, smoothness and low adsorption characteristic of CFs results in the chemical inertness [3, 4], which limits their bonding with matrices and leads to weak interfacial interaction between filaments and matrices in the composites.

To solve these issues, surface functionalization of CF has been widely investigated. The general goal of the modification is to improve the chemical compatibility between the CF surface and the polymer through chemical methods, therefore to enhance CFs adhesion and dispersion with and in the polymer. Chemical methods include employing nitric acid, $KMnO_4$, H_2SO_4, chromic acid and electrolytic NH_4HCO_3.

Research on chemical functionalization of CFs has focused on introducing acidic functional groups to the surface of CFs through oxidation methods such as aqueous electrochemical treatment [5-7]. King et al. [6] oxidized pitch-based CFs in ammonium sulfate electrolyte and found interfacial shear (IFSS) strength increased through single fiber tensile test. Fukunaga and Ueda [8] anodically oxidized pitch-based CFs in 0.1 M NH_4HCO_3 and a superior IFSS was also observed. However, CFs functionalizing processes with aqueous electrochemical treatment not only produce waste but also might cause surface degradation when using nitric acid as the electrolyte [9].

Among the methods for CFs treatment, plasma technology is of great interest because of the advantages of rapid treatment, scalability for high-quantity production and being non-polluting, which is highly desirable for industry. Several studies on surface functionalization of CFs through plasma modification technology have been reported [10, 11]. Lopattananon et al. [12] employed acrylic acid (AAc) and 1,7-octadiene as precursors to modify CF through plasma technology and produced composite materials. From their results with the polymer coatings, improved adhesion and an increased tensile strength and modulus over the untreated-unsized CF was measured. Among plasma technologies, the atmospheric pressure plasma (APP) process has received attention, since it operates effectively under atmospheric pressure and ambient temperature, providing a potential method for surface modification on thermal sensitive materials such as polymers. Bai et al. [13] developed an atmospheric plasma

polymerization route using AAc as precursor to enhance micromechanical adhesion between CFs and an elastomeric matrix by around 60%.

During the research to improve interfacial adhesion between the fibers and the matrices, self-healing has also received a great attention in the study of advanced composite materials. Matrix cracking and delamination caused by external mechanical loading or impact have played critical roles in composite material degradation, which leads to failure and limits the application. The vulnerability of composite materials to impact damage results in a costly burden of maintenance and inspection for detecting and preventing the presence of damage. To solve this issue, a self-healing function of composite materials has been demonstrated through various methods, including the hollow fiber approach [14-16], the capsule-based healing system [17-19] and the application of intrinsic healing polymers [20-22]. Among these approaches, an intrinsic healing polymer offers a healing mechanism through reversible reactions, such as chain mobility and entanglement, ionic interaction, reversible polymerization and melting of the thermoplastic phase, which can be triggered by external impact or damage. Different from hollow fiber and capsule-based healing approaches, the intrinsic healing mechanism is capable of multiple crack healing events, since it does not consume the healing agents stored inside microcapsules or hollow channels [23]. An approach based on an intrinsic healing mechanism has been made by Varley et al. [24] utilising a diglycidyl ether of bisphenol-A (DGEBA) based ionomer healing agent. The ionomer healing agent, which kept its miscibility inside the epoxy resin matrix network by

controlling its concentration under 7.5 wt%, was connected to the epoxy resin network through hydrogen bonding. When the healing mechanism was triggered by heat, the healing agent decoupled from the epoxy resin network, diffused to the crack and ionically entangled together to close the fracture. Since the healing agent diffuses through nano-interspace in a material during the healing process, it promises the advantage of repairing micro-fractures before the fractures turn into catastrophic failure. Therefore, combining the ionomer healing system with CFs, a self-healing composite material, with the capability of fixing the debonding between the matrix and the fibers, can be envisaged.

1.2 Aims and Objectives

The main aim of this project is the surface functionalization of CFs using a novel APP with subsequent AAc vapour grafting to introduce carboxylic acid functional groups on the CFs, so the functionalized CFs can react with an ionomer-modified epoxy resin, which was developed in this study, to prepare a self-healing composite. This APP process produces little waste and is a possible rapid route to optimize the adhesion between the CFs and the resin. Furthermore, it provides a mechanism for the healing of the interface using the functional groups reaction between the carboxylic acid groups and the ionomer healing agent in the matrix.

In this work, a Pyrex chamber was tailored to reduce precursor fragmentation during

plasma treatment and retain a higher percentage of functional groups. The effects of different parameters of APP treatment, especially working gas and grafting time, on surface wettability, stability, functional group labelling and chemical composition, were first investigated via water contact angle measurements and X-ray photoelectron spectroscopy (XPS) on silicon wafers before applying them to CFs. Silicon wafers have a flat, plane surface suitable for estimating the degree of surface functionalization. Subsequently, these parameters can be applied to the CF surfaces with confidence. The healing efficiency of the ionomer-modified epoxy resin network (via single-edge notched bending tests) and functional group reactions between the ionomer healing agent and the functionalized silicon and CF surfaces (via XPS), were also studied to estimate the self-healing function.

Chapter 2 Literature Review

2.1 Introduction

The literature review in this chapter presents a general introduction to carbon fibers (CFs), including its characteristics and properties, which attract attention from both academia and industry to apply CFs for composite materials. Some approaches made to prepare carbon fiber (CF) composite, and the main challenge these approaches have encountered, are also provided in this chapter. A survey of several solutions to the challenge, including CF sizing, oxidation treatment, plasma polymerization and atmospheric pressure plasma treatment, are provided here along with their advantages and limitations. This literature review also contains an overview of different concepts of designing a self-healing matrix, the advantage of using a self-healing polymer as the matrix in the composite material and a comparison between these concepts of design. Finally, after concluding the review of the materials, challenges, approaches and methods, the goals of this study are presented at the end of this chapter.

2.2 Carbon fibers

A CF is a fibrous bundle-like substrate, which contains at least 92 wt % of carbon and is composed of thousands of carbon filaments, each of diameter 5–10 μm. CFs are generally prepared by an adjusted pyrolysis of stabilized precursor fibers. A CF is mainly produced by initially converting a carbonaceous precursor into fiber form, heating the fiber to 200 - 300 °C in air and stabilizing the fiber by an oxidization process. The heated precursor fiber is then heated under 1200 to 3000 °C in an inert atmosphere

to eliminate the non-carbon elements, such as hydrogen, oxygen and nitrogen, and finally converting the precursor to a CF. Hence, CF properties are highly dominated by the precursor material and conditions during processing, including carbon content, crystallinity, molecular orientation and the amount of defects.

The history of CFs dates back to 1878 when Thomas Edison converted bamboo into CF for one of the candidates for a lamp filament [2] . The first industrial scale manufacture was in 1959, when CFs were prepared from synthetic rayons through carbonization for missile development [25]. During the 1960s, high performance CFs were developed, which used polyacrylonitrile (PAN) as a precursor. PAN, which contains 68% of carbon, can be prepared from acrylonitrile via polymerization by utilizing peroxides as the initiators. The manufacturing of PAN-based CFs requires the participation of an oxidation process and thermal treatment and was summarized (Figure 2.1) into three steps: oxidative stabilization; carbonization under high temperature (1000 ℃ in nitrogen); graphitization (2500 °C in argon) [26, 27]. This offers a process with higher carbon yields (30% for rayon while 50% for PAN) and better physical properties than rayon-based methods [28, 29]. Later, a process was achieved by carbonizing pitches, which contains at least 80% of carbon, into CFs. Pitch can be obtained from the refining of petroleum and the gasification of coal or via the pyrolysis of synthetic polymers such as polyvinyl chloride. Although coal pitch (2/3 of its compounds are aromatic [30]) is more aromatic than petroleum pitch, it possesses a high content of carbon particles, which results in filament breakage during extrusion and thermal treatment [27]. Among

these kinds of pitches, mesophase pitches were applied as precursors due to their superior molecular orientation, which can be carbonized into a graphitic crystalline structure during the process, and became the most popular material for manufacturing ultra-high modulus CFs [31]. Compared to using PAN as a precursor, pitch precursors have lower material costs. However, the processes of pitch purification, mesophase formation and fiber spinning to achieve high performance CFs increase the costs significantly.

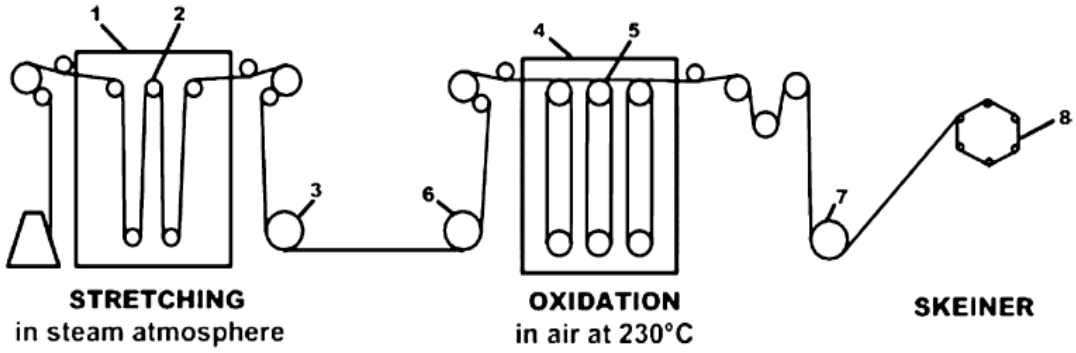

Figure 2.1 Semi-batch production of CFs from PAN fiber [27] (SKEINER means winder).

Similar to the structure of graphite, in CFs, carbon atoms are located on a hexagonal pattern with each basal plane as an aromatic ring. Preparing CFs from different precursors and manufacturing processes can lead to different arrangement of carbon atom layer planes in CFs, resulting in a graphitic or a turbostratic structure of them (Figure 2.2).

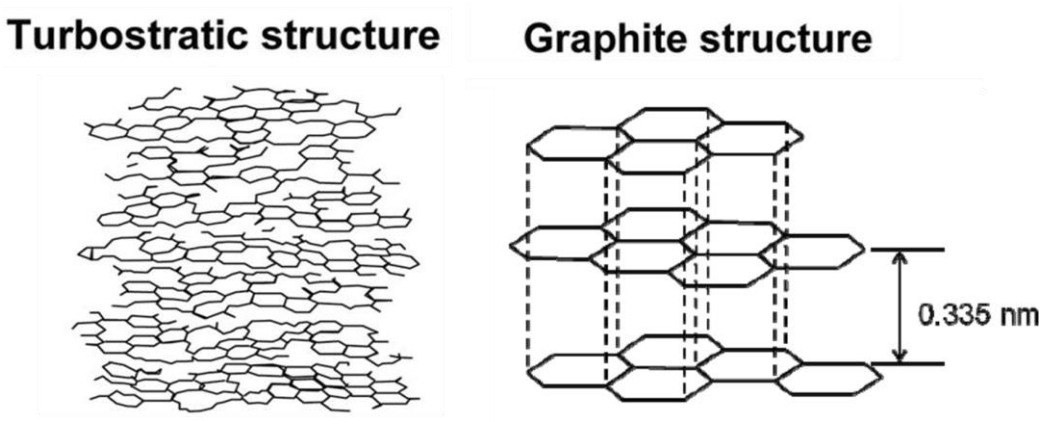

Figure 2.2 Schematics of turbostratic and graphite structures [32].

In the CFs with a graphitic structure, the hexagonal planes are stacked parallel to each other in a regular arrangement. The atoms in the same plane are bonded covalently via sp^2 bonding, while those between different layers are bonded with Van der Waals forces. In contrast, in a turbostratic structure, the parallel graphene layers are stacked in a tilted or irregular order. Mainly, mesophase pitch-based CFs show a graphitic structure, while PAN-based CFs were observed in a turbostratic structure [33]. Figures 2.3 to 2.5 show the cross-sectional SEM images of three various based CFs [34].

It can be observed that the structure of PAN-based CFs is more folded and contains turbostratic layers of carbon. This structure is similar to that of the PAN precursor, which results in a lower degree of graphitization, compared to pitch-based CFs. The imperfectly aligned and misoriented structure however is responsible for the high-strength property of PAN-based CFs. The strength of PAN-based CF is determined by

misoriented graphite planes since there are low forces between graphite planes. Misoriented crystals arrive from when graphitization around impurities in the PAN dope occurs. When a stress occurs paralleled to the axis of the PAN-based CFs, the layers align until their movement is limited by the disclination within the structure. As for pitch-based CFs, compared to the PAN-based CFs, a higher degree of alignment of the graphitic layers was observed, which makes them more flaw-sensitive but offers better lattice-dependent properties. Thus, PAN-based CFs exhibit a mechanical property of high tensile strength and low modulus, while pitch-based CFs are low tensile strength and high modulus.

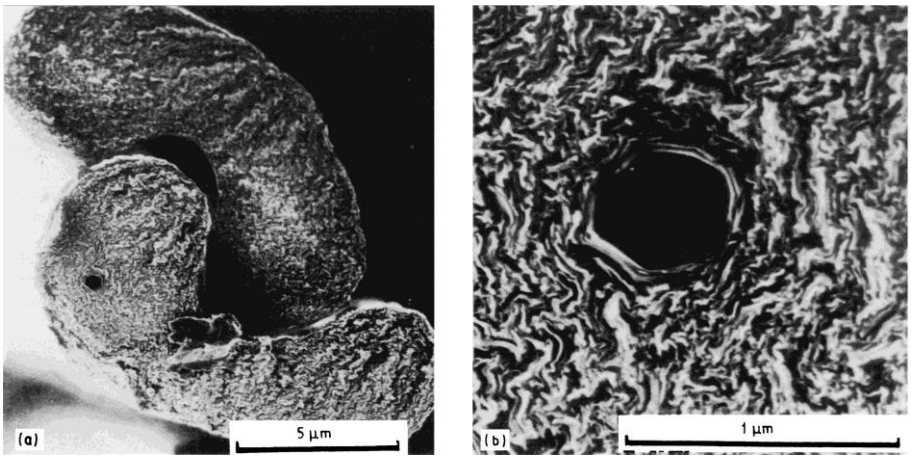

Figure 2.3 Cross-sectional SEM images of PAN-based CFs [34].

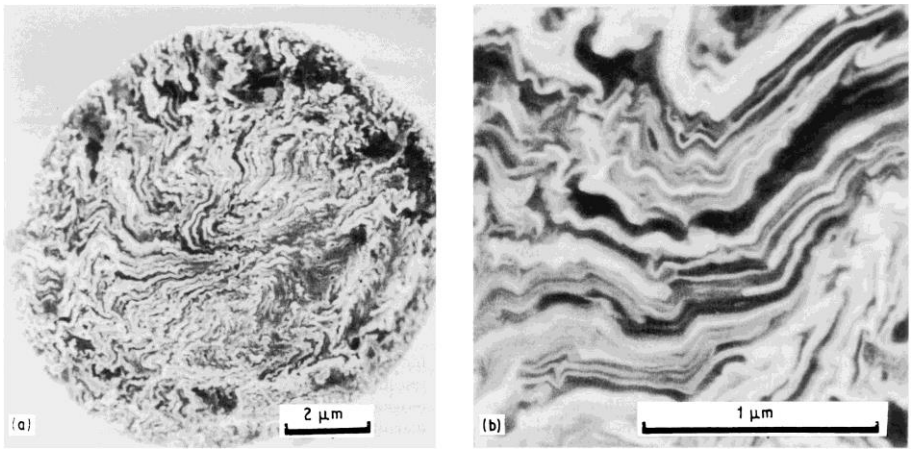

Figure 2.4 Cross-sectional SEM images of pitch-based CFs [34].

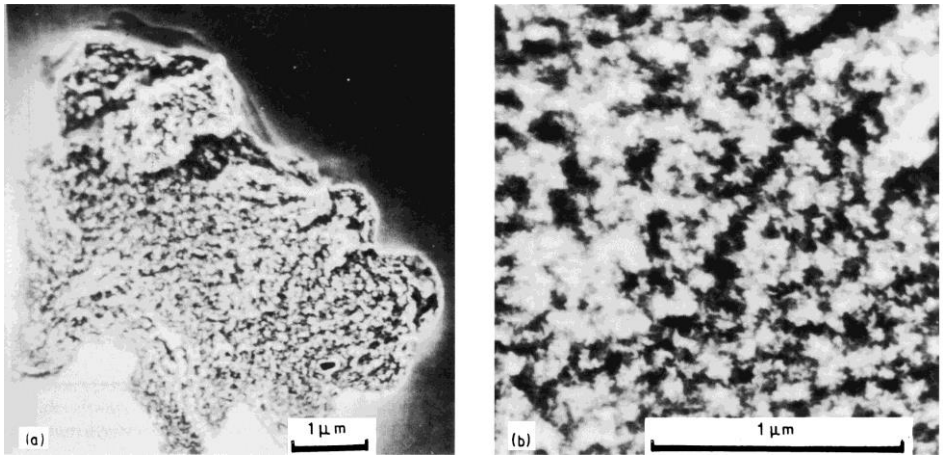

Figure 2.5 Cross-sectional SEM images of rayon-based CFs [34].

The microstructure of a CF further affects its mechanical properties and thermal and electrical conductivities.

Because of the high content of delocalized π electrons and the aligned graphene planes along the fiber axis, CFs exhibits excellent thermal (between 21–125 W/mK) and electrical conductivities, which are similar to those of metals [27]. Compared to PAN-based CFs, a higher electric conductivity can be achieved by pitch-based CFs due to the higher crystal orientation they possess [35].

CFs with high crystallinity and well alignment of crystals in the fiber direction tend to exhibit a higher modulus. Compared to PAN-based CFs, which mostly consist of turbostratic crystals, pitch-based CFs were found with a greater size of crystallites [36]. However, the larger crystallites in the microstructure of pitch-based CFs lead to higher stress concentrations on grain boundaries. Therefore, while pitch-based CFs generally

exhibit higher tensile modulus and better thermal and electrical conductivities along the fiber direction, PAN-based CFs possess a higher tensile strength due to the smaller turbostratic crystallites in their structures [37-40]. Table 2.1 illustrates the tensile properties of three major CFs categorized by various precursor applied during preparation [2].

Table 2.1 Comparison of mechanical properties of CFs from different precursors.

Precursor	Tensile strength (GPa)	Tensile modulus (GPa)	Elongation at break (%)
PAN	2.5-7.0	250-400	0.6-2.5
Mesophase pitch	1.5-3.5	200-800	0.3-0.9
Rayon	~1.0	~50	~2.5

Although PAN-based CFs have been observed with superior tensile and compressive strength compared to pitch-based CFs, the compressive strength of both pitch- and PAN-based CFs are found to be reduced with increased modulus [34, 38]. It has also been demonstrated that compressive strength not only is highly related to shear modulus between basal planes [40], but also rises with reduced orientation, density and increased inter-planar space and void content [41]. In 1996, Miwa et al. [42] investigated the effects between compressive strength and fiber diameter and found that compressive strength grows with reduced diameter but maintains almost the same level when fiber diameter ranges smaller than 10 μm. These reports further give rise to the interest of preparing CF-reinforced composite materials, which is expected to utilize one or more

of CF's intrinsic characteristics, such as high strength and stiffness, light weight, good fatigue and corrosion resistance and improved friction and wear qualities.

2.3 Carbon fiber functionalization for composites

Since the initiation of commercial CF products, investigators [27, 33, 35, 43] have studied and revealed the characteristic physical properties of CFs, such as electrical, mechanical and thermal (described in Chapter 2.2). To date, an increasing number of studies have focused on the development and understanding of fiber-reinforced composite materials in various load bearing applications [44]. Ideal reinforcing fibers include glass, carbon and aramid fibers. Considering their outstanding mechanical performance (high tensile strength up to 7 GPa and high modulus up to 800 GPa), it is very popular to use CFs as reinforcement in polymer matrices, which are either thermoplastic or thermoset. Thermoset polymer matrices include the application of epoxies, cyanates, polyesters and bismaleimides (BMI), while it is common to utilize high molecular polymers, such as aromatic polyimides, polyphenylene sulfide and polyarylene, for thermoplastic composite matrices [45].

Initial studies of CF/epoxy composites have put a lot of efforts into utilizing pristine CFs to reinforce the matrices [44, 46, 47]. However, lower than predicted tensile strength and interlaminar shear strength (ILSS) were found, as a result of inferior wettability due to the chemical inert nature of CFs in polymer matrices.

Although CF-reinforced composites have been widely utilised, the adhesion between filaments and matrices is still a critical element for composite performance. Therefore, surface functionalization of filaments has become an essential topic for optimizing the adhesion of CFs in polymer matrices.

In order to optimize the adhesion of CFs in polymer matrices, several surface treatment approaches have been studied. Various techniques for augmenting the interfacial bonding in composites include, for example, gaseous or wet oxidation [48, 49], electrochemical methods [7, 50, 51], plasma treatment [11, 52] and polymer coating [53, 54]. With elevated surface free energy and immobilized functional groups on the fibers, improved interfacial properties were observed [55-57].

2.3.1 Oxidation treatment

To effectively transfer external tensile load from CFs to a polymer matrix and augment the handling of the fibers, optimum chemical bonding between each other is required [58]. A large amount of studies have been reported for the chemical functionalization of CFs.

Li [59] employed an acid treatment for functionalizing CFs to improve interfacial reaction with polyimide matrices. XPS results indicated that the oxidation treatment not only raises the oxygen concentration but also converts hydroxyl-type oxygen on the

surface into carboxyl functional groups. Zhang et al. [60] oxidized pitch based CFs with 65 to 68 wt% HNO_3 under 90°C for 1.5 hours. An increased amount of functional groups (–O–C–, –C=O, –O–C=O) or sites on the fiber surface was achieved, which increased surface energy and polarity and contributed to interfacial adhesion between the filaments and polyimide matrix. However, functionalizing CFs through acid treatment not only produces polluted wastes but was also found to be complicated and time consuming in processes [61].

Compared to acid (HNO_3) treatment, electrochemical oxidation offers a faster, uniform, and mass production suited process. Electrolytes such as ammonium bicarbonate, ammonium sulfate, ammonium oxalate and sodium bicarbonate have been widely employed [5, 6, 62-64]. Liu et al. [64] functionalized PAN-based CFs via an electrochemical oxidation process using ammonium oxalate (0.5 M) as electrolyte with the electric current density of 0.6 mA cm^{-2}. The functionalized CFs showed an improved (by 16.6%) tensile strength and exhibited an 8.6% increase on ILSS with epoxy matrix. Park and Park [62] electrochemically modified unsized PAN-based CFs using 5 wt% sodium bicarbonate as electrolyte and observed increased ILSS between fibers and DGEBA matrix. An increase of ILSS between CFs and DGEBA matrix from 79 MPa to 93 MPa was reported by Denison et al. [65] after the CFs were modified by an electrochemical oxidation treatment using ammonium bicarbonate as the electrolyte. Liu et al. [66] employed a mixture of ammonium bicarbonate (0.6 mol/L) and ammonium oxalate monohydrate (0.5 mol/L) in a ratio of 1:1 as the electrolyte solution

to electrochemically oxidize the PAN-based CFs. Improvements of the tensile strength (by 17.1%) and the ILSS between the CFs and epoxy matrix (by 14.5%) were observed after the CFs electrochemical oxidation. Ryu et al. [63] have also reported improved ILSS between the DGEBA matrix and the unsized CFs, which were electrochemically treated with 5 wt% ammonium carbonate. However, the electrochemical process took a longer treatment time (from 60 to 90 minutes) and produced chemically polluted liquid waste, which is not environmentally friendly [9, 67, 68]. In light of these drawbacks as described above, researchers have turned their interests to plasma technologies.

2.3.2 Carbon fiber sizing

Sizing is commonly used by fiber manufacturers to "size" or coat their fibers, which can involve providing an acceptable surface coating to protect fibers from damage or fuzzing caused by yarning or contacts during manufacturing. Sizing materials, commonly applied around 0.5 to 1.5 wt%, not only offer protection to the filaments bulk but also improve the composite processibility and adhesion between fibers and matrices, which play a major role in the preparation of composites with tailored interface properties. The effect is mainly contributed by the chemical reactions between the polymer matrix and the covalently bonded functional groups on the surface of CFs [69].

To achieve the optimal interaction, for different kinds of matrix and fibers, various

sizing agents are required [70]. Commonly applied sizing agents can be categorized into two types: the solution type (a sizing agent dissolved in an organic solvent) and emulsion type (an emulsified sizing agent dispersed in water) [71]. For the solution type of sizing, sizing agents such as polyvinyl alcohol, epoxy resin and vinyl acetate polymer are commonly utilized [72, 73]. Blackketter et al. [72] utilized epoxy-sized CFs (PAN-based) and an epoxy resin (EPON 828) to prepare a CF-reinforced thermoset matrix composite. Compared to the composite made by unsized CFs, improved short beam shear (39.6 MPa to 73.1 MPa) and transverse flexural strengths (29.6 MPa to 78.2 MPa) were observed, indicating better unidirectional composite shear and transverse tensile strengths of the composite prepared with epoxy-sized CFs. Taking factors of economy, safety and hygiene into account, the emulsion type sizing agents are widely applied. However, the challenge for utilizing an emulsion type sizing agent is the ratio of the emulsifier to the sizing agent. As the emulsifier is a poor bonding agent and tends to limit reduce the bonding of the dried emulsion finish to the CFs, it is preferable to limit the amount of emulsifier during the process. A typical sizing process is schematically described in Figure 2.6 [71]. Generally, the sizing is first sprayed or dipped to the surface of CFs, then dried up to evaporate the solvent or water to leave the sizing agents on and fuses to the CFs surface.

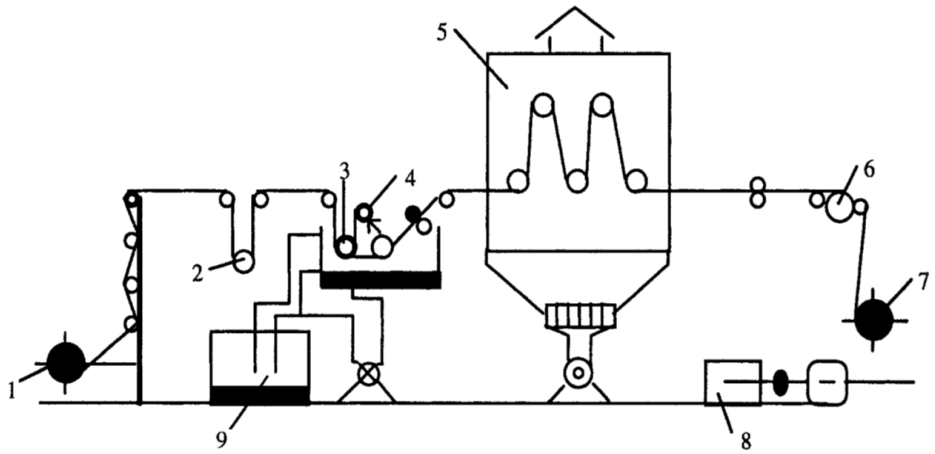

Experimental sizing line (Zoltec Co.). 1—unwinding mechanism. 2—precise tension adjustment unit. 3—bath. 4—sprayer. 5—drying box. 6—drawing mechanism. 7—winding mechanism. 8—motor and speed control. 9—reservoir circulation.

Figure 2.6 Schematic diagram of a typical sizing process [71].

In a study by Liu et al. [74], emulsion type vinyl ester resin sizing agent (HMSA-1) was prepared through phase inversion emulsification and applied to CF sizing. A HMSA-1 sized CF/vinyl ester composite was observed with 20.7% improvement in ILSS as HMSA-1 offers reactive groups on the CF surface and possesses superior compatibility with vinyl ester matrix.

Li et al. [75] reinforced phenolic resin matrices with CFs sized with phenol, m-phenylenediamine or acrylic acid through electropolymerization. The composites exhibited an increase in impact strength, flexural strength and ILSS by 44 %, 68% and 87% with m-phenylenediamine sized CFs, 66%, 100%, and 112% with phenol sized CFs, and 20%, 80 %, 100% with acrylic acid, respectively. Enhancement of ILSS was also reported in both woven CF/epoxy and CF/polyethersulfone when utilizing epoxy sized CFs as reinforcing fiber material [76, 77].

However, an inferior interfacial performance between sizing and epoxy matrix was also monitored in epoxy composites reinforced by polyurethane and polyetherimide sized CFs. ILSS shows a decrease in both polyurethane (14 MPa) and polyetherimide (19 MPa) sized CFs composites, compared to that using unsized CFs (28 MPa). The poor fiber/matrix adhesion may be due to the adsorption of polyurethane and polyetherimide sizing onto the CF surface, which limits the diffusion of sizing materials into the polymer matrix during composite fabrication. Since dissolving of sizing materials into matrices provides a chemical reaction between fibers and matrices and further benefits interface performance, the adsorption of sizing may diminish functional groups on the filament surface and within sizing materials and leads to weak interfacial bonding [78]. This is supported by a study of Yumitori et al. [76], which indicated that a reduction of interfacial shear strength may occur if the sizing layer existed as a distinct layer.

It has been suggested that fiber/sizing compatibility plays a crucial role during composite development. Although sizing application contributes to the improvement of abrasion resistance and bending strength of CFs, the mechanical performance (e.g. ILSS) tends to decrease when the CF sizing shows lack of compatibility with the matrix [79-81].

2.3.3 Plasma polymerization

First in 1920, Tonks and Langmuir [82] began to study the phenomenon of “plasma” and further used the term in 1929 to describe this process of gas ionization. When substrates are given energy by high temperature, accelerated electrons or ions, reactions such as excitation, dissociation and ionization occur, thus producing a mixture of molecules, atoms, excited species, electrons, positive ions, negative ions, free radicals and UV or visible light, which is called a plasma. Therefore, besides gas, liquid and solid, plasma is recognized as the forth state of matter.

Plasma polymerization has been widely investigated and applied for the modification of surfaces through depositing thin films on them [83, 84]. In this process, gaseous monomers are introduced into the plasma as precursors. After collisions with high-energy electrons in the plasma, most precursor molecules are fragmentized into reactive species and react with each other and eventually deposit a cross-linked polymer film on the surface.

This technology exhibits several advantages. First of all, the thickness of the thin film, from approximately hundred nanometres to one micrometre, can be easily controlled. Conformal coatings with specific physical or chemical properties can also be prepared on nearly any substrate, such as polymers, metals, glass, ceramic and semiconductors. With the above-mentioned characteristics, surface modification of fibers through plasma polymerization to improve their adhesion to epoxy resin in fiber-reinforced

composite materials was achieved. By plasma coating, functional groups can be immobilized on the surface of fibers to create chemical bonds between them and the resin, resulting in a more effective load transfer and further prevent fiber damaged during handling. Dilsiz et al. [85] utilized a radio frequency (RF) plasma with xylene as monomer on PAN-based CFs. The interfacial adhesion between CFs and epoxy resin was found to be improved as the ILSS increased from 65.62±0.59 MPa (Untreated CFs) to 70.01±2.40 MPa (RF plasma treated with xylene). Feih and Schwartz [86] employed an RF plasma using a mixture of oxygen/acetylene (at a ratio of 1:2) as precursor for functionalization of PAN-based CFs. The interfacial performance between CFs and epoxy resin was observed to be improved as the ILSS was increased from 30 MPa (Untreated CFs) to 45 MPa (RF plasma treated with oxygen/acetylene).

Reports have demonstrated improvement of single filament strength and modulus on plasma coated reinforcing fibers [87-89]. Precursors, including acrylic acid, allylamine and allyl alcohol, have been applied for plasma polymerization on CFs and glass fibers to introduce functional groups such as carboxylic acid and amine [12, 88-90]. Swait et al. [91] coated E-glass fibers through plasma polymerization with an acrylic acid/1,7-octadiene copolymer as precursor. These fibers were used to fabricate unidirectional composite panels. From their results, the longitudinal tensile strength of the composites exhibited a 20% increase, while a further 30% increase of tensile strength was achieved with an optimal ratio of composition (40% acrylic acid) of the coating. The increased performance of plasma-polymerized fiber composites may be the result of the reduction

in the variability of fiber strength caused by the plasma polymer coating [89]. Another possibility is the improved stress transfer between the filaments and the matrix due to the mechanical properties of the plasma polymer (which exhibits a modulus slightly higher than that of the matrix, but much lower than that of the fibers).

2.3.4 Atmospheric pressure plasma treatment

Although some studies related to the surface modification of fibers through plasma polymerization have been previously reported [12, 87-90], all these processes were carried out at low pressure, which requires expensive vacuum systems (seals, transfer chambers and pumping) and is usually found with low deposition rates. In contrast, APP processes possess advantages such as rapid treatment times, environmental friendliness and lower production costs. Therefore, atmospheric pressure plasmas have received increasing attention recently to deposit plasma polymer films on various substrates [92-94].

Atmospheric plasma processes can be classified into four major categories: Implantation (e.g., utilizing oxygen or nitrogen gas for –OH or $–NH_3$ immobilization), etching (e.g., oxidation of organic polymer through oxygen or N_2O gas), activation (e.g., applying argon or helium to introduce free radical) and deposition of polymers.

In a previous study, the author employed an atmospheric plasma system assembled by Chen et al. [95] in a V-type glass tube for surface activation and polymerization. With ethanol and helium mixed working gases, new grafted oxygen containing polar groups such as C-O and O-C=O and improved hydrophilicity were observed on the surface of a glass slide. The same effects have also been reported in this system as the author utilized He and N_2 mixed working gases for polyurethane nonwoven treatment, while employing tetramethylsilane vapour enhanced hydrophobicity on a glass surface (Figure 2.7) [95-97].

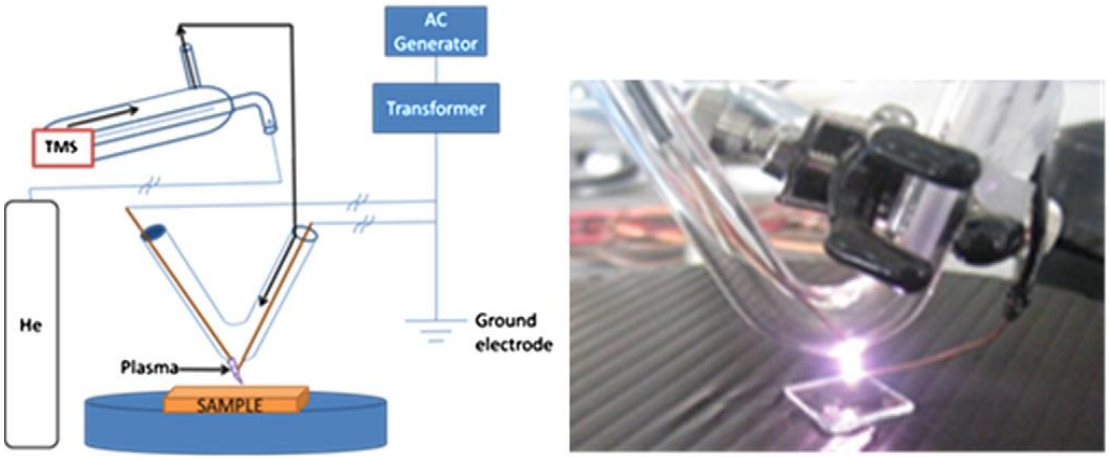

Figure 2.7 Schematic diagram of atmospheric plasma treatment system and plasma glow in the V-type glass tube [95].

O'Hare et al. [98] prepared organic coatings with a rate of 40 nm/min by feeding an acrylic acid precursor into the post discharge of a radio frequency atmospheric pressure helium plasma torch. Nisol et al. [99] deposited acrylic acid films by introducing an acrylic acid vapour in an helium dielectric barrier discharge plasma (Figure 2.8).

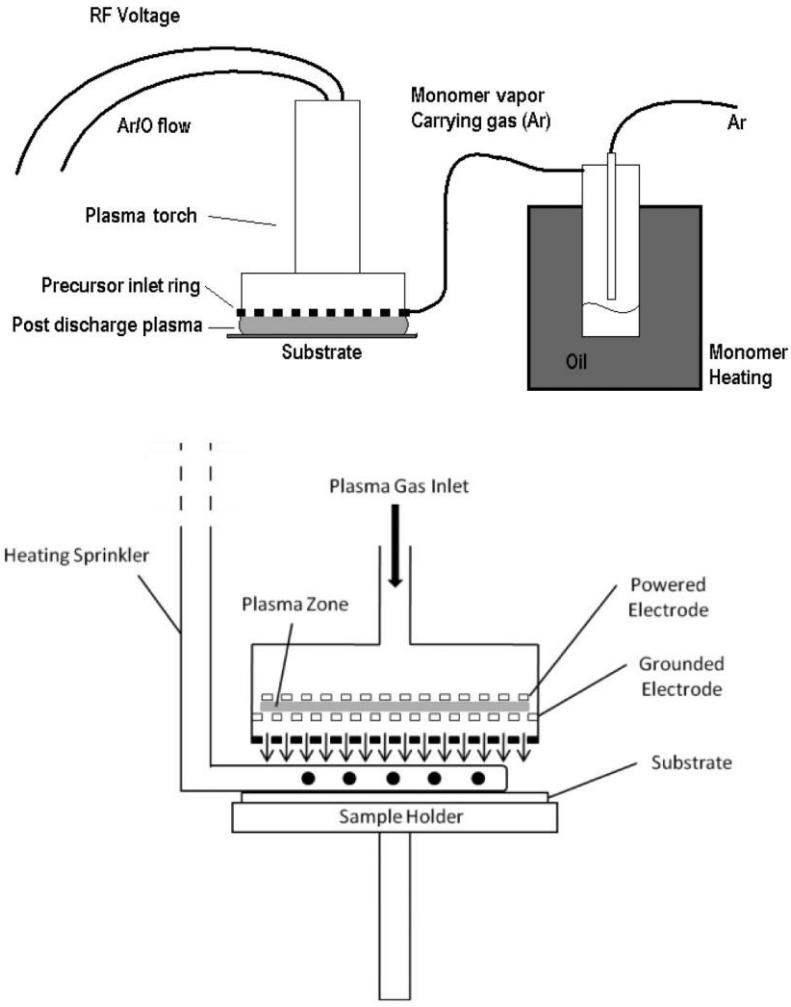

Figure 2.8 Schematic of the atmospheric pressure plasma process using the RF torch [99].

A study has also been reported by Bai et al. [100], who employed an atmospheric pressure plasma with acrylonitrile as precursor to deposit a thin functional polymer layer on the surface of CFs, to improve their adhesion to an elastomeric resorcinol formaldehyde latex (RFL) matrix. The single fiber fragmentation test revealed that the adhesion between CFs and RFL was enhanced, as the interfacial shear strength increased by 30% for fibers with 4.2 min residence in plasma zone. In another research [13], they replaced the precursor by acrylic acid and utilized an atmospheric pressure plasma for CF functional coatings (Figure 2.9). The results of this study exhibited a

nearly 60% improvement in adhesion behaviour between the CFs and the elastomeric matrix.

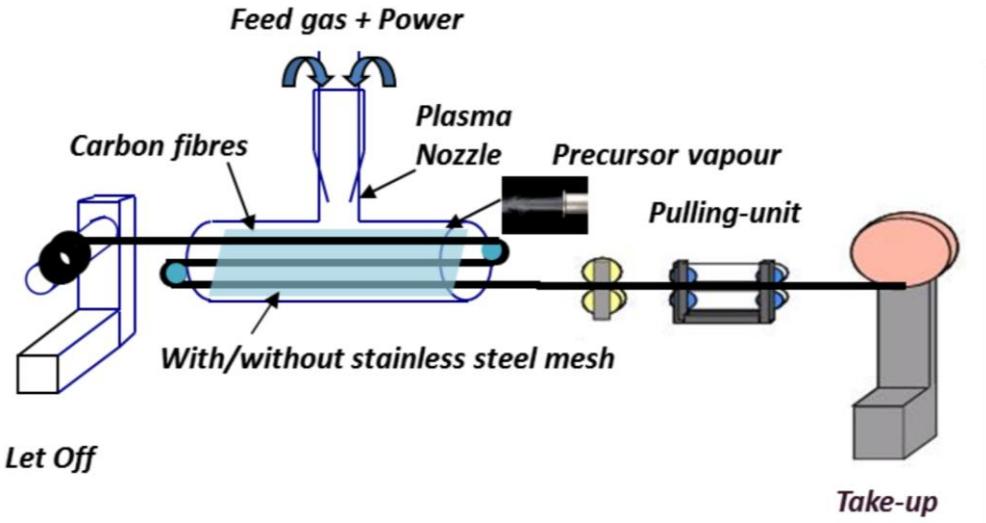

Figure 2.9 Schematic of continuous atmospheric plasma polymerization treatment set-up for CFs [13].

In 2012, Carton et al. [101] deposited carboxylic group containing films on a substrate for biomedical application by using an atmospheric nitrogen plasma jet with acrylic acid as precursor (Figure 2.10). Two years later, to improve the water stability of deposited films, a precursor consisting of acrylic acid and a cross-linking agent methylene-bis-acrylamide was introduced for plasma polymerization through an atmospheric pressure air plasma jet [102]. In this study, higher deposition rates, ranging from 1 to 10 μm/min, compared to 1 μm/min in the previous study, as well as the retention of carboxylic moieties were reported.

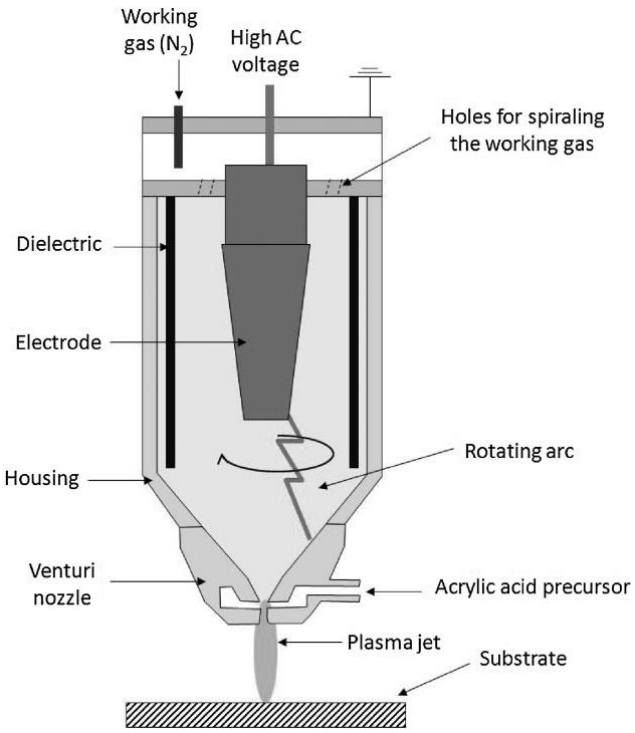

Figure 2.10 Schematic of the atmospheric nitrogen plasma jet system [101].

It can be summarized that plasma polymerized acrylic acid coatings have the potential to increase the interfacial bonding between fibers and matrices in composite materials, leading to a superior transfer of stress from matrix to fibers. Furthermore, the success of acrylic acid polymerization through atmospheric pressure plasma makes this process a promising method to enhance the mechanical properties of CF/epoxy composite materials.

2.4 Self-healing matrices for composites

CF-reinforced polymer systems, compared to steel, aluminium and wood, exhibit superior specific strength and modulus and offer a degree of variety in design and manufacture. These composite materials are promising for developing high strength,

lightweight and multi-functional composite materials and have been widely employed in various industrial applications including aerospace, civil engineering and electro-optical industry [103].

However, these composites are vulnerable to external impact, which results in microcracking in the matrices and further leads to various damages including fiber/matrix debonding and structural delamination [104, 105]. The delamination is difficult to observe as it occurs deep inside the structure. Therefore, to sustain the structural integrity, frequent inspection and maintenance are required. Currently, various methods have been proposed for delamination repair [106-108], including injection of resin to the crack through an access channel and bonding the composite structure with a reinforcing patch, though, all processes are time consuming and require a trained technician. Therefore, the application of a self-healing system on the matrix of composites has attracted an increasing worldwide interest as an achievement to enhance damage tolerance and durability.

The idea of developing a remendable intelligent network, which is defined as self-healing system, has been highly influenced by the bio-inspired materials system. The concept was originally inspired by the natural biological function of healing within the living organism, such as the capability of skin to heal the trauma autonomously after being triggered by injury. By utilizing the same concept of healing processes within living organisms into standard materials, it provides a prospective chance and benefit

to improve the performance of a material. A well-designed self-healing material promises the characteristic of initiating the healing process autonomously to response the crack or damage caused on it, which further recovers the function and prolongs the lifetime of the material.

The main approaches for developing self-healing systems share a similar concept and general mechanism of the self-remendable process is showed in Figure 2.11. After the damage happened, the healing function is triggered by the crack or initiated by external stimuli such as heat. Unlike standard materials, self-remendable materials contain "mobile components", called healing agents, which are able to flow or diffuse towards the crack of the damaged material. Then the healing is proceeded by closing the damage site via physical or chemical reactions performed by the healing agents, including entanglement or polymeric cross-linking. After the healing performance, this "mobile" healing agent becomes immobilized again.

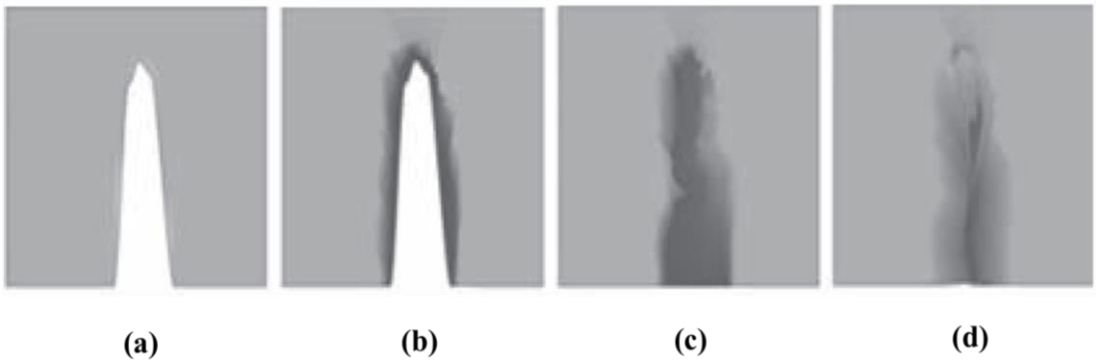

Figure 2.11 General healing mechanisms of a self-healing material (a) the damage site occurs (b) healing agent responses to the damage site (c) the mobile healing agent fixes the crack (d) healing process accomplished and the healing agent become immobilized [109] (no scale bar shown in original source).

To date, the approaches can be categorized into three aspects: capsule-based healing systems, vascular healing systems and intrinsic healing polymers.

2.4.1 Capsule-based healing matrices

In capsule-based healing systems, healing agents are encapsulated and embedded into a polymeric matrix. When damage takes place due to external force and breaches the capsules, a self-healing function is triggered as healing agents are released and react in the damage site (Figure 2.12). It is also common to enclose a catalyst in the matrix to initiate polymerization [110, 111]. White et al. [112] manufactured a self-healing polymer with microencapsulated dicyclopentadiene (DCPD) healing agent and Grubbs' first-generation catalyst within an epoxy matrix and demonstrated about 75% recovery of the virgin fracture load. The healing mechanism is based on Grubbs' catalyzed ring-

opening metathesis polymerization of DCPD, which was activated when a crack propagated into the microcapsules, releasing the monomer and polymerization was initiated by contact with the embedded catalyst. Research employing encapsulated DCPD healing agent and wax dispensed Grubbs' catalyst exhibited high healing efficiencies (90%) and extended fatigue life (213%), as discussed by Brown et al. [113-115]. However, because the capsules containing healing agents at the damaged site were emptied and ruptured after the healing event, it can only be performed once per damaged site.

.

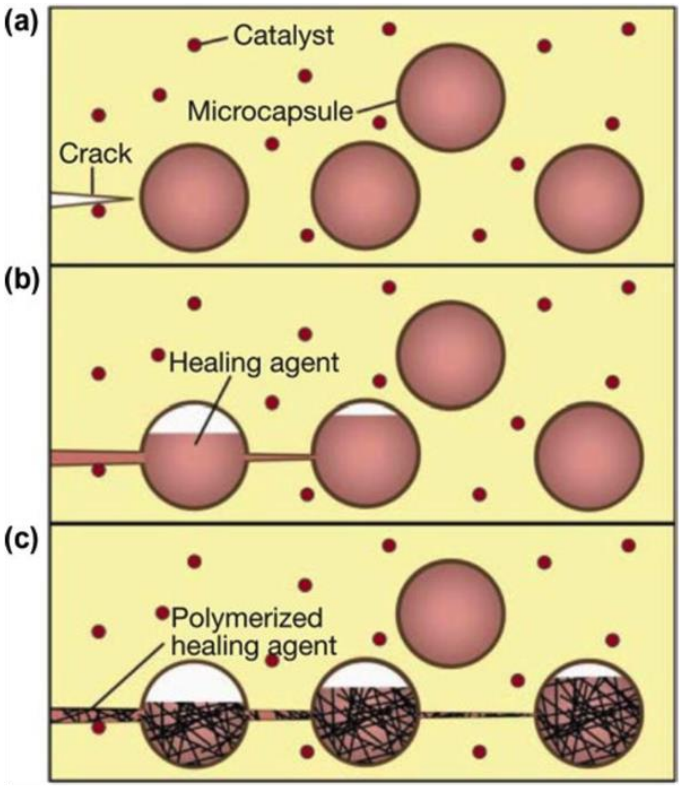

Figure 2.12 Capsule-based self-healing composite reported by White et al. [116].

2.4.2 Vascular healing matrices

In a vascular healing system, vascular mimic networks filled with healing agent are fabricated inside the matrix. After the healing function is triggered, it is possible to support the healing agent into the same damaged site from and through the connected channels inside the matrix, allowing for multi-healing events (Figure 2.13).

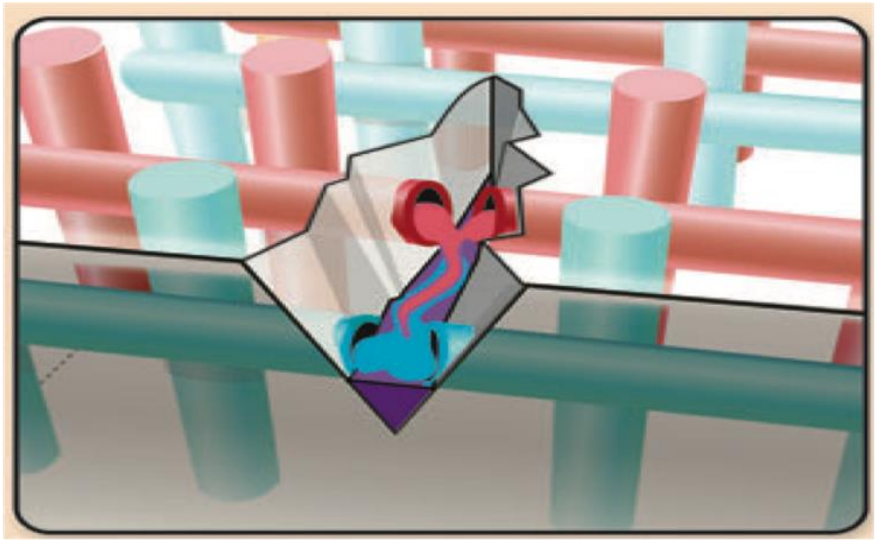

Figure 2.13 In a vascular healing system, the hollow tubes inside the material contain healing agent. When a crack happens, these tubes will be ruptured and release healing agent [117].

Toohey et al. [118, 119] developed a 3D vascular healing system in an epoxy resin matrix by mimicking epidermal tissue structure. DCPD was applied as healing agent and stored in the 3D microchannel (~200 μm) network of the matrix, while Grubbs' catalyst was introduced into the epoxy resin matrix. From the results of four-point bending, healing efficiencies between 38 to 70% were observed. For both capsule-based and vascular healing systems, the disadvantage of these methods is the

requirement of introducing foreign bodies like microcapsules [116] or hollow fibers [120] for the storage of healing components.

2.4.3 Intrinsic healing matrices

The application of intrinsic healing polymers focuses on repairing damage through intrinsic reversible bonding of the matrices (Figure 2.14) and exhibits advantages such as being repeatable, which possesses the possibility to repair damage at the same location several times, and being able to stay dormant until required [121-123].

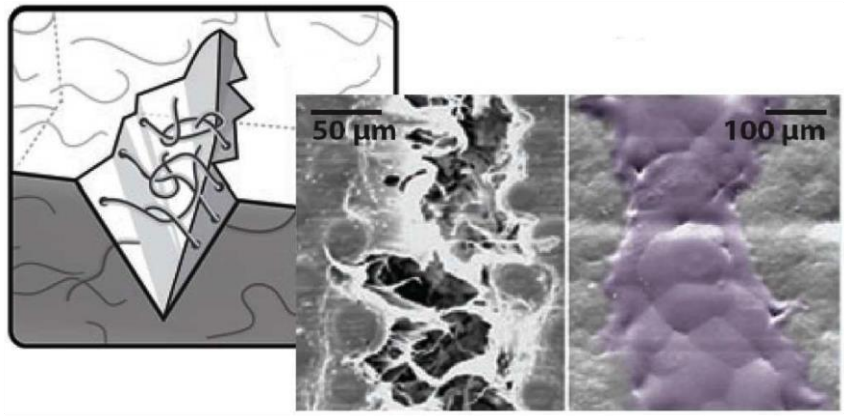

Figure 2.14 Scheme of one of the approaches of intrinsic self-healing materials: The healing is carried out by melting and subsequent flow of the thermoplastic material into the damage site to entangle chains that span the crack surfaces [117].

Compared to capsule-based and vascular healing systems, the introduction of a microencapsulate or hollow channel is not required. The introduction of microcapsules or hollow fibres and related systems introduces local stresses, which can reduce the

strength of the material. The fractured healing agent 'containers' add additional local stresses. These disadvantages can be mitigated by using a self-healing matrix. A thermal-triggered self-healing system based on Diels-Alder reaction was developed and applied on furan-maleimide polymers by Chen et al. [121, 124] and an 83% healing efficiency was observed. A similar system on furan-maleimide polymers was also studied by Plaisted and Nemat-Nasser [125] and increased healing efficiency (Maximum 100%) and repeatable healing ability of the polymer were reported. Self-healing functionality was also established by Park et al. [126, 127] using a novel polymer (Mendomer 401) derived from cyclopentadiene through the Diels-Alder reaction. The developed self-healing polymer was applied as matrix in a CF composite, which exhibited a maximum 94% healing efficiency. Luo et al. [21] incorporated phase-separated poly caprolactone (PCL) in a thermally remendable epoxy matrix. The PCL melted and initiated a volumetric thermal expansion to close the crack. By investigating the peak fracture load, it revealed a greater than 100% healing efficiency, as quantified healing measurement in the healed case is larger than the virgin case.

Approaches to self-healing via molecular diffusion have also been illustrated [128, 129]. In this approach, the healing agent, which is hydrogen bonded to the matrix, is able to diffuse to the damage site through the matrix after thermal stimulation and activate healing function. This mechanism is illustrated in Figure 2.15.

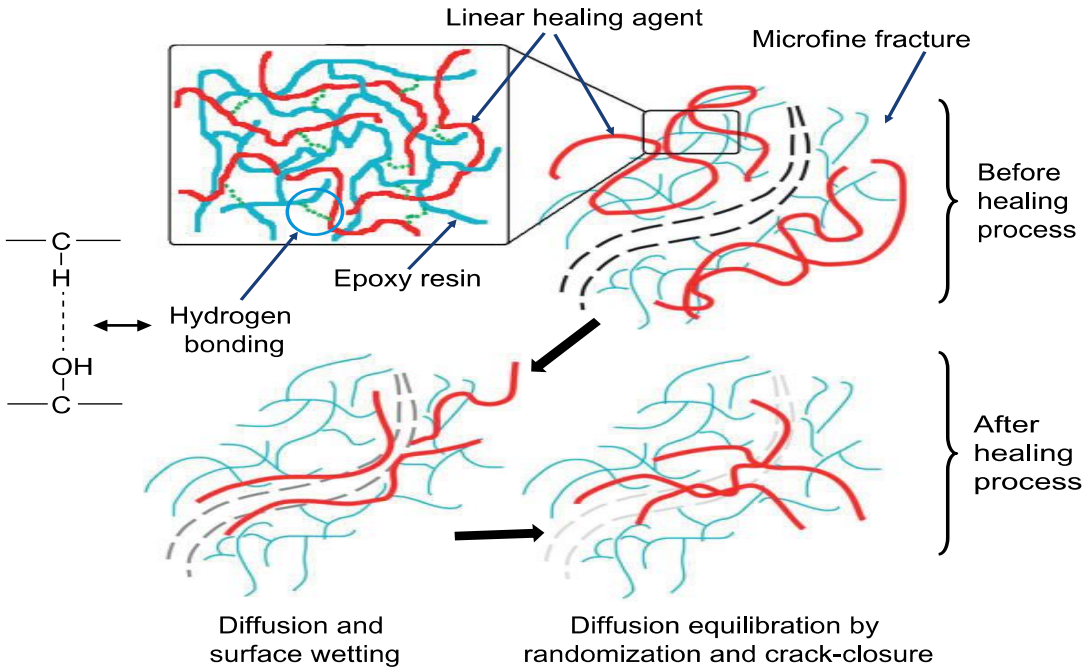

Figure 2.15 Schematic of diffusional solid-state healing showing the role of a linear polymeric healing agent [130].

Yamaguchi et al. [131, 132] reported an autonomic self-healing mechanism through inter-diffusion and aggregation of dangling chains in a polyurethane gel. Healing efficiency was estimated by tear experiments, which revealed that for healed specimens, those with longer dangling chains showed about 80% tear strength recovery.

A solid-state repair system has been reported by Hayes et al. [20], where a DGEBA combined with poly(bisphenol-A-co-epichlorohydrin) is capable of repeated thermal healing, and a healing efficiency between 50% and 70% was reported.

Rahmathullah et al. [133] elevated molecular diffusion through thermal treatment (185°C for 1 hour) of an epoxy–amine matrix (DGEBA and 4,4’-methylene biscyclohexanamine) with excess amine curing agent and observed a healing efficiency of over 100% from the results of compact tension tests, which may be due to the covalent bonds formed by polyetherification or homopolymerization reactions of unreacted epoxy groups at the damaged interface.

Varley et al. [24] demonstrated a mendable DGEBA matrix with ionomer mechanism (Figure 2.16). Glycidyl end-capped poly (bisphenol A-co-epichlorohydrin) was end-capped 4-amino-sodium salicylate and employed as a healing agent in this paper. The healing agent is soluble and originally attached to the polymer network via hydrogen bonding and as healing temperature is achieved (185°C), it can uncouple from the matrix and diffuse to the damage for healing. The DGEBA matrix with the presence of healing agents exhibited significant load recovery even after 3 healing cycles, while that without healing agents were found decayed with 2 healing events. It also indicated that when the healing agent reacted with carboxylic acid or sodium neutralized carboxylic acid groups, an even better mendability, compared to high-molecular-weight phenoxy healing agents, could be reached, suggesting the potential for employing ionomer healing system to composite matrices.

In light of these advantages, the DGEBA-based self-healing system presented by Varley et al. [24] was modified, then utilized with the APP-functionalized CF in this study to offer a novel and rapid method for preparing CF self-healing composite.

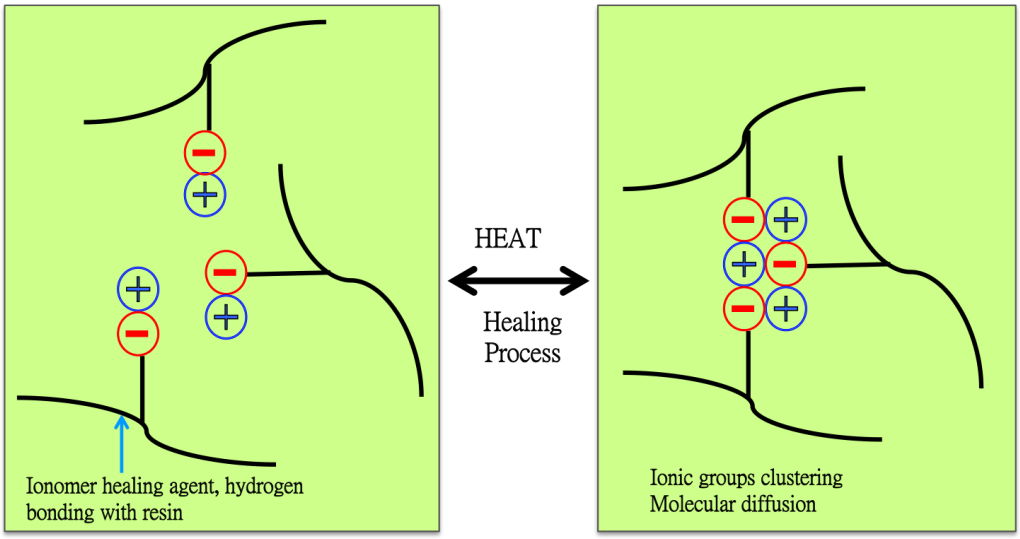

Figure 2.16 Triggered by heat, ionomer systems offer remendability through hydrogen bonding, ionic clustering and molecular diffusion in polymers.

2.5 Summary

The literature review in this study describes:

1. CF's structure and intrinsic characteristics, such as high strength and stiffness, light weight, good fatigue and corrosion resistance, and improved friction and wear qualities.

2. The approaches and benefits of preparing CF-reinforced composite materials, which are suitable for applications where strength, stiffness, lighter weight and excellent

fatigue characteristics are requirements.

3. The challenges encountered during development of CF-reinforced composite materials, which are poor adhesion and bonding between the chemically-inert CF surface and the matrix. Therefore, surface functionalization of CFs is required.

4. The advantages of utilising atmospheric pressure plasma with acrylic acid for surface functionalization. Compared to other methods, including employing nitric acid, $KMnO_4$, H_2SO_4, chromic acid and electrolytic NH_4HCO_3, atmospheric pressure plasma possesses advantages as a rapid treatment process, showing good scalability for high-quantity production and being non-polluting.

5. Self-healing composites exhibit benefits and potentials, including reducing expenditure on maintenance and prolonging service life. Various self-healing systems and their applications to composite materials have been studied. Among these systems, the ionomer self-healing system shows advantages such as repeatability, which possesses the possibility to repair damage at the same location several times, and being able to stay dormant until required.

In light of these points from the review, this research aims towards the employment of an atmospheric pressure plasma using an acrylic acid precursor for surface functionalization of CFs. The functionalization process provides carboxylic acid groups

on the CFs to improve their adhesion to ionomer-modified epoxy resin, which is also developed in this research, to further enhance the load carrying capability of and provide self-healing function to CF/epoxy self-healing composites.

Chapter 3 Materials and Methods

3.1 Materials

CFs (Figure 3.1) used in this work were provided by Carbon Nexus (Geelong, Australia) in an untreated and unsized form of high performance CFs produced from a polyacrylonitrile (PAN) precursor. The 7 μm CFs are composed by 12000 filament tows, with reported values of the modulus and strength of 238 GPa and 3.4 GPa, respectively. Silicon wafers (n-type), which were purchased from San Chih Semiconductor Co., Ltd, Taiwan, were cut into a size of 1 cm^2 and used as specimens. The substrates were cleaned ultrasonically in 99.5% isopropanol solvent (Purchased from Aldrich Chemical Company, UK, HPLC grade) and distilled water (Purchased from Fisher Scientific, UK, HPLC grade) for 15 min and left to dry in an oven (40°C, 1 atm) to remove contaminants and organic matters from the surface. The precursor for plasma polymerization was acrylic acid purchased from Aldrich Chemical Company, UK, with 99% purity. The epoxy resin and hardener under the trade name of Araldite LY 5052 and Aradur 5052, respectively, were purchased from Mouldlife, UK. For preparing the healing agent, diglycidyl bisphenol A-co-epichlorohydrin (DGEBA) with a viscosity average molecular weight of 1075 g mol^{-1} and 4-amino-sodium salicylate were purchased from Sigma-Aldrich. For surface carboxyl derivatisation, 2,2,2-trifluoroethanol (TFE), di-*tert*-butylcarbodiimide (Di-tBuC) and Pyridine were purchased from Aldrich Chemicals (all reagents 99% purity).

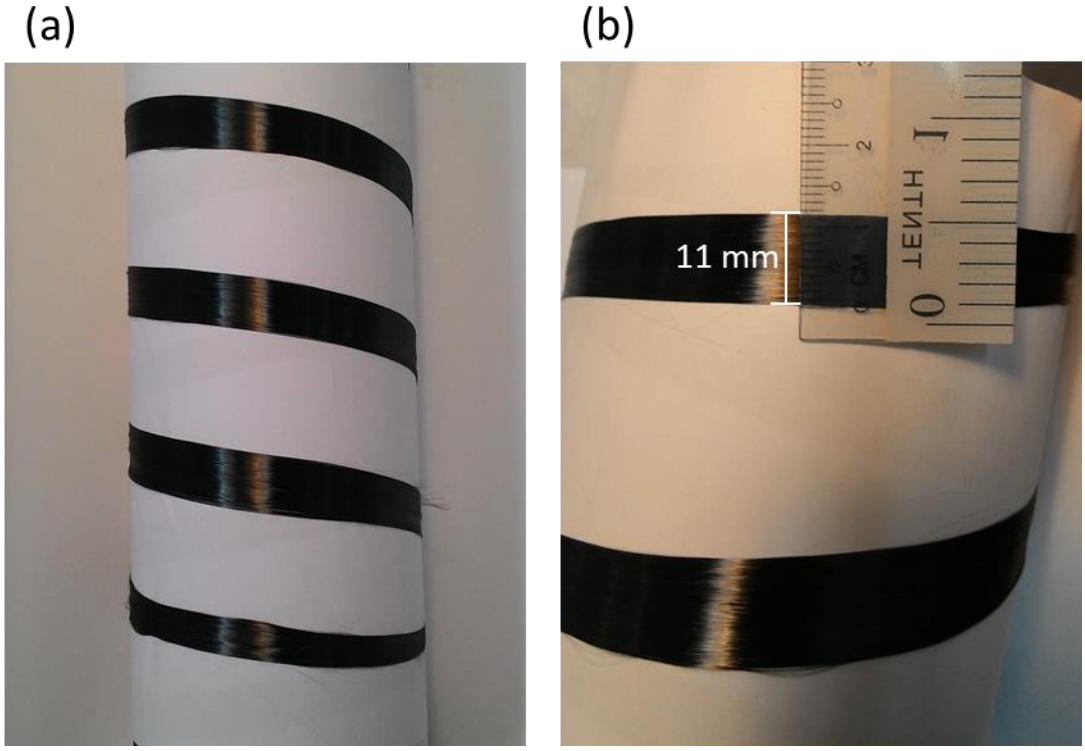

Figure 3.1 Images of (a) the unsized high performance CF bundles and (b) the diameter of the CF bundles provided by Carbon Nexus.

3.2 Atmospheric pressure plasma functionalization

3.2.1 Design of the atmospheric pressure plasma chamber

A V-shape atmospheric pressure plasma chamber has been designed and utilized in other studies by the author [95-97] for tailoring surface wettability and introducing functional groups. This design based on the fundamental concept of creating atmospheric pressure plasma, which is composed of two electrodes (a cathode and an anode) and a plasma working gas injection system. This concept has been widely applied in different atmospheric pressure plasma nozzle models, such as arc plasma torches, corona discharge devices, RF atmospheric pressure plasma jets, RF cold

plasma torches (with RF cathode and grounded anode) (Figure 3.2) [134] and OPENAIR® Plasma System (Plasmatreat GmbH), which was employed in this study.

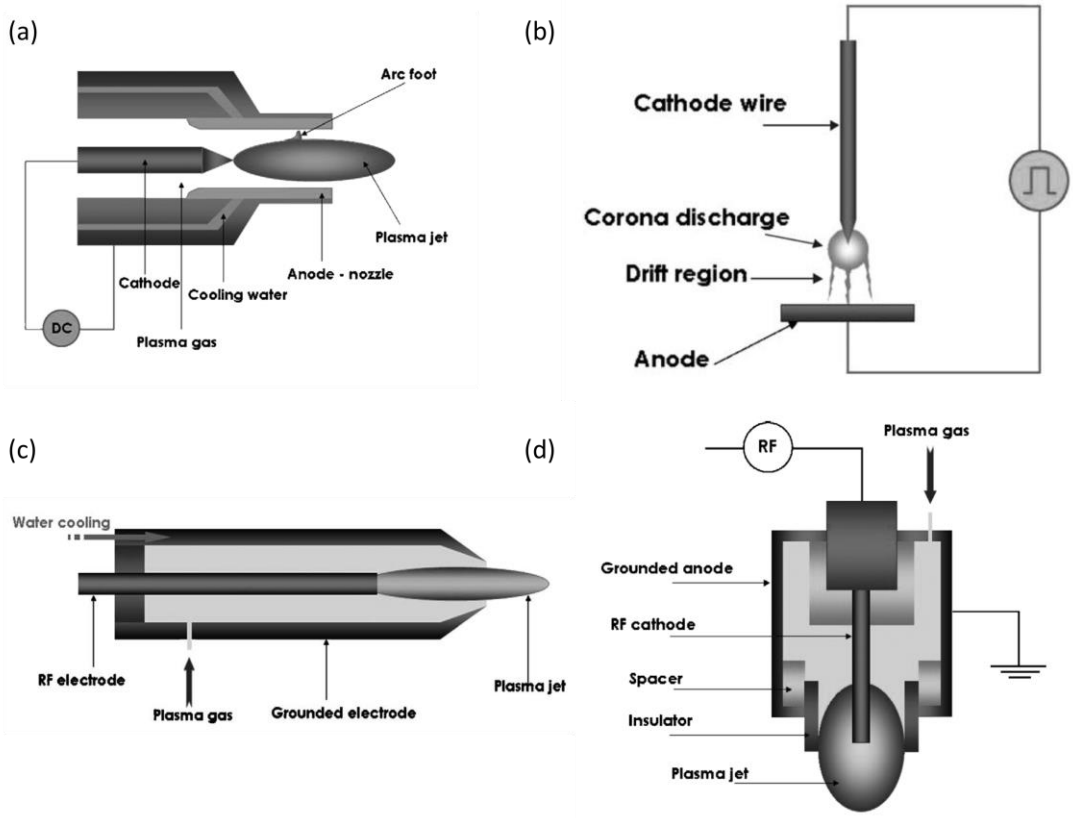

Figure 3.2 Principle structure of (a) an arc plasma torch (b) a corona discharge device (c) an atmospheric pressure plasma jet and (d) a cold plasma torch [134].

The V-shape atmospheric pressure plasma chamber exhibited the capability of improving both the hydrophilicity (e.g. using helium/ethanol mixture working gas) and hydrophobicity (e.g. using helium/tetramethoxysilane mixture working gas). In the works utilizing the V-shape chamber, the precursor was blended with and

introduced into the chamber by helium working gas and a pair of copper conduction wires was placed in the V-shape glass column separately to act as electrodes to create plasma at the tip of the chamber. In this case, the reaction is closer to the idea of plasma polymerization, which means some bonds of the precursor (e.g. C-C, C-H) were broken, turned into free radicals and at the end cross-linked on the surfaces of the substrates.

However, in this project, an APP nozzle was purchased for surface modification of CFs. Therefore, the focus and tasks have turned from designing an APP nozzle into a chamber for APP functionalization.

As mentioned in Chapter 2, for CF-reinforced composites, the interface between CFs and the matrix plays an important role on the performance of mechanical properties. Therefore, when an atmospheric process is utilized to introduce functional groups, it is beneficial to limit the influence from the atmospheric gas and retain the monomer structure of the precursor. Taking these two points into account, a cylindrical Pyrex chamber (details were described in a published paper) was manufactured and combined with an APP nozzle to create a remote atmospheric plasma system. The chamber stands vertically with the nozzle installed at the top, a sample platform

downstream and an AAc vapour inlet, which is 52 mm from the end of the plasma nozzle and 25 mm from the sample platform, on the chamber wall.

This system is categorized as a remote atmospheric plasma system as it not only has a glass chamber to prevent the process from being affected by atmospheric gas but also a distance of 52 mm between the plasma nozzle and precursor vapour inlet to prevent the precursor from monomer fragmentation. However, the diameter and dimension of the chamber have limited the potential for continuous functionalization of large fabric rolls or continuous CFs, which is popular for industrial application.

Thus, another cylindrical Pyrex chamber was prepared for and utilized in this study. Compared to the chamber described above, this chamber aims towards offering the possibility to treat a short bundle of CFs (fixed on the sample platform and shifted via the rails, for purpose of fundamental studies) or continuously a long length of CF bundle (where the CFs are pulled from one side through the chamber for treatment and collected on the opposite side after treatment using a roller feed system). The same concept of preventing the precursor from monomer fragmentation was also considered, thus the distance between the plasma nozzle and the precursor vapour inlet was set at 100 mm, which is almost a twofold increase of that in the previous chamber (52 mm). Since the length of atmospheric pressure plasma glow of argon

(0.6 mm) is different with air (1.2 mm), a certain amount of flexibility (e.g. 10 mm) for the distance between the plasma nozzle and the sample is essential.

To sum up, this chamber was designed to cover ideas including:

1. Flexibility for adjusting the distance between the plasma nozzle and the sample (after measured the atmospheric pressure plasma glow length of argon and air).

2. Reducing the effects of atmospheric gas on the process without using a complex device/design (As keeping the APP process as a simple and rapid method is the main advantage of using it and popular for industrial application).

3. Limiting the monomer fragmentation of the precursor, which retains the structure of the precursor to potentially obtain a more homogeneous surface with a higher atomic percentage of desired functional groups (As this chamber is designed for carrying out an APP surface activation followed by surface grafting, instead of plasma polymerization).

In light of the concept and ideas discussed in this chapter, this Pyrex chamber was designed and then applied in this study. Details and setup will be given and described in the next chapter.

3.2.2 Atmospheric pressure plasma setup

The system designed in this study was built with an atmospheric pressure plasma system and a bespoke chamber, as schematically shown in Figure 3.3. The plasma nozzle (OPENAIR® Plasma System), which was purchased from Plasmatreat GmbH, Germany, is equipped with a DC pulsed plasma source and a plasma nozzle for treatment/activation (Figure 3.4).

The chamber was constructed with a Pyrex column, custom-made by the glassblower in the Department of Chemistry, University of Sheffield. The chamber is 250 mm in length, 50 mm in outer diameter and 46 mm in inner diameter, with a pair of 8 mm Pyrex glass rods in the middle of the glass column to act as rails for the mobile specimen holder, which provides the platform for the atmospheric plasma treatment of the flat specimen (e.g., silicon wafer in this study) or fibers (e.g., CF bundles) for estimating the effects of surface grafting of functional groups. The Pyrex chamber has two holes on top of it, one for the atmospheric plasma nozzle to fit in, which offers surface activation, another one for introducing the precursor (e.g., acrylic acid vapour in this research) for grafting, and a hole at the bottom of it for releasing gases (Figure

3.5). The hole for fitting in the atmospheric pressure plasma nozzle is 28 mm in inner diameter and 32 mm in outer diameter, with a height of 10 mm to offer the availability for adjusting the distance between the sample platform and the plasma nozzle. Another hole on top of the chamber, which was designed for introducing the precursor, is 10 mm in outer diameter with a rippled surface for tube connection. These two holes on top of the chamber are separated by a distance of 100 mm, with a hole in the middle to release gases from the bottom of the chamber. Built by a 4-mm-thick Pyrex, the gas releasing hole, which is 30 mm in outer diameter and 26 mm in inner diameter, is able to be connected with a ventilation system if necessary. The purpose of separating the precursor and plasma nozzle holes is to prevent precursor monomers from fragmentation, which may be caused by the atmospheric pressure plasma. By reducing precursor fragmentation, it is expected to obtain a higher percentage of functional groups from the precursor, which is beneficial for this work and further applications, including continuously functionalization of CFs. By utilizing this bespoke chamber, it not only minimizes the effect of atmospheric gas on the treatment but also promises a rapid process for surface activating and grafting.

(a)

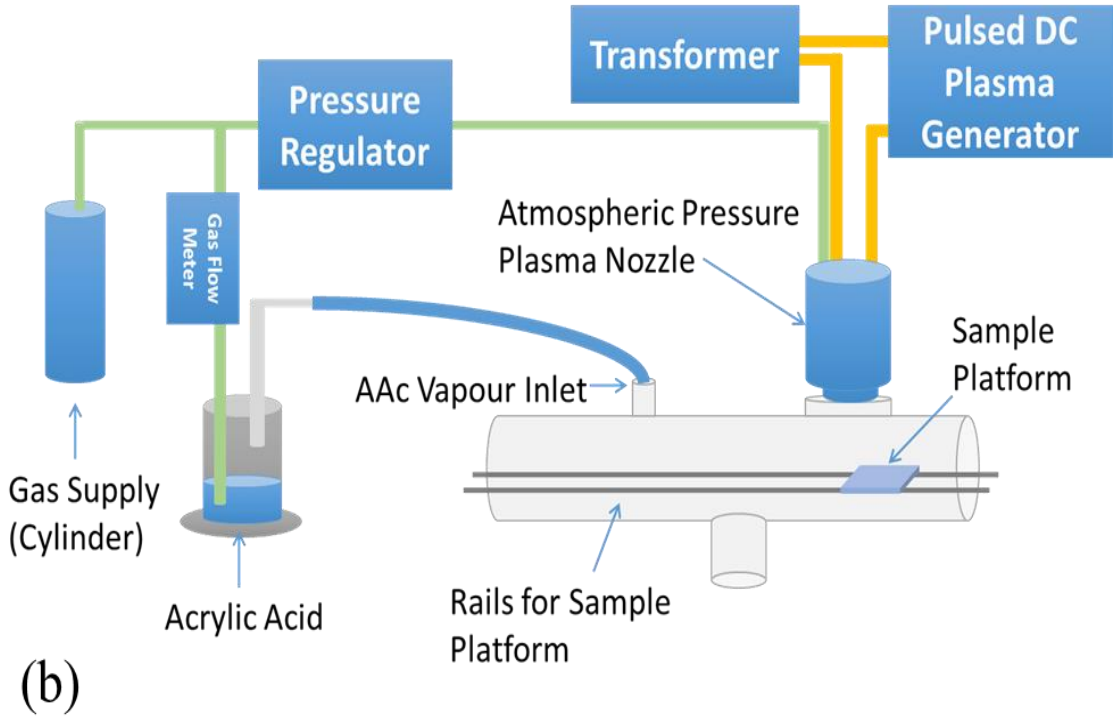

(b)

Figure 3.3 (a) Schematic diagram (b) image of the atmospheric pressure plasma system.

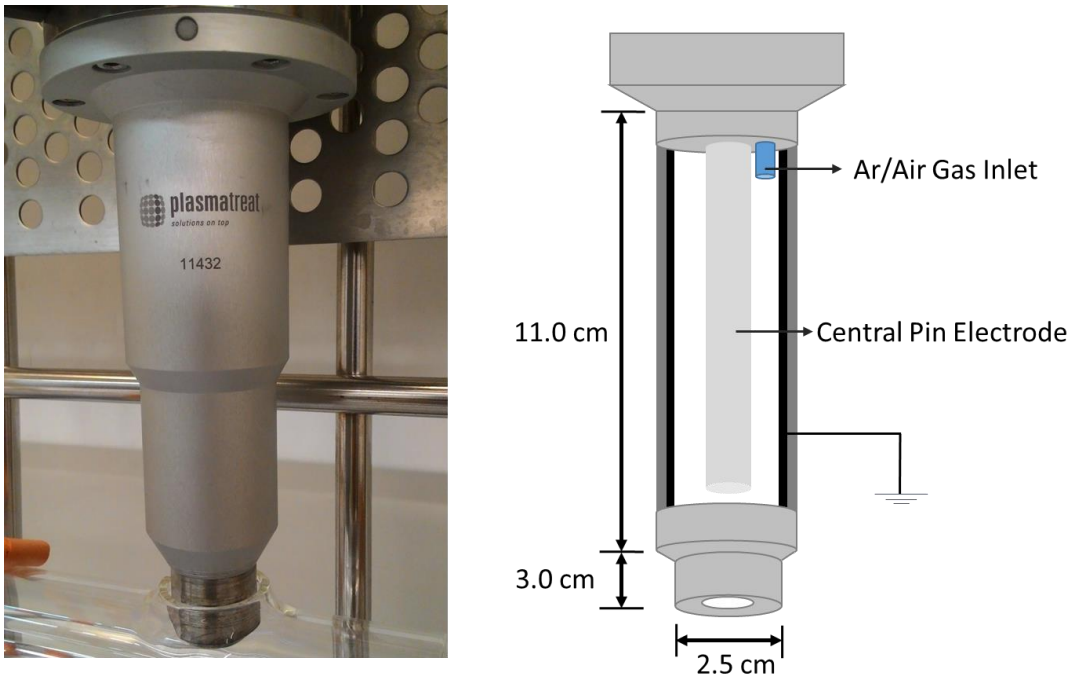

Figure 3.4 Atmospheric pressure plasma nozzle.

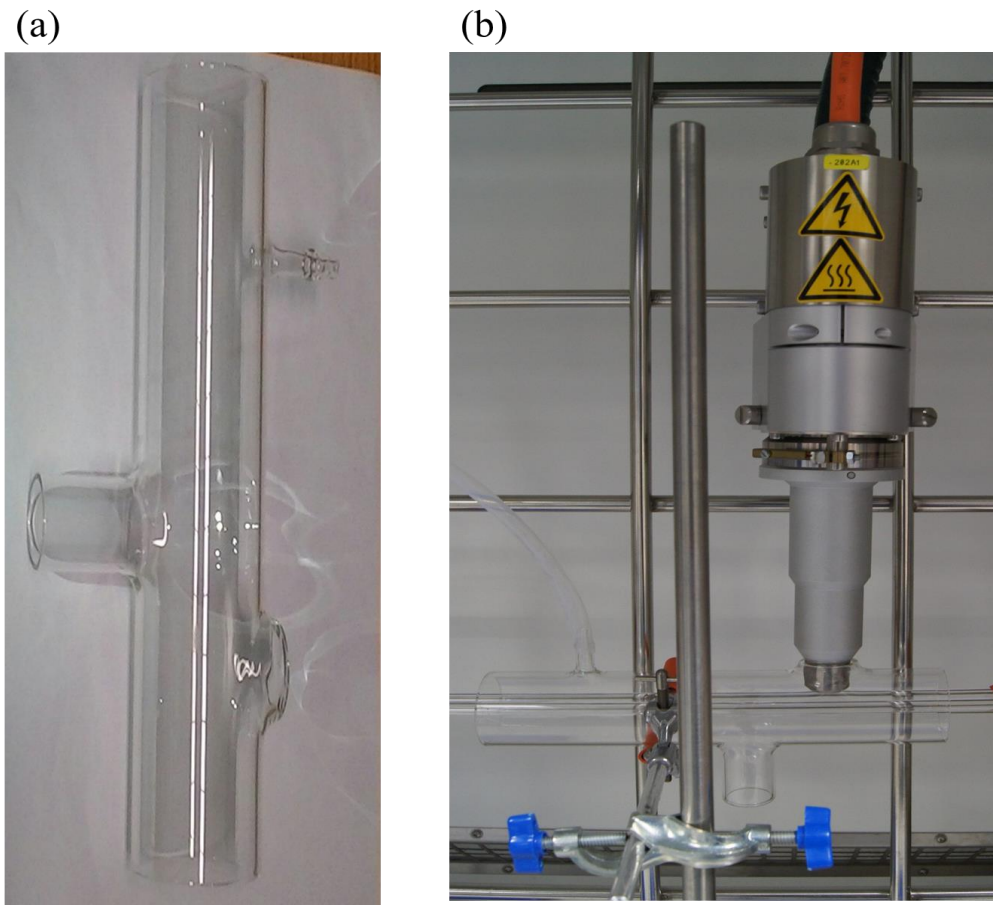

Figure 3.5 Schematic diagrams of (a) the bespoke Pyrex chamber and (b) combination of the atmospheric pressure plasma nozzle and the Pyrex chamber.

3.2.3 Atmospheric pressure plasma functionalization

In this study, samples were first activated by argon (Ar-APP) or air atmospheric pressure plasma (Air-APP) (Figure 3.6) and then exposed to acrylic acid (AAc) vapour for surface grafting by moving the samples downstream to the precursor hole. AAc (Figure 3.7) was applied as precursor in this process and was expected to introduce carboxylic acid functional groups on the specimen surface. Argon or compressed air at a flow rate of 35 standard litres per minute (SLM) was fed into the plasma nozzle as plasma working gas and AAc vapour was introduced by argon (20 SLM) from a bubbler into the reactor chamber as precursor, respectively.

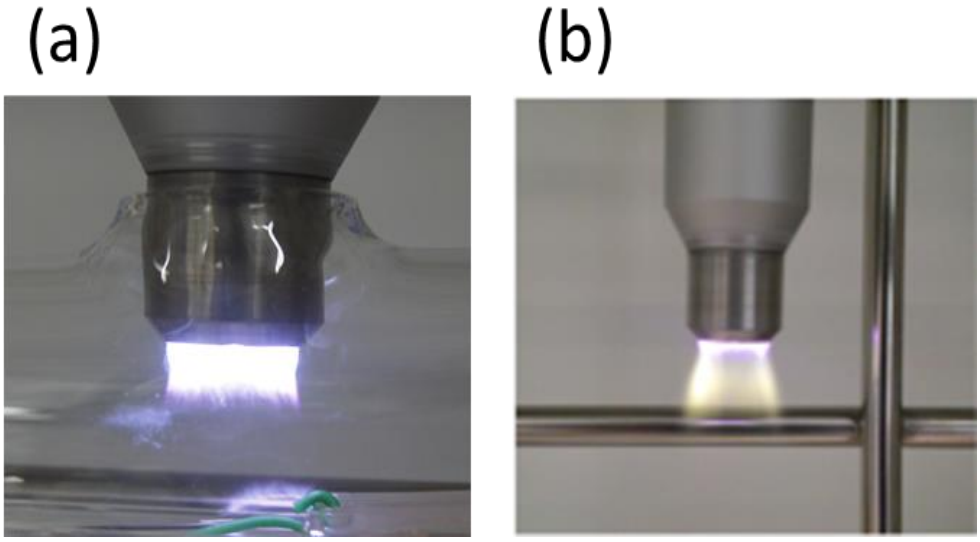

Figure 3.6 Plasma glow of (a) argon and (b) air atmospheric pressure plasmas.

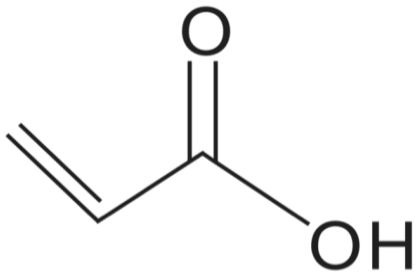

Figure 3.7 Chemical structure of acrylic acid.

The n-type silicon wafers (1 cm^2) were mounted on the mobile specimen holder and placed in the chamber at a distance of 6 mm (Ar-APP) or 12 mm (Air-APP) from the tip of the plasma nozzle.

For the functionalization of CF bundles, two versions (Version-1 and Version-2) of sample platforms were developed. In the Version-1 sample platform, CF bundles (45 mm in length, 3 mm in width and 1 mm in thickness) were fixed on a customized steel frame. As shown in Figure 3.8, one side of the CF bundles (70 mm in length, 3 mm in width and 1 mm in thickness) was fixed on the table by tape and the other side was pulled vertically by a force of 0.014 N to keep the bundles straight before fixing them on the steel frame with a length of 45 mm. The CF bundles, which were fixed on the steel frame, were separated from the original part of the bundles, which were taped on the table. The Version-1 platform (with CF bundles on it) was then mounted on the mobile specimen holder and placed in the chamber at a distance of 6 mm (Ar-APP) from the tip of plasma nozzle. The Version-1 platform offers the advantage of being

easy to transfer the aligned CF bundles to moulds for sample preparation for further mechanical tests. However, mounting CF bundles on the Version-1 platform is time-consuming. Moreover, due to the APP and strong plasma working gas, damage (broken CFs) was observed on the activated CF bundles. Although increasing the distance between the nozzle and CF bundles to 8 mm was able to address this problem, the maximum effective distance between the nozzle and the sample for APP activation is 6 mm, according to the studies on silicon surfaces in this work.

To address these issues, the Version-2 sample platform, which was a cleaned (same protocol as Si-wafer cleaning) slide glass of 75 mm x 25 mm x 1 mm, was utilized in this study. Both sides of the CF bundles (60 mm in length, 11 mm in width and 1 mm in thickness) were taped on the platform without any typical pulling force to keep them strictly aligned, which is beneficial for load bearing under plasma and APP penetration for activating the backside of the bundles on this slide glass (Version-2 platform). The Version-2 platform (with CF bundles on it) was mounted on the mobile specimen holder and placed in the chamber at a distance of 6 mm (Ar-APP) from the tip of the plasma nozzle. Although fiber damage may occur, a larger amount of CF bundles gives a higher flexibility for sample selection for further studies.

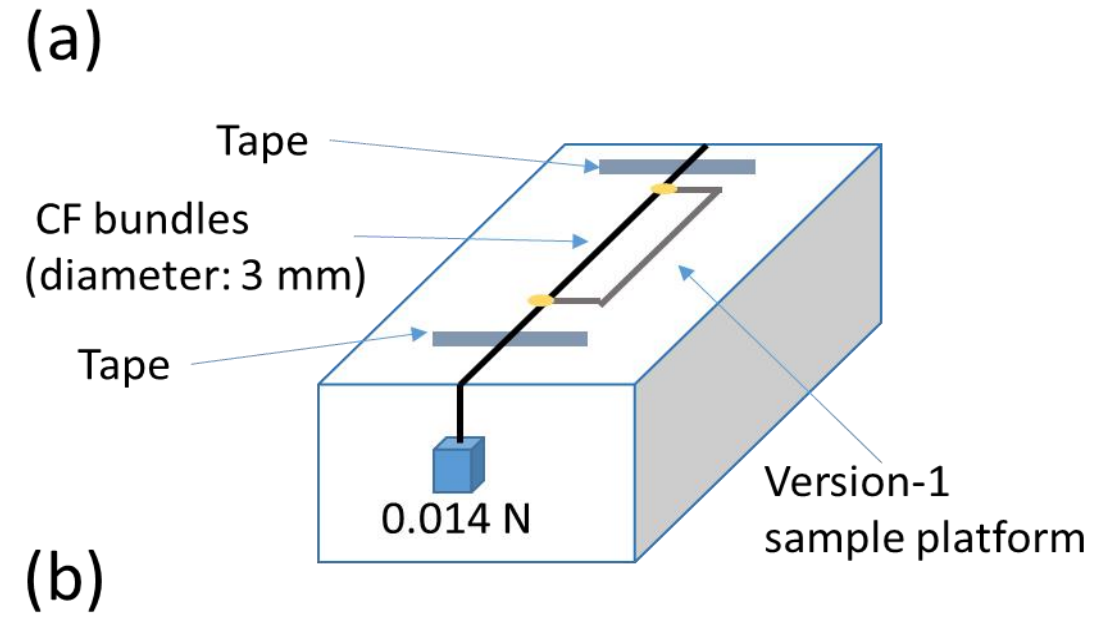

Figure 3.8 (a) Schematic diagram and (b) image of Version-1 sample platform for CF bundles.

As illustrated in Figure 3.9, the silicon wafers or CFs were activated by argon (activating time: 5 or 10 seconds) or air plasma (activating time: 5 seconds) first and subsequently grafted by acrylic acid vapour (grafting time: 1, 3, 5 or 10 minutes) for

immobilizing high-concentration carboxylic acid groups on the surface. For the purpose of comparison, a conventional Ar-APP process using the same OPENAIR® Plasma System nozzle and parameters, however, introducing the AAc precursor gas in direct contact with the plasma glow, was employed to treat silicon specimen for 60 seconds.

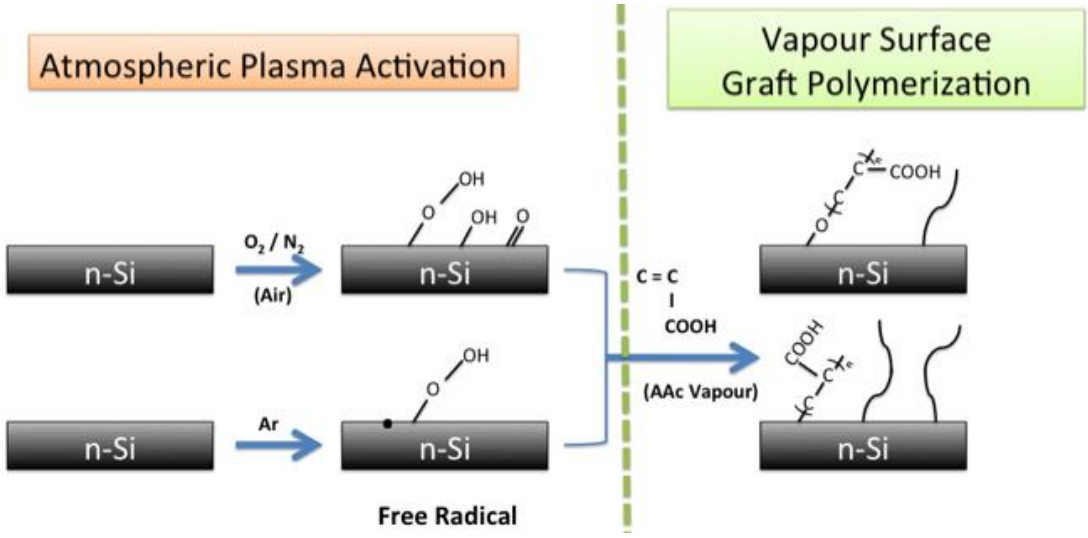

Figure 3.9 Schematic diagram of the APP activation/AAc vapour grafting process developed in this study. Free radicals and peroxide groups were first created on the surface via APP activation, then reacted with AAc vapour to deposit carboxylic acid functional groups on the surface.

3.3 Surface characterisation

Before treating CFs with the APP functionalization developed in this study, flat silicon wafers (n-type) were treated by this process to estimate the effects of the APP on surface properties.

3.3.1 Surface wettability

Prior to XPS analysis, the wettability of the silicon wafers with/without plasma coatings was evaluated with water contact angle (WCA) measurements as a preliminary step to confirm the effect of plasma deposition. A Dino-Lite digital microscope was set up for observing water contact angles (WCAs) (Figure 3.10). Data was collected as the average of 5 readings with the 0.03-ml sessile drop method and calculated by the Dinocapture 2.0 software.

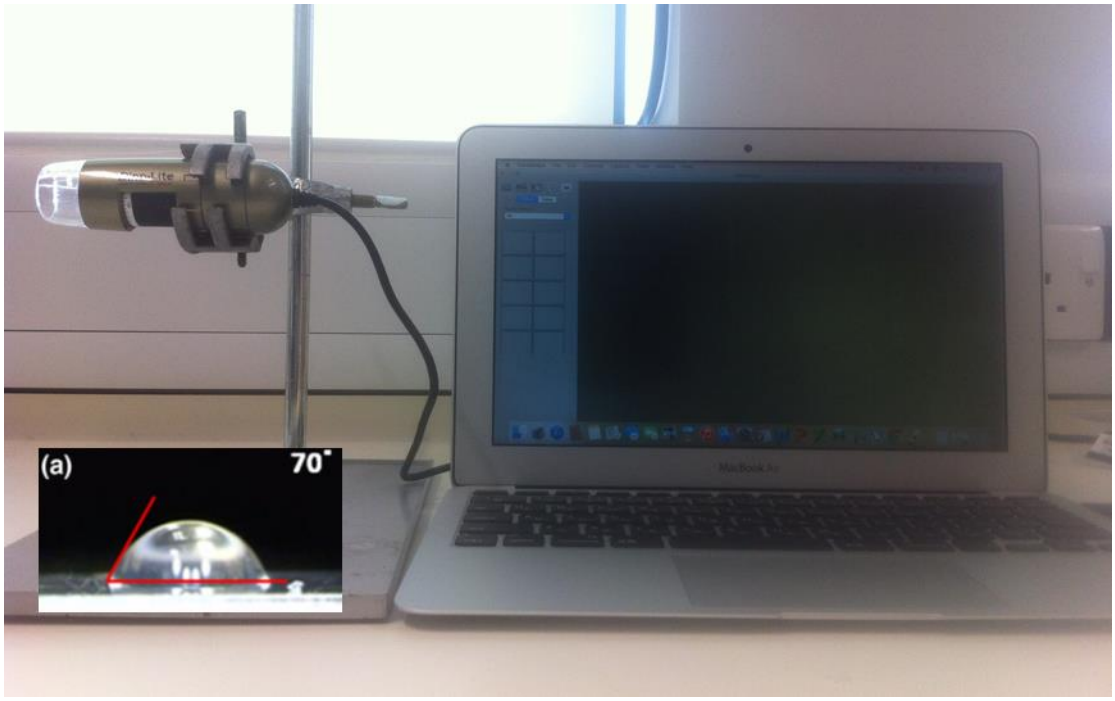

Figure 3.10 Dino-Lite digital microscope for contact angle measurement [96].

3.3.2 Surface stability of functionalized silicon specimens

The WCAs of silicon specimens were recorded 2, 4 and 8 days after treatment. By observing the change of the contact angle of a specimen, the stability of the surface can be examined. A smaller change in the contact angle over time suggests a more stable

surface.

3.3.3 X-ray photoelectron spectroscopy

The chemical composition of the coatings was obtained by XPS using an AXIS Supra or Ultra DLD spectrometer with a monochromatic Al Kα radiation (1486.6 eV) source at a power of 225 W (Supra) or 150 W (Ultra) and a take-off angle of 90 degrees relative to the specimen surface. The X-ray analysis area was 700 μm by 300 μm. All measurements were carried out in the fixed analyzer transmission mode with the pressure of the instrument below $5 \cdot 10^{-9}$ mbar. The spectra of survey scans were recorded over a binding energy range from -5 eV to 1200 eV with an energy resolution of $\Delta E = 1.000$ eV. For measurements of C1s core spectra, a binding energy range from 270 eV to 292 eV with an energy resolution of $\Delta E = 0.100$ eV was employed. The pass energies used for survey scans and high resolution scans were 160 eV and 20 eV, respectively. To prevent the specimen surfaces from being affected, neither an ion/electron neutralizer nor an argon sputtering cleaning process was performed during the measurements. The acquisition time to obtain the C1s core spectra was 5 minutes. The C1s core spectra of the surfaces were fitted using Gaussian-Lorentzian product lineshapes GL(30) via CasaXPS software (version 2.3.16), Shirley background subtraction was utilized and sample charging was considered by referencing all peaks relative to the hydrocarbon peak at 285.0 eV.

Specimens were enclosed in aluminum foils, transported and analyzed by XPS

immediately after preparation to limit their exposure to atmosphere.

Silicon wafer specimens were directly mounted on the sample holder covered with double sided carbon tape.

For CFs analysis, the process of mounting CF samples were initiated by putting a long piece of double sided tape on the sample holder and then a small piece of indium foil in the middle of the tape. The CF samples were then draped across the indium foil and adhered to the exposed sticky tape (on either side of it). All analyses were recorded from the CFs above the indium foil and the direction of the X-ray was parallel to the longitudinal axis of the CFs. In this way, the samples should be electrically isolated to avoid any differential charging, and the signal amount that has not come from the CFs but instead from exposed substrate will be indicated by a strong indium signal in the survey scan.

3.4 Carboxyl derivatization

In this study, XPS was utilized to estimate the present of carboxylic acid functional groups on the APP process modified surface. However, the energy peak at 289.2 eV in the C1s core level presents both COOR/COOH functional groups. Therefore, to further confirm the presence of the 289.2 eV peak that stands for carboxylic acid functional, which is desired in this process, the 2,2,2-trifluoroethanol (TFE) derivatization

technique in conjuction with XPS analysis was employed. TFE reacts only with carboxylic acid groups, thus, promises advantages on the analysis of surfaces that are not amenable to be investigated directly by XPS.

The mechanism of TFE on a carboxylic surface is shown in Figure 3.11. The specimens were fixed on a microscope slide and placed inside a glass jar. TFE (0.9 mL), pyridine (0.4 mL, as catalyst) and di-*tert*-butylcarbodiimide (Di-tBuC, 0.3 mL, as drying agent) were sequentially introduced into the glass jar (below the microscope slide) at 15-min intervals [135].

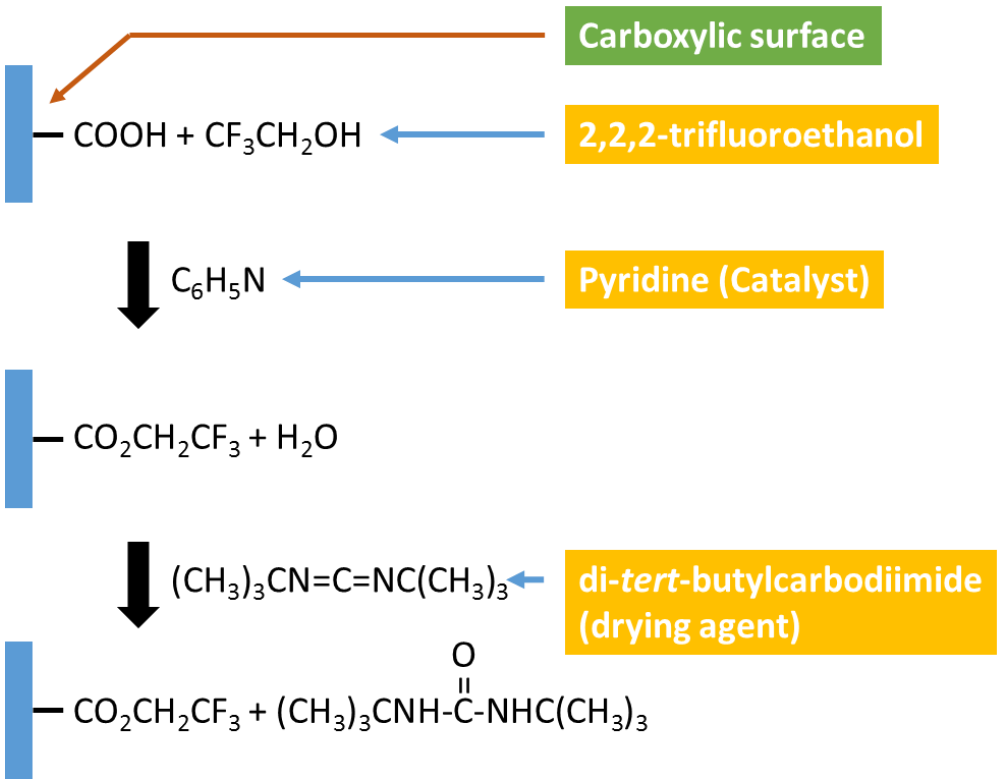

Figure 3.11 TFE derivatization reaction with carboxylic acid groups.

3.5 Design of the healing agent

The design of the ionomer self-healing network in this research was inspired by the concept reported by Hayes et al. [20, 129]. With the participation of the ionomer healing agent, a thermo-induced healing event can be executed.

This research proposed an ionomer healing agent synthesized by end-capping DGEBA with 4-amino-sodium salicylate. The most commonly used DGEBA possesses a high molecular weight of 44000 g/mol, which results in the difficulty for the healing agent to diffuse during the healing event due to an increased viscosity. Jones et al. [136] addressed this issue by using a low-molecular-weight (6100 or 4000 g/mol) DGEBA to prepare the healing agent. However, the DGEBA with a molecular weight of 6100 or 4000 g/mol has been discontinued from the product line. Therefore, DGEBA with a molecular weight of around 1075 g/mol was utilized in this work.

This low-molecular-weight DGEBA-based ionomer healing agent was designed to be blended into LY 5052 epoxy resin, which acts as the matrix for the self-healing composite. In the cured epoxy resin, the ionomer healing agents bond with the polymer network via hydrogen bonds or with each other due to ion agglomeration, which creates a higher molecular size of the healing agent and further reduces the impact on the mechanical properties of the epoxy resin matrix.

When fracture or debonding occurs, the healing event can be triggered by raising the

temperature, which results in uncoupling the ionomer healing agents from the rigid epoxy resin network and each other, then diffusing and migrating to the fracture or debonding site, finally reacting with each other or functional groups on the fiber surface, for repairing fracture or debonding, respectively.

The feature of the ionomer healing agent is that it assembles reversibly so that the diffusion of a low-molecular-weight healing agent during healing event is more efficient, but for the stable healed resin it reassembles to a higher molecular weight and ensures molecular entanglement across the crack or debonding.

3.6 Synthesis of the ionomer healing agent

The healing agent designed in this study was prepared by end-capping DGEBA with 4-amino-sodium salicylate (Figure 3.12). The concept for designing this ionomer healing agent has been described in Chapter 3.5 and the process for the ionomer healing agent synthesis was inspired from studies of Jones et al. [136, 137]. The DGEBA was blended with the 4-amino-sodium salicylate in a 1:2 stoichiometric formulation and ground into fine powder using mortar and pestle. The mixture was then placed in a vacuum oven at 130°C for 45 minutes to react and grinded into fine powder again after reaction.

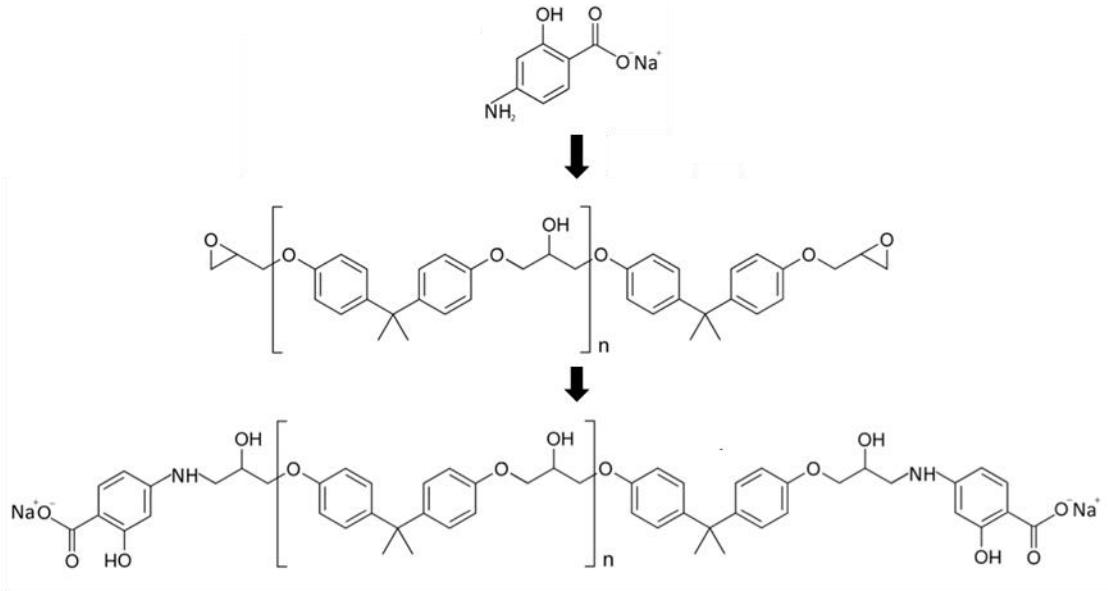

Figure 3.12 Preparation of ionomer: 4-amino-sodium salicylate end-capped DGEBA [137].

3.7 Sample preparation for testing

3.7.1 Preparation of epoxy resin samples

To prepare unmodified epoxy samples, Araldite LY 5052 resin was blended with Aradur 5052 hardener to a 100:38 formulation. The blended resin was degased for 15 minutes in a rotary evaporator at 23°C, then cast into silicone moulds for curing at 23°C for 1 day and post-cured for 4 hours at 100°C.

3.7.2 Preparation of ionomer-modified epoxy resin samples

For the ionomer-modified specimens, the healing agent (ionomer-modified DGEBA) was dissolved in Araldite LY 5052 resin, which was prepared by the process described

in Chapter 3.7.1, at a concentration of 7.5 wt% to maintain complete miscibility of the ionomer healing agent in the Araldite LY 5052. The mixture was heated in an oil bath (Figure 3.13) and stirred at 130°C for 3 hours, then removed from the oil bath and cooled down to room temperature. After being degassed for 30 minutes in a rotary evaporator, the ionomer-modified Araldite LY 5052 resin was blended with Aradur 5052 hardener to a 100:38 formulation.

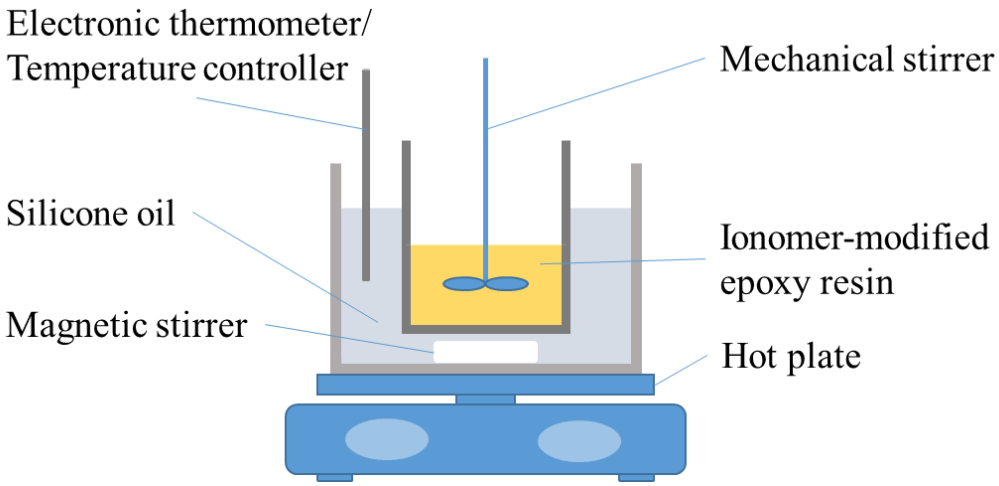

Figure 3.13 Schematic diagram of the experimental setup for preparing ionomer-modified epoxy resin.

3.8 Single-edge notched beam test

Before being applied as the matrix for the self-reassemble CF composite, the healing efficiency of the ionomer system, Araldite LY 5052 resin containing 4-amino-sodium salicylate end-capped DGEBA, was studied using a modified single-edge notched bending (SENB) test reported by Ma et al. [138]. Specimens (virgin and ionomer

modified) were prepared basing on ISO 13586 standard in a size of 11.0 mm (width), 4.5 mm (thickness) and 68.0 mm (overall length), and a pre-crack was made by lightly tapping a razor blade in each sample.

The ISO 13586 standard for preparing a conventional SENB specimen suggests manufacturing a notch on the specimen, then creating a pre-crack across the root of the notch by tapping a fresh razor blade into it. Compared to the conventional SENB specimen (Figure 3.14), the modified specimen does not require manufacturing a notch. This addresses the concern that the remaining width of the SENB specimen after notch preparation (which takes around 3 mm in this case) is not sufficient to accommodate an instantly sharp pre-crack initiated by the tapping.

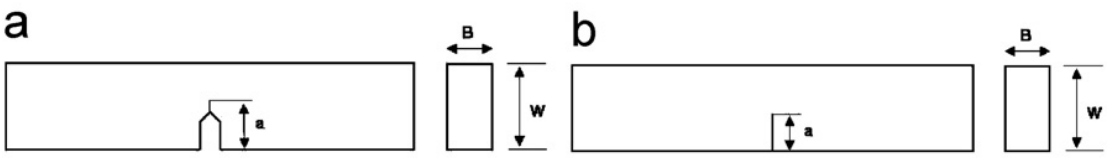

Figure 3.14 Geometry of the (a) conventional single edge-notch bending specimen (b) modified single edge-notch bending specimen.

Specimens were mounted on the platform of a three-point bending machine, with a span of 44 mm, and loaded to failure by a Lloyd universal testing machine using a 500-N static load cell. The fractured surfaces of the tested specimens were placed and gently clamped together, then put into an oven at 120 °C for 2 h to trigger and perform healing

(1st healing event). The specimen after the 1st healing event was then loaded to failure again using the method described above and the failure load (N) was recorded. This healing process was employed on the same specimen one more time (2nd healing event), then loaded to failure again. Healing efficiency (%) was calculated by dividing the failure load of a sample after the 1st or 2nd healing event to that before healing.

3.9 Simulation of potential interface healing using ionomer adsorption

The mechanism of an ionomer healing system has been described in Chapter 2. Based on the ionomer mechanism, the approach of designing self-healable composite materials in this study is to develop an ionomer healing agent by end-capping DGEBA with 4-amino-sodium salicylate, which introduces sodium carboxylate functional groups on the two end groups of DGEBA. These sodium carboxylate functional groups can ionically react not only with each other for repairing crack(s) inside the matrix but also with carboxylic acid functional groups from APP/AAc-grafted CFs to repair debonding and heal interfaces between the matrix and the fibers.

Therefore, after examining the capability of thermo-induced self-healing on ionomer-modified epoxy resin, the interaction of functional groups between the ionomer healing agent and the APP/AAc-grafted surface is also an important topic to investigate.

As the sodium carboxylate functional groups are located on the 4-amino-sodium salicylate end-capped end groups, a neat or Ar-APP/AAc-grafted silicon specimen was immersed in 7.5 wt% of 4-amino-sodium salicylate in isopropanol. After a 5-minute immersion, the silicon surface was washed three times with isopropanol, dried at room temperature and then analysed by XPS. By observing the presence of sodium and nitrogen, which can only be obtained from the ionomer healing agent, the effects of functional groups reactions between the APP- functionalized surface and the ionomer healing agent can be evaluated. The result of the evaluation can further demonstrate the potential of applying the self-healing system and the APP process to the preparation of self-healing composites.

After preliminary results had observed the performance of functional groups reaction, the same immersion procedure was utilized on: (a) neat or Ar-APP/AAc-grafted silicon specimens immersed in isopropanol (as control to estimate the effects of isopropanol on this experiment); (b) neat or Ar-APP/AAc-grafted silicon specimens immersed in 7.5 wt% of ionomer healing agent in isopropanol; and (c) neat or Ar-APP/AAc-grafted

CF bundles immersed in 7.5 wt% of ionomer healing agent in isopropanol. Samples were then analysed via XPS to estimate the functional groups interaction between the functionalized surfaces (carboxylic acid groups) and the ionomer healing agents (sodium carboxylate groups).

3.10 Interfacial healing performance

To further examine the interfacial healing performance, APP-functionalized CF bundles were embedded into ionomer-modified epoxy resin to prepare self-healing composite samples (shown in Figure 3.15). The sample was in a size of 10 mm (width), 5 mm (thickness) and 35 mm (overall length) and with a transverse bundle of CFs (3 mm in width) in the middle of it. It was loaded to failure to create a debonding along the interface between the ionomer-modified matrix and the APP-functionalized CF bundle. The fracture surface (debonding site) of a tested sample was placed and gently clamped together, then put into an oven at 120°C for 2 h to trigger and perform interfacial healing (1^{st} healing event). The sample was loaded to failure again and the same healing process was performed (2^{nd} healing event). The interface between the APP-functionalized CF bundle and the ionomer-modified epoxy resin matrix was observed by a Dino-Lite digital microscope before and after every healing event.

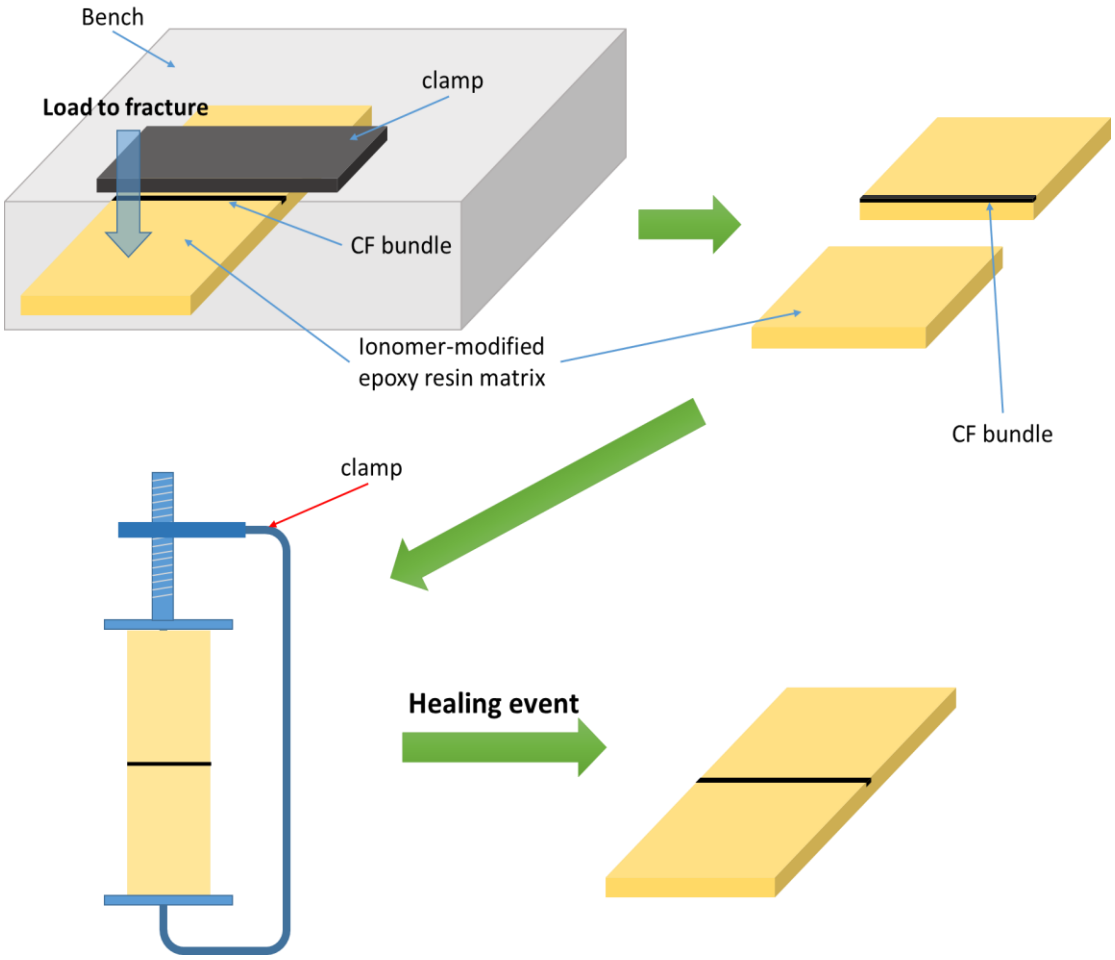

Figure 3.15 Diagram of the observation of interfacial healing performance.

Chapter 4 Results

4.1 Wettability

4.1.1 Introduction

The wettability was assessed by recording the contact angle with water to preliminarily indicate the effects of the functionalization. WCA measurements of specimens treated with different parameters, which are neat silicon wafer (control), silicon wafer with argon or air plasma activation only, and silicon wafer with argon or air plasma activation followed by AAc vapour grafting, were monitored. Table 4.1 and 4.2 illustrate the parameters of specimen treatments and the abbreviations of them.

Table 4.1 Parameters of argon atmospheric pressure plasma treatments.

Abbreviation	Argon plasma treatment time	Acrylic acid vapour grafting time
CTRL	0 second	0 minute
Ar-APP	5 seconds	0 minute
Ar-1	5 seconds	1 minute
Ar-3	5 seconds	3 minutes
Ar-5	5 seconds	5 minutes
Ar-10	5 seconds	10 minutes
Ar-APP-10	10 seconds	0 minute
Ar-1-10	10 seconds	1 minute
Ar-3-10	10 seconds	3 minutes
Ar-5-10	10 seconds	5 minutes
Ar-10-10	10 seconds	10 minutes

Table 4.2 Parameters of air atmospheric pressure plasma treatments.

Abbreviation	Air plasma treatment time	Acrylic acid vapour grafting time
Air-APP	5 seconds	0 minute
Air-1	5 seconds	1 minute
Air-3	5 seconds	3 minutes
Air-5	5 seconds	5 minutes
Air-10	5 seconds	10 minutes

4.1.2 Surface wettability of silicon specimens

The images presented in Figure 4.1 exhibit an observable difference only between the neat silicon surface and the APP/AAc-grafted surface. However, a significant change of WCA after plasma activation and AAc vapour grafting can be observed in Figure 4.2. The silicon surfaces became more hydrophilic after atmospheric pressure plasma activation. The APP-activated silicon surface was found to be more hydrophobic after AAc-grafting, which preliminarily confirmed the effects of the functionalization.

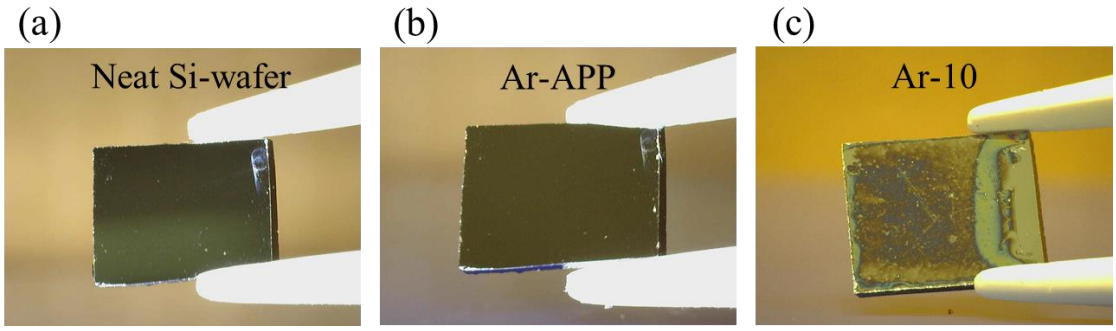

Figure 4.1 Images of silicon surfaces (a) neat (b) activated by a 5-second argon plasma (c) activated by a 5-second argon plasma with 10-minute AAc-grafted (samples are 10 mm x 10 mm).

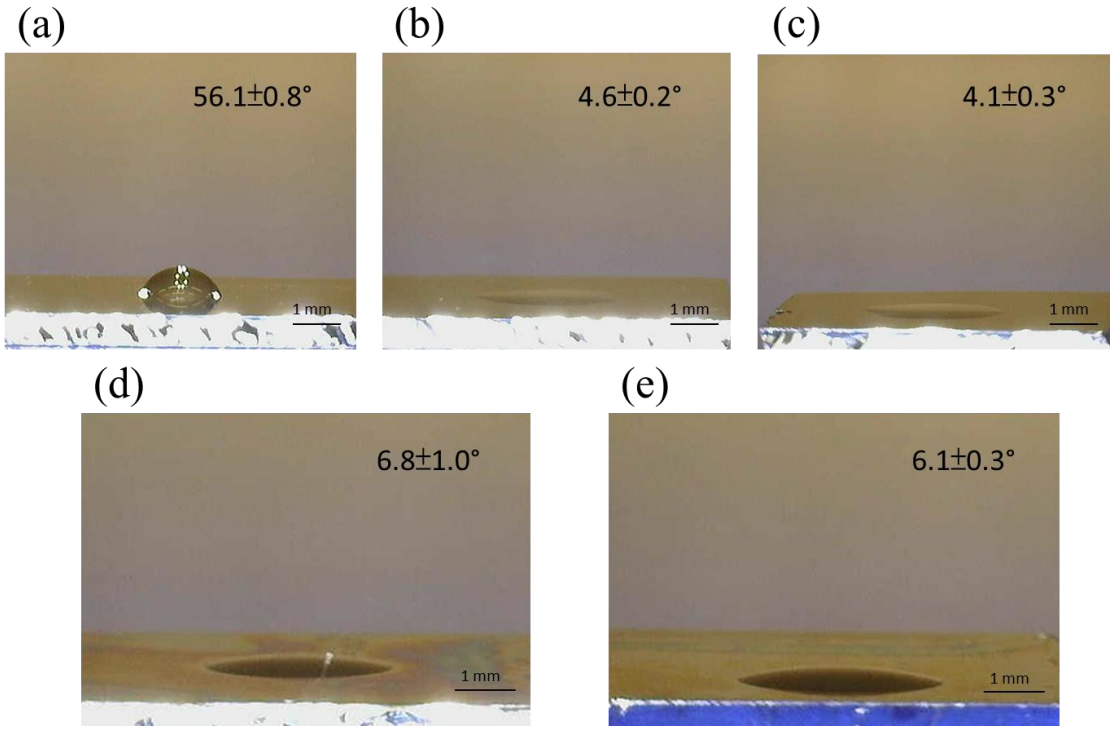

Figure 4.2 Images of WCA on silicon wafers (a) neat (b) 5-second argon plasma activated (c) 10-second argon plasma activated (d) 5-second argon plasma activated with 10-minute AAc-grafted (e) 10-second argon plasma activated with 10-minute AAc-grafted.

To further estimate the effects of plasma working gas, plasma treatment and AAc grafting time on the surface wettability of the silicon surface, more results were collected and illustrated for comparison.

From Table 4.3, it can be seen that the WCA of the silicon wafers dropped from 56.1± 0.8° (neat) to 4.6±0.2° after a 5-second argon plasma activation, then rose to 10.5±0.4°, 10.8±0.6°, 9.5±3.4° or 6.8±1.0° after AAc vapour grafting for 1, 3, 5 or 10 minutes, respectively.

Table 4.3 Summary of WCA measurement of Ar-APP (5s) and AAc grafted silicon specimens.

Sample	CTRL	Ar-APP	Ar-APP activation (5s)/AAc grafting			
			Ar-1	Ar-3	Ar-5	Ar-10
WCA (degrees)	56.1±0.8	4.6±0.2	10.5±0.4	10.8±0.6	9.5±3.4	6.8±1.0

Table 4.4 shows that the WCA of the silicon wafers decreased from 56.1±0.8 degrees (neat) to 4.1±0.3° degrees after a 10-second argon plasma activation and increased to 5.4±1.0°, 6.9±0.8°, 4.8±0.3° or 6.1±0.3° degrees after AAc vapour grafting for 1, 3, 5 or 10 minutes, respectively.

Table 4.4 Summary of WCA measurement of Ar-APP (10s) and AAc grafted silicon specimens.

Sample	CTRL	Ar-APP-10	Ar-APP activation (10s)/AAc grafting			
			Ar-1-10	Ar-3-10	Ar-5-10	Ar-10-10
WCA (degrees)	56.1±0.8	4.1±0.3	5.4±1.0	6.9±0.8	4.8±0.3	6.1±0.3

As for silicon wafers activated by a 5-second air plasma, the WCA dropped from 56.1 ±0.8 degrees (neat) to 8.2±0.2 degrees after a 5-second air plasma activation and elevated to 13.3±1.4, 13.7.±1.9, 14.5±0.7 or 16.1±0.2 degrees after AAc vapour grafting for 1, 3, 5 or 10 minutes, respectively (Table 4.5).

Table 4.5 Summary of WCA measurement of Air-APP (5s) and AAc grafted silicon specimens.

Sample	CTRL	Air-APP	Air-APP activation (5s)/AAc grafting			
			Air-1	Air-3	Air-5	Air-10
WCA (degrees)	56.1±0.8	8.2±0.2	13.3±1.4	13.7±1.9	14.5±0.7	16.1±0.2

4.1.3 Surface stability of functionalized silicon specimens

The WCAs of silicon specimens were recorded 2, 4 and 8 days after the treatments. By observing the change of contact angle of a specimen, the stability of the surface can be examined.

The contact angles with water from silicon specimen treated with different parameters are illustrated in Table 4.6. While the neat silicon surface exhibited a contact angle of 56.1±0.8°, the WCA changed from 4.6±0.2° to 11.5±0.4°, then to 10.5±0.6° and to 20.9±1.2° 2, 4 and 8 days after Ar-APP activation, respectively. Similar results were observed on the Air-APP activated silicon surface, as the WCA rose from 8.2±0.2° (Day 0) to 14.0±0.9° (Day 2), 14.6±1.0° (Day 4) and 21.3±0.6° (Day 8). The wettability change of the Ar-APP activated/AAc vapour grafted silicon surface with time was also monitored, which showed an increase of WCA from 6.8±1.0° (Day 0) to 16.4±1.9° (Day 2), 19.1±1.7° (Day 4) and 22.2±1.7° (Day 8). For silicon treated by Air-APP activation/AAc vapour grafting, its WCA altered from 16.1±0.2° (Day 0) to 21.8±1.8° (Day 2), 30.4±2.3° (Day 4) and 26.6±1.3° (Day 8).

Table 4.6 WCAs of silicon specimens after different APP treatments.

APP parameters	Time After APP Treatment (Day)				Decay of Hydrophlicity*
	0	2	4	8	
Ar-APP	4.6±0.2°	11.5±0.4°	10.5±0.6°	20.9±1.2°	16.3°
Ar-10	6.8±1.0°	16.4±1.9°	19.1±1.7°	22.2±1.7°	15.4°
Air-APP	8.2±0.2°	14.0±0.9°	14.6±1.0°	21.3±0.6°	13.1°
Air-10	16.1±0.2°	21.8±1.8°	30.4±2.3°	26.6±1.3°	10.5°

*8 days after APP treatment.

4.2 X-ray photoelectron spectroscopy

4.2.1 Introduction

In this study, XPS was utilised to identify the presence of carboxylic acid functional groups on the surface, which further indicates the effects of the functionalization. The peak at the binding energy of 289.2 eV was used to determine the contribution of the carboxylic acid groups deposited onto the surface because it not only fits into -COOH components in the C1s spectrum of poly-AAc [139] but also was absent in the C1s spectrum of the untreated silicon wafer.

The intensity of the 289.2 eV peak in the C1s core level spectrum of silicon specimen treated with different parameters was summarized and compared in Table 4.7.

Table 4.7 Summary of surface carboxylic acid functional groups on silicon wafers modified by APP or AAc grafting (XPS: C1s 289.2 eV).

Parameter		Atomic percentage of carboxylic acid groups (%)
CTRL (untreated) (Figure 4.3)		0
Ar- or Air-APP Activation (Figures 4.4 and 4.5)		0
Ar-APP activation (5s)/ AAc grafting (Figure 4.6)	Ar-1	3.65
	Ar-3	13.89
	Ar-5	16.88
	Ar-10	19.72
Ar-APP activation (10s)/ AAc grafting (Figure 4.7)	Ar-1-10	8.75
	Ar-3-10	17.14
	Ar-5-10	17.33
	Ar-10-10	16.33
Air-APP activation (5s)/ AAc grafting (Figure 4.8)	Air-1	15.64
	Air-3	18.30
	Air-5	17.91
	Air-10	20.30
Conventional Ar-APP	Ar-60s-Mix	13.36

4.2.2 Argon atmospheric pressure plasma activated silicon surfaces

From the untreated silicon wafer surface, there was no retention of carboxylic acid groups as no peak at 289.2 eV was detected (Figure 4.3). After a 5-second (Figure 4.4) or 10-second (Figure 4.5) Ar-APP activation, similar to the neat silicon wafer, oxygen,

silicon and a small percent of carbon were identified on the surfaces. Compared to the neat silicon surface, peak intensities at 285.0 eV and 286.7 eV were similar after a 5-second argon plasma activation (86.29% and 13.71%, respectively), but altered after a 10-second argon plasma activation (75.79% and 24.21%, respectively). No peak at 289.2 eV was observed after Ar-APP activation.

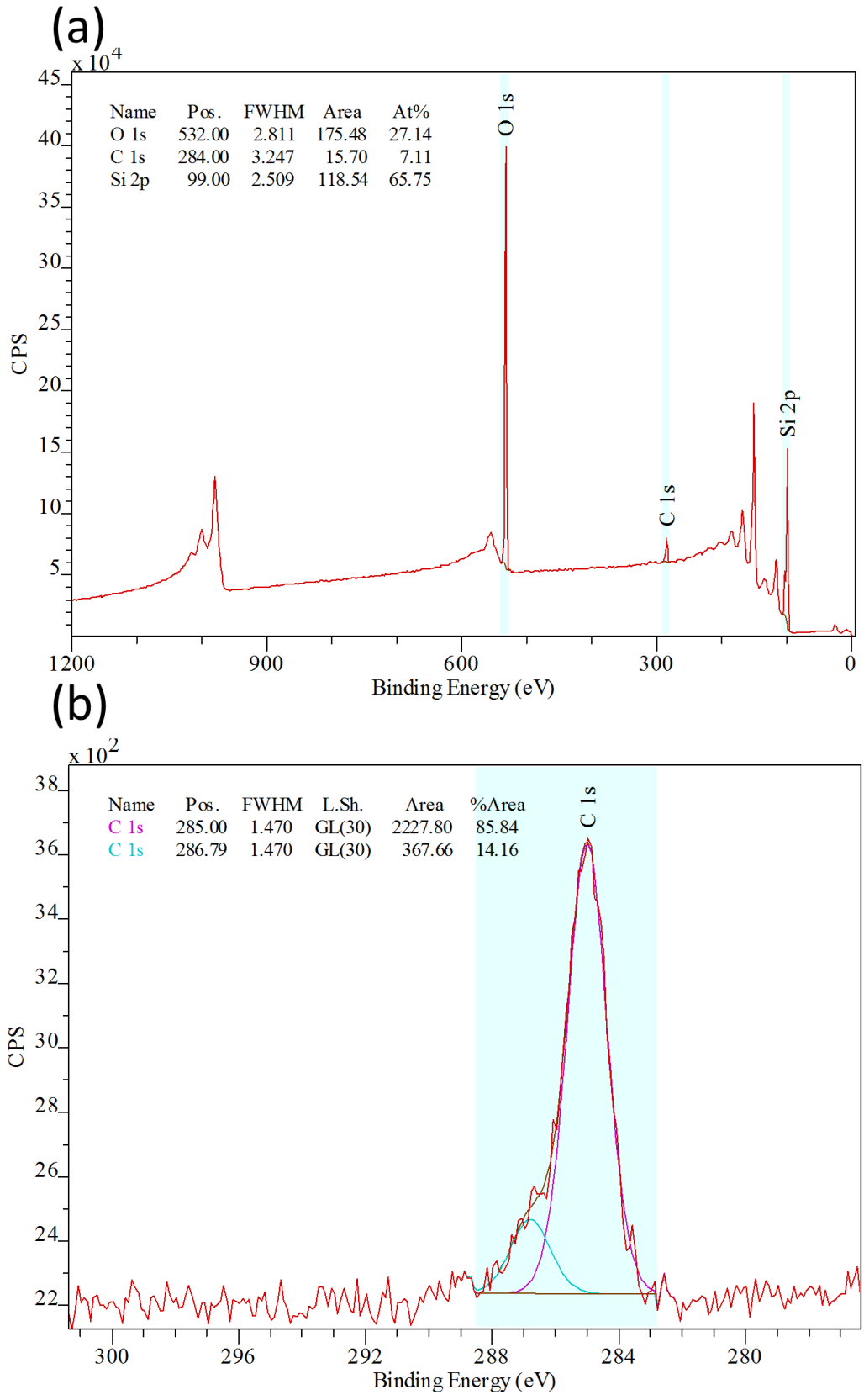

Figure 4.3 XPS survey scan (a) and C1s core level spectrum (b) from a neat silicon wafer surface.

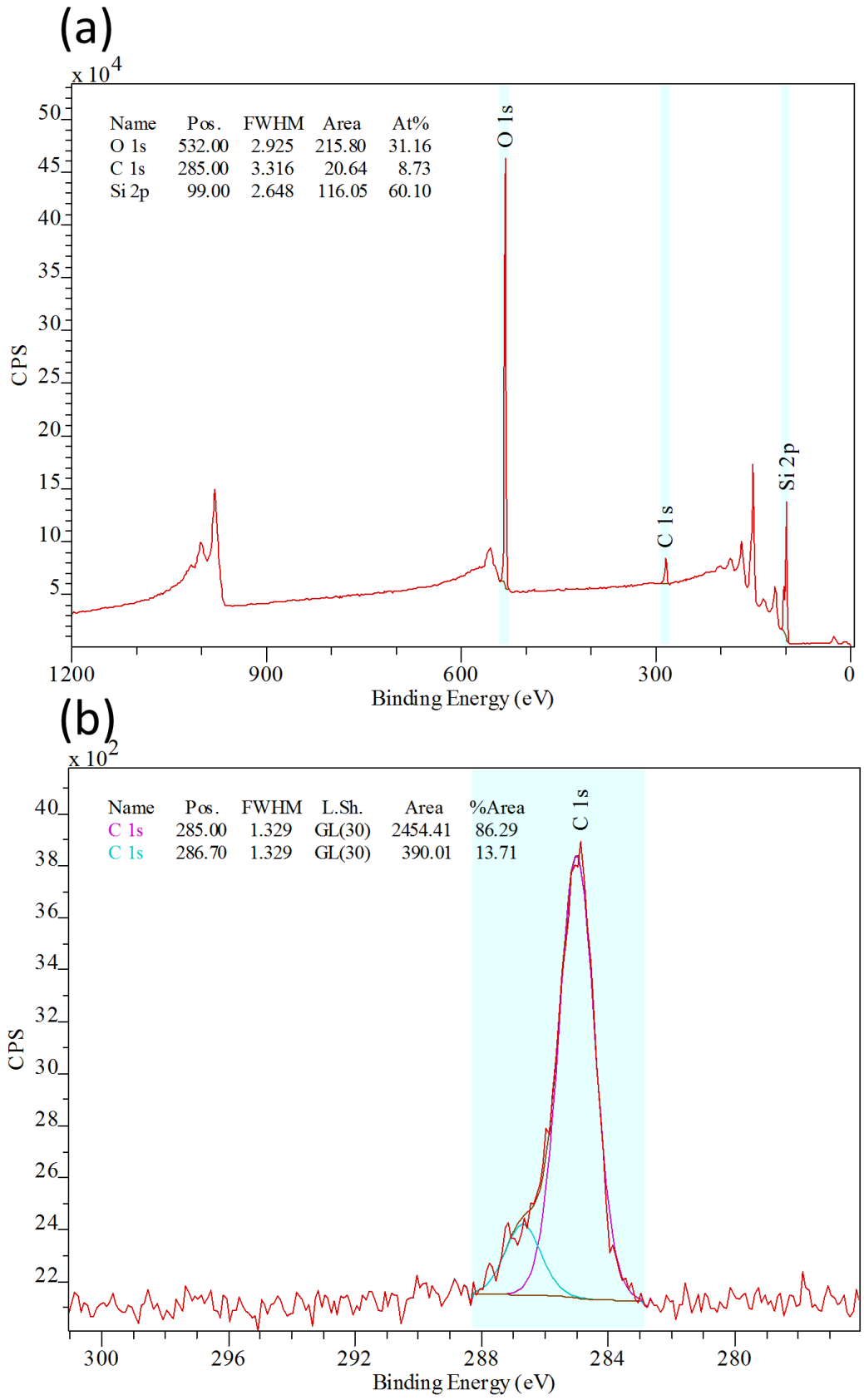

Figure 4.4 XPS survey scan (a) and C1s core level spectrum (b) from a 5-second Ar-APP activated silicon wafer surface.

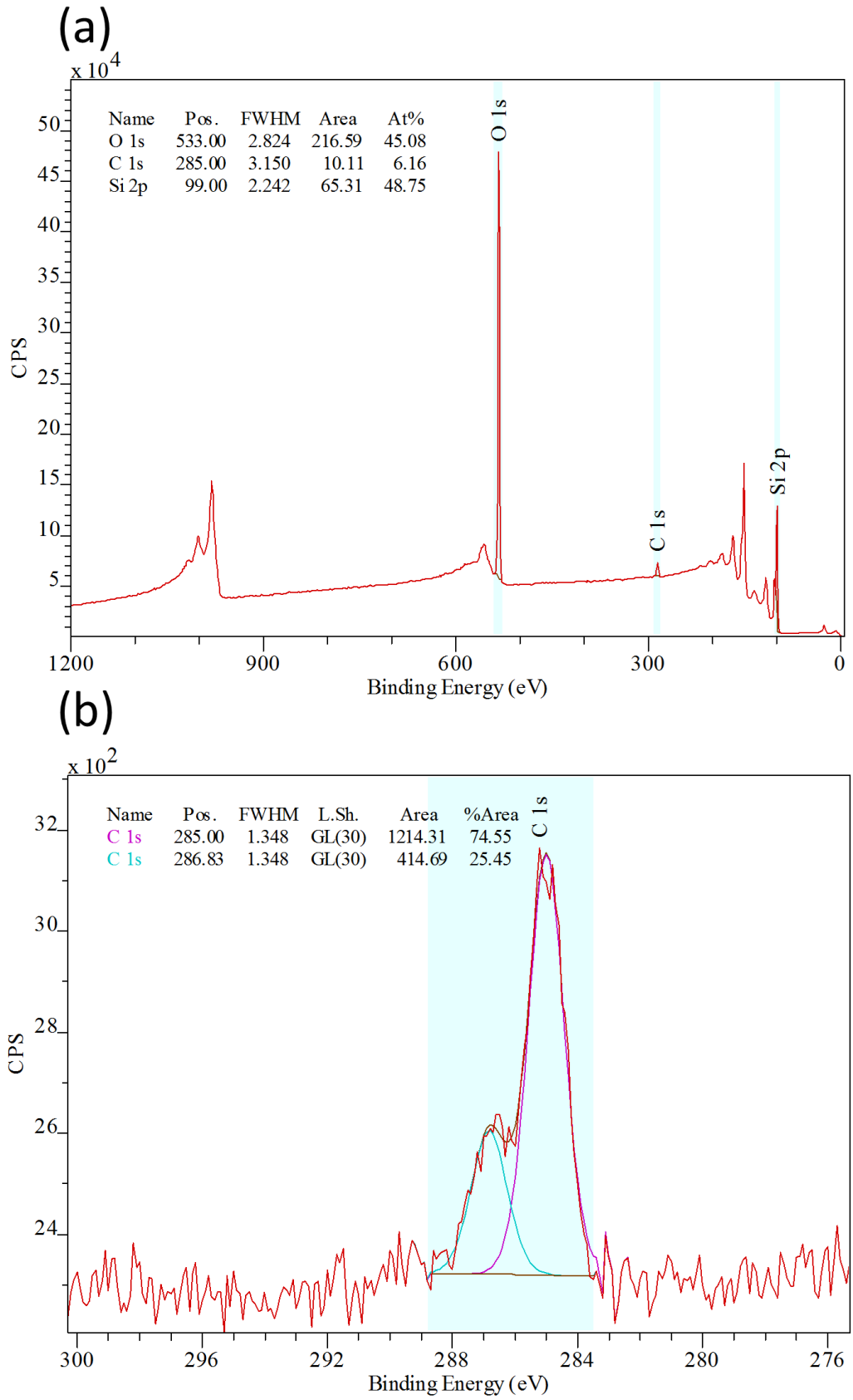

Figure 4.5 XPS survey scan (a) and C1s core level spectrum (b) from a 10-second Ar-APP activated silicon wafer surface.

For the 5-second Ar-APP activated silicon, after the subsequent AAc vapour grafting, the peak intensity at 289.2 eV increased from 0% to 3.65% (1 min grafting), 13.89% (3 min grafting), 16.88% (5 min grafting) and 19.72% (10 min grafting) (Figure 4.6).

(a)

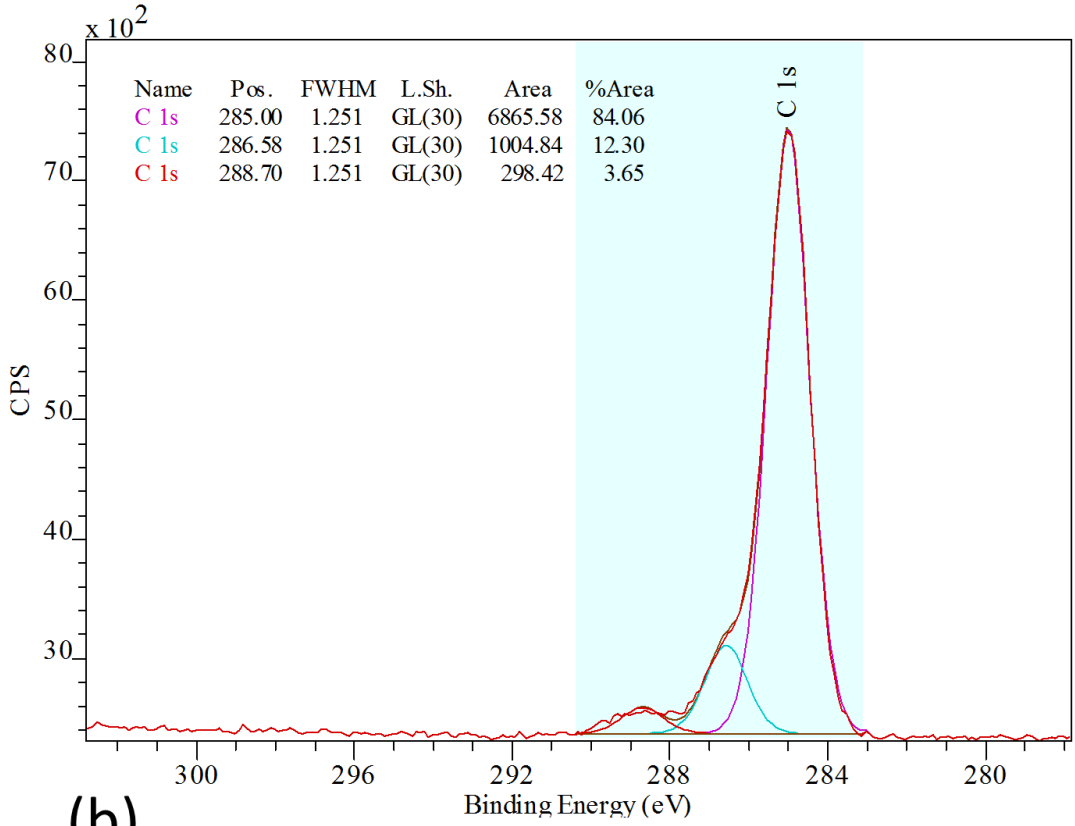
x 10^2
Name Pos. FWHM L.Sh. Area %Area
C 1s 285.00 1.251 GL(30) 6865.58 84.06
C 1s 286.58 1.251 GL(30) 1004.84 12.30
C 1s 288.70 1.251 GL(30) 298.42 3.65
C 1s
CPS
Binding Energy (eV)

(b)

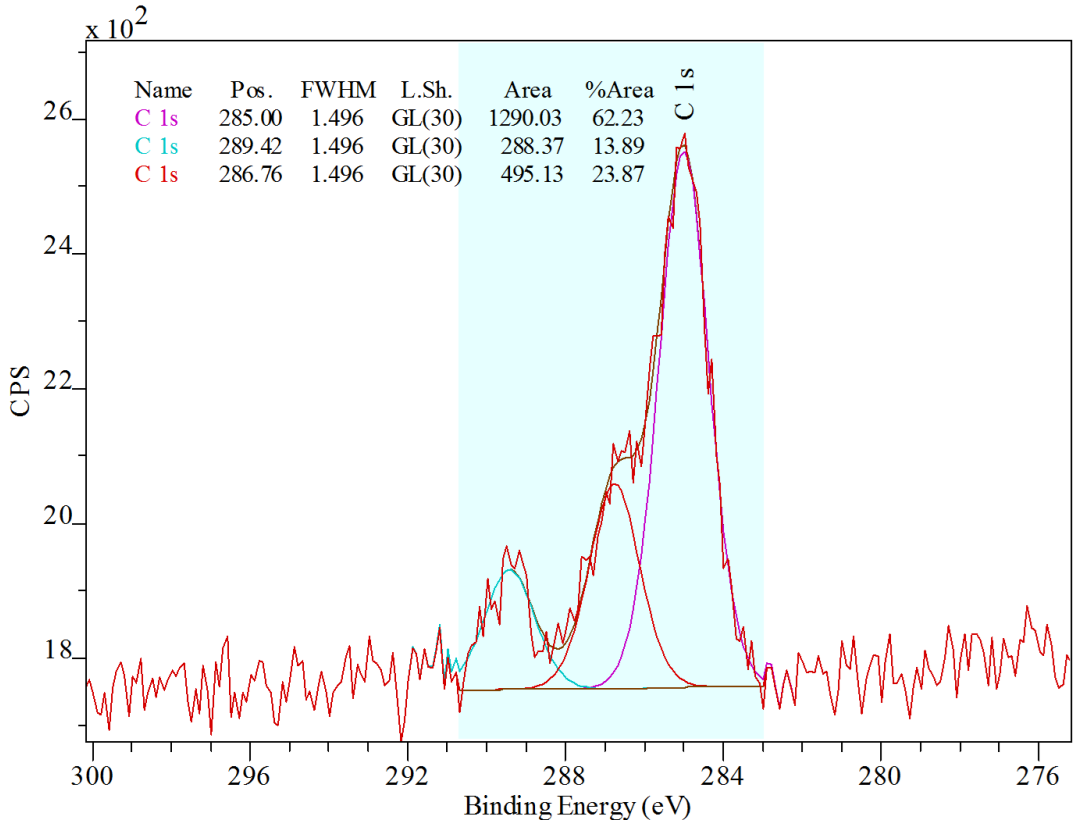
x 10^2
Name Pos. FWHM L.Sh. Area %Area
C 1s 285.00 1.496 GL(30) 1290.03 62.23
C 1s 289.42 1.496 GL(30) 288.37 13.89
C 1s 286.76 1.496 GL(30) 495.13 23.87
C 1s
CPS
Binding Energy (eV)

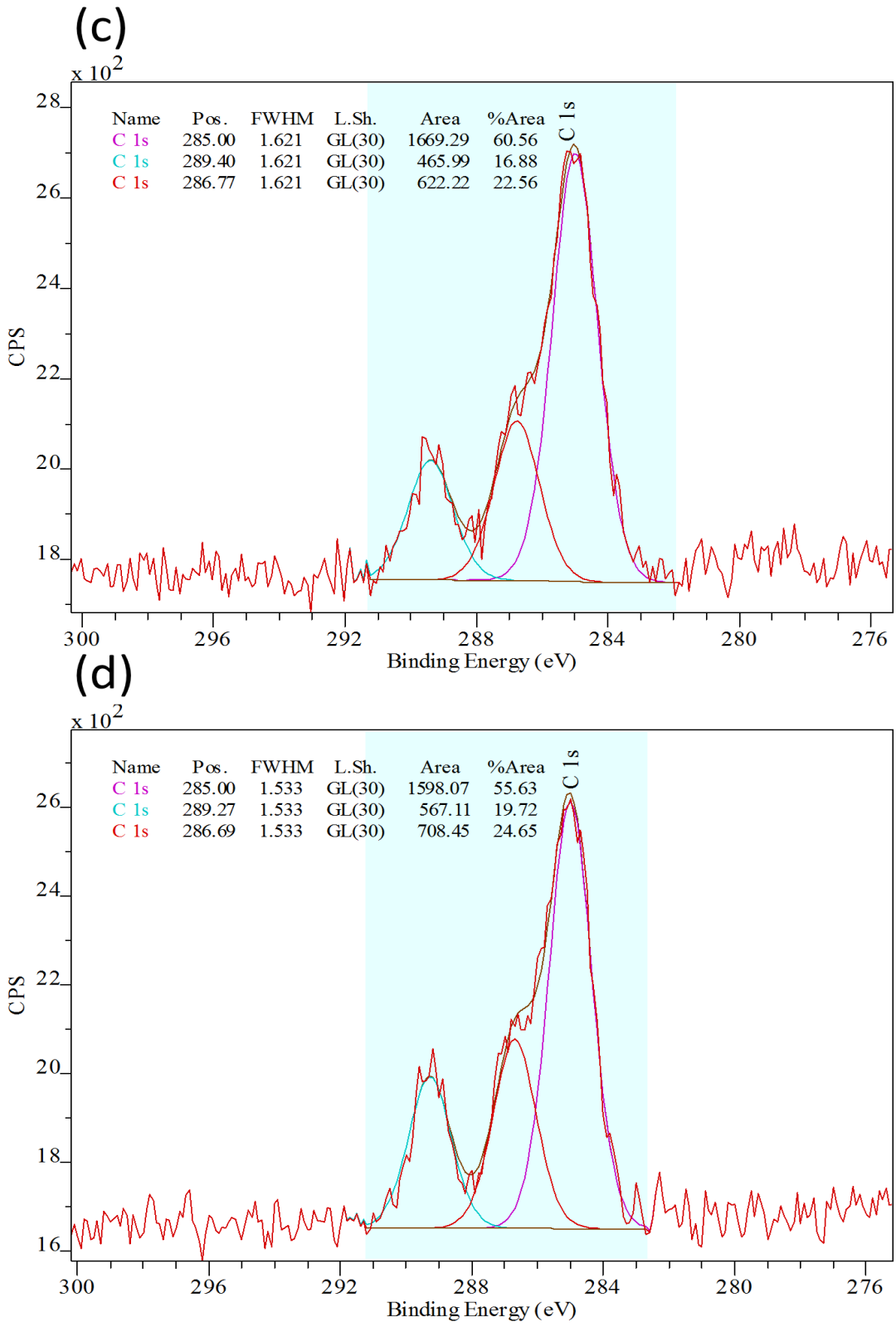

Figure 4.6 C1s core level spectra from silicon surfaces activated by the 5-second Ar-APP with AAc vapour grafting for (a) 1 minute (b) 3 minutes (c) 5 minutes and (d) 10 minutes.

A similar trend was observed on silicon after a 10-second Ar-APP activation and subsequent AAc vapour grafting. By increasing the AAc grafting time from 0 to 1 minute, 3 minutes, 5 minutes and 10 minutes, the atomic percentage of 289.2 eV in C1s altered from 0% to 8.75%, 17.14%, 17.33% and 16.33%, respectively (Figure 4.7).

(a)

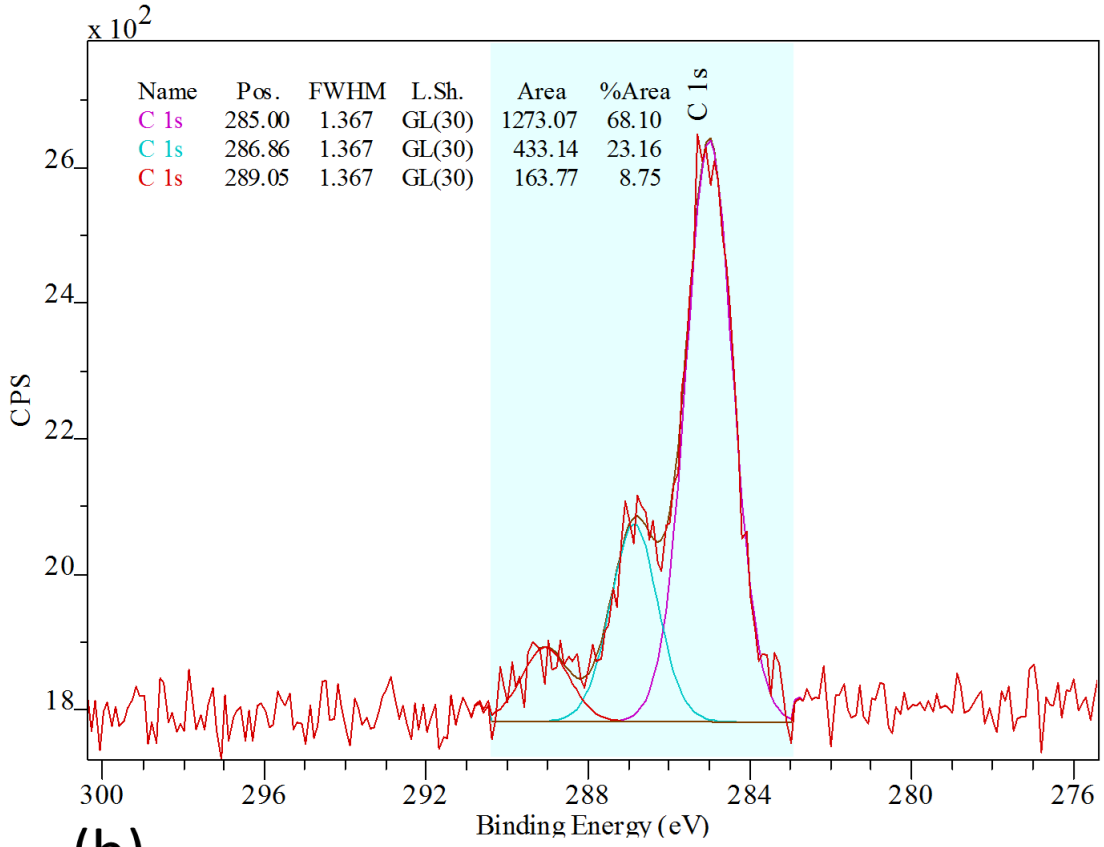
x 10^2
Name Pos. FWHM L.Sh. Area %Area
C 1s 285.00 1.367 GL(30) 1273.07 68.10
C 1s 286.86 1.367 GL(30) 433.14 23.16
C 1s 289.05 1.367 GL(30) 163.77 8.75
C 1s
CPS
26
24
22
20
18
300
296
292
288
284
280
276
Binding Energy (eV)

(b)

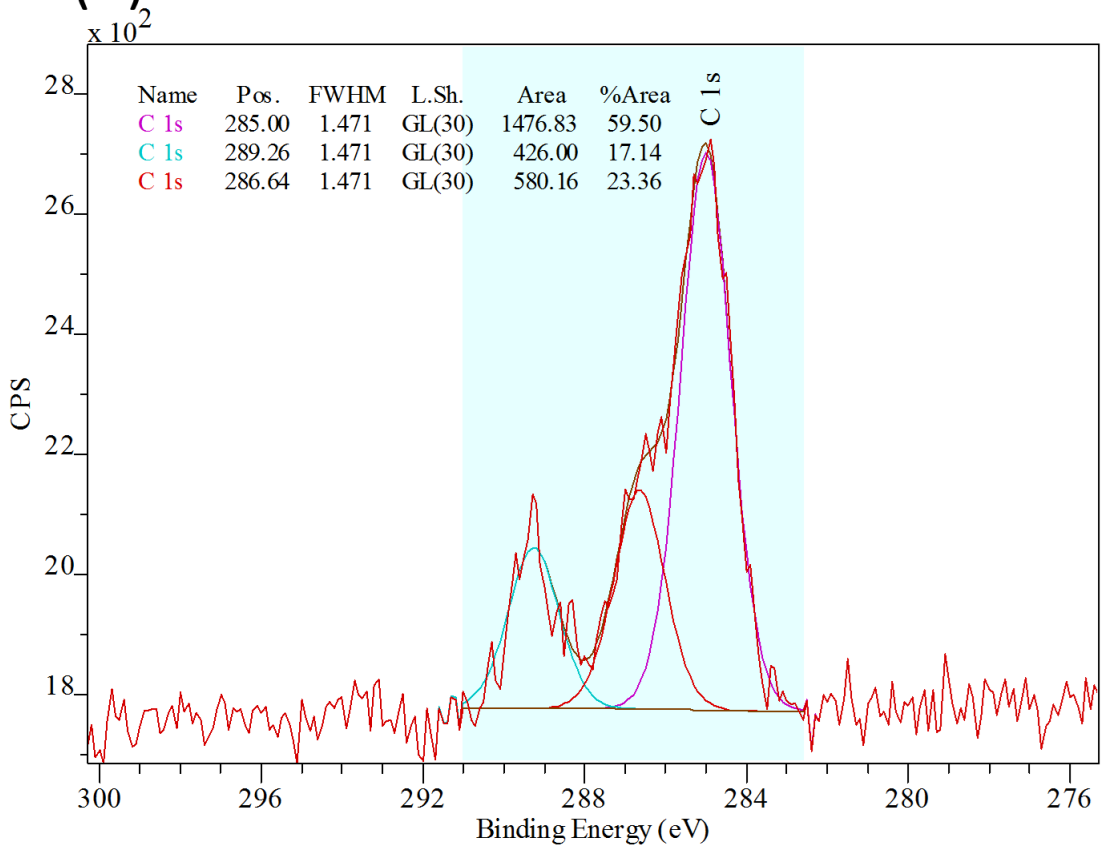
x 10^2
Name Pos. FWHM L.Sh. Area %Area
C 1s 285.00 1.471 GL(30) 1476.83 59.50
C 1s 289.26 1.471 GL(30) 426.00 17.14
C 1s 286.64 1.471 GL(30) 580.16 23.36
C 1s
CPS
28
26
24
22
20
18
300
296
292
288
284
280
276
Binding Energy (eV)

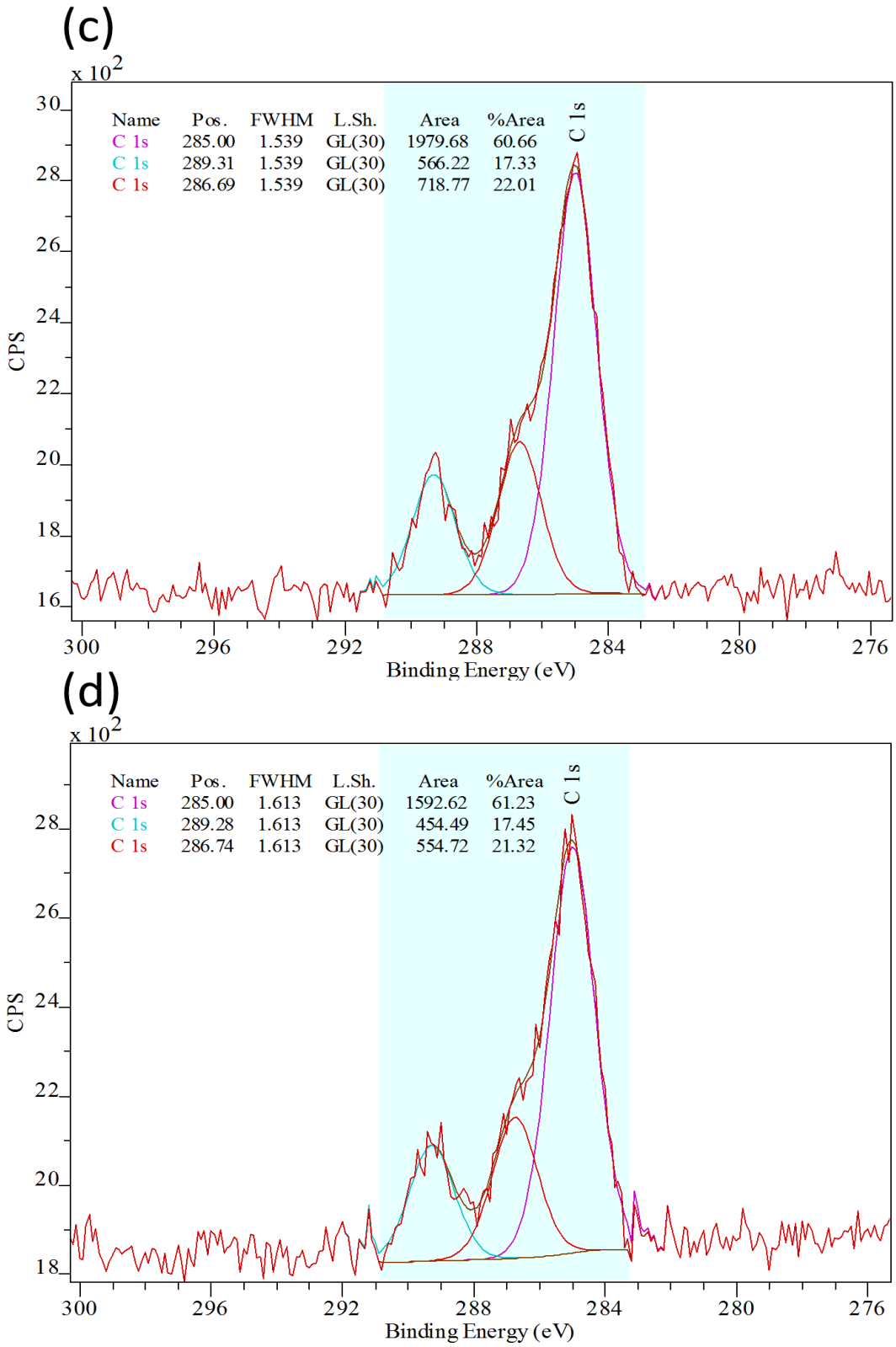

Figure 4.7 C1s core level spectra from silicon surfaces activated by the 10-second Ar-APP with AAc vapour grafting for (a) 1 minute (b) 3 minutes (c) 5 minutes and (d) 10 minutes.

4.2.3 Air atmospheric pressure plasma activated silicon surfaces

In the case of silicon activated by a 10-second Air-APP activation, the peak intensity at 289.2 eV was observed to increase from 0% to 15.64%, 18.30%, 17.91% and 20.30%, after the subsequent AAc vapour grafting for 1 minute, 3 minutes, 5 minutes and 10 minutes, respectively (Figure 4.8).

(a)

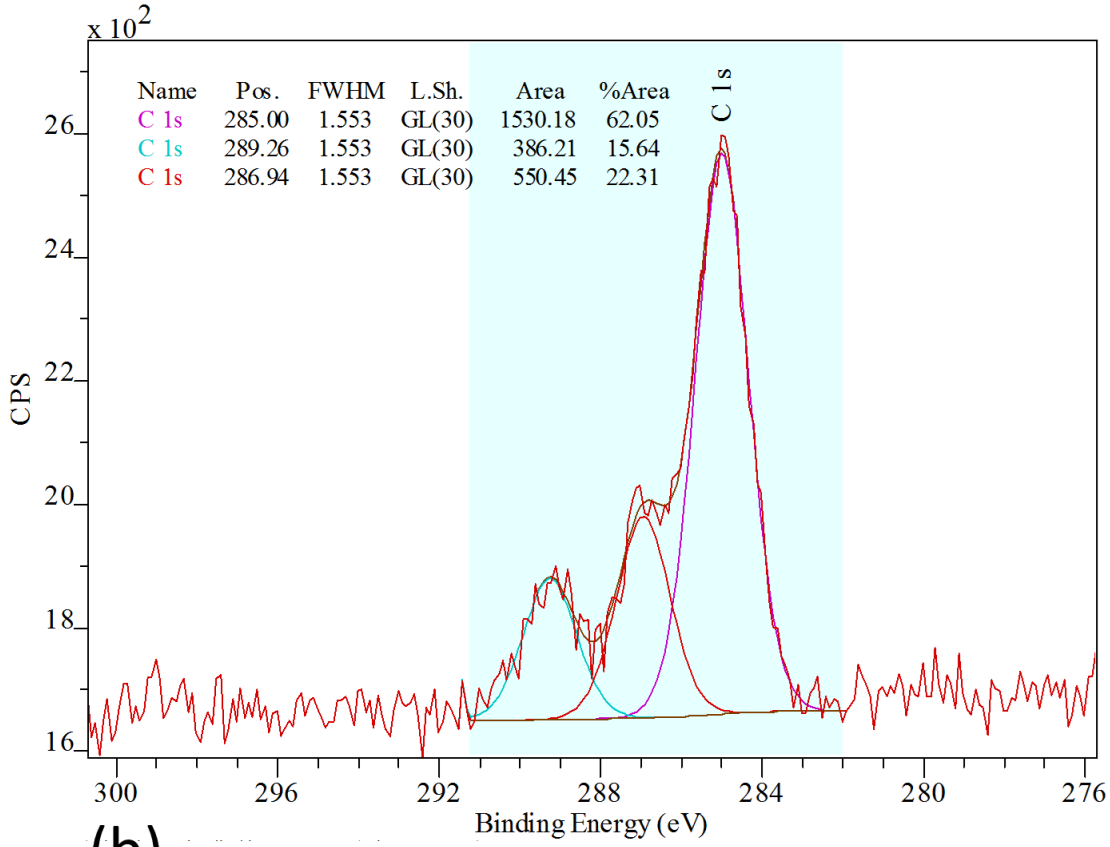
x 10^2
Name Pos. FWHM L.Sh. Area %Area
C 1s 285.00 1.553 GL(30) 1530.18 62.05
C 1s 289.26 1.553 GL(30) 386.21 15.64
C 1s 286.94 1.553 GL(30) 550.45 22.31
C 1s
CPS
26
24
22
20
18
16
300
296
292
288
284
280
276
Binding Energy (eV)

(b)

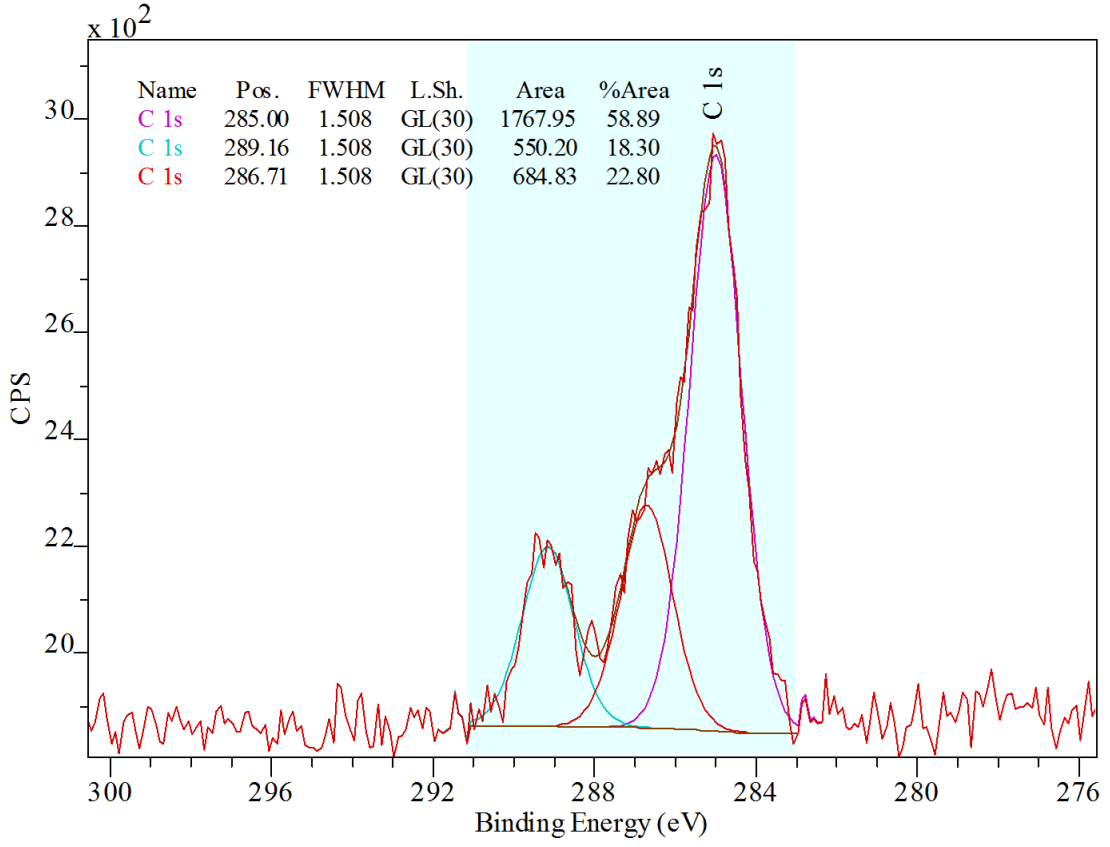
x 10^2
Name Pos. FWHM L.Sh. Area %Area
C 1s 285.00 1.508 GL(30) 1767.95 58.89
C 1s 289.16 1.508 GL(30) 550.20 18.30
C 1s 286.71 1.508 GL(30) 684.83 22.80
C 1s
CPS
30
28
26
24
22
20
300
296
292
288
284
280
276
Binding Energy (eV)

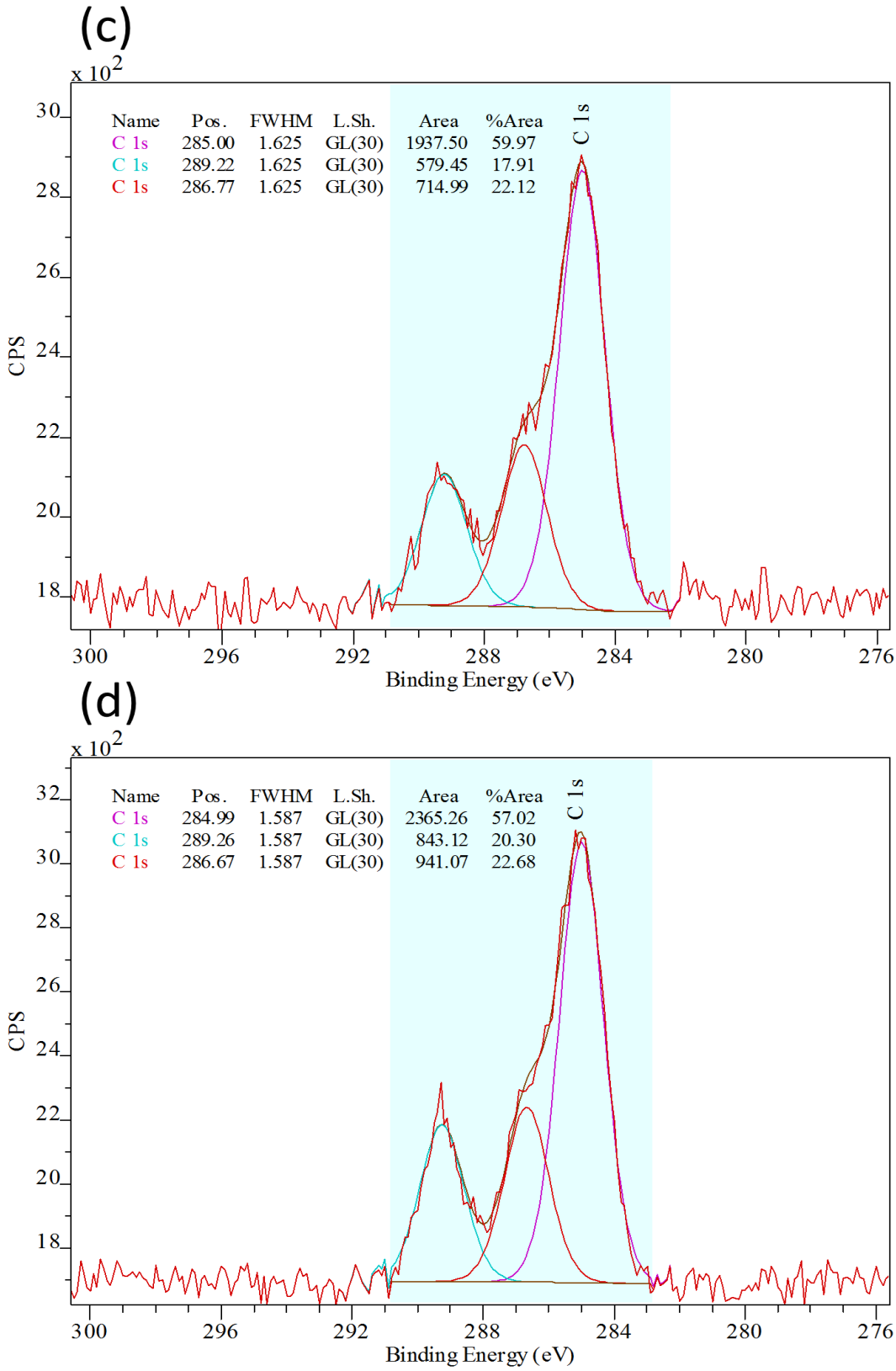

Figure 4.8 C1s core level spectra from silicon surfaces activated by the 5-second Air-APP with AAc vapour grafting for (a) 1 minute (b) 3 minutes (c) 5 minutes and (d) 10 minutes.

4.2.4 Conventional argon atmospheric pressure plasma activated silicon surface

For silicon treated by the conventional Ar-APP process, which exposed the AAc vapour directly under a plasma glow for 60 seconds, a 13.36% intensity of carboxylic acid group was identified (Ar-60s-MIX in Table 4.7).

4.2.5 Argon atmospheric pressure plasma functionalized carbon fibers

After the effects of the APP activation/AAc vapour grafting process on silicon were studied, the XPS analysis was also employed on CFs treated by the same process. As the analyses of CF samples were recorded from the fibers above the indium foil on the sample holder, the survey spectra of CF samples were checked and compared to the survey scan of the indium foil for the purpose of data selection to confirm the spectra are from CF samples, instead of the indium foil on the sample holder. XPS results (C1s core spectra) of the functionalized CFs after data selection are shown in Figure 4.9. For 5-second Ar-APP activated CFs, the percentage of carboxylic acid functional groups (at around 289.2 eV) was observed to increase from 0% to 3.70%, 4.12%, 3.89% and 4.92%, after the subsequent AAc vapour grafting for 1 minute, 3 minutes, 5 minutes and 10 minutes, respectively. The main peak at 285.0 eV corresponds to the graphitic peak of CFs. Other peaks in C1s spectra at binding energies around 286.5 eV, 287.9 eV and above 291.0 eV are assigned to the C-OR type groups, the C=O group and the π-π^* shake up satellite, respectively [140, 141].

(a)

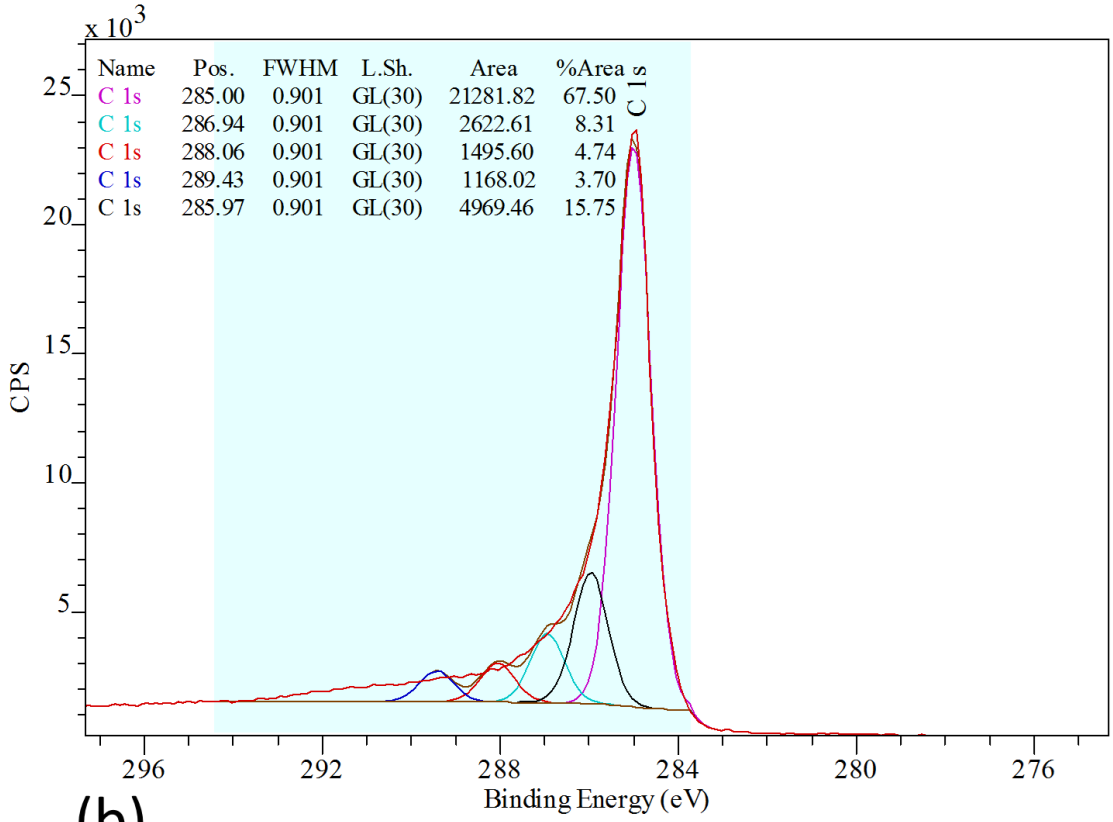
x 10^3
Name Pos. FWHM L.Sh. Area %Area
C 1s 285.00 0.901 GL(30) 21281.82 67.50
C 1s 286.94 0.901 GL(30) 2622.61 8.31
C 1s 288.06 0.901 GL(30) 1495.60 4.74
C 1s 289.43 0.901 GL(30) 1168.02 3.70
C 1s 285.97 0.901 GL(30) 4969.46 15.75
C 1s
CPS
25
20
15
10
5
296
292
288
284
280
276
Binding Energy (eV)

(b)

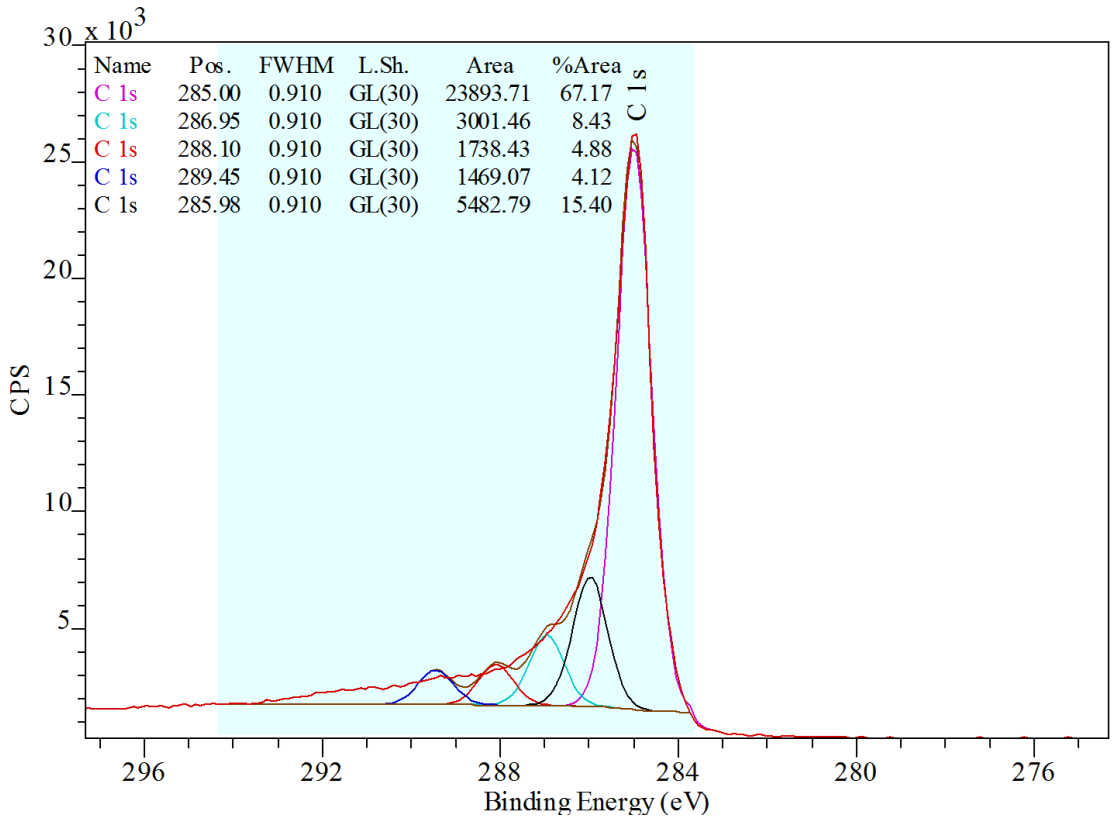
x 10^3
Name Pos. FWHM L.Sh. Area %Area
C 1s 285.00 0.910 GL(30) 23893.71 67.17
C 1s 286.95 0.910 GL(30) 3001.46 8.43
C 1s 288.10 0.910 GL(30) 1738.43 4.88
C 1s 289.45 0.910 GL(30) 1469.07 4.12
C 1s 285.98 0.910 GL(30) 5482.79 15.40
C 1s
CPS
30
25
20
15
10
5
296
292
288
284
280
276
Binding Energy (eV)

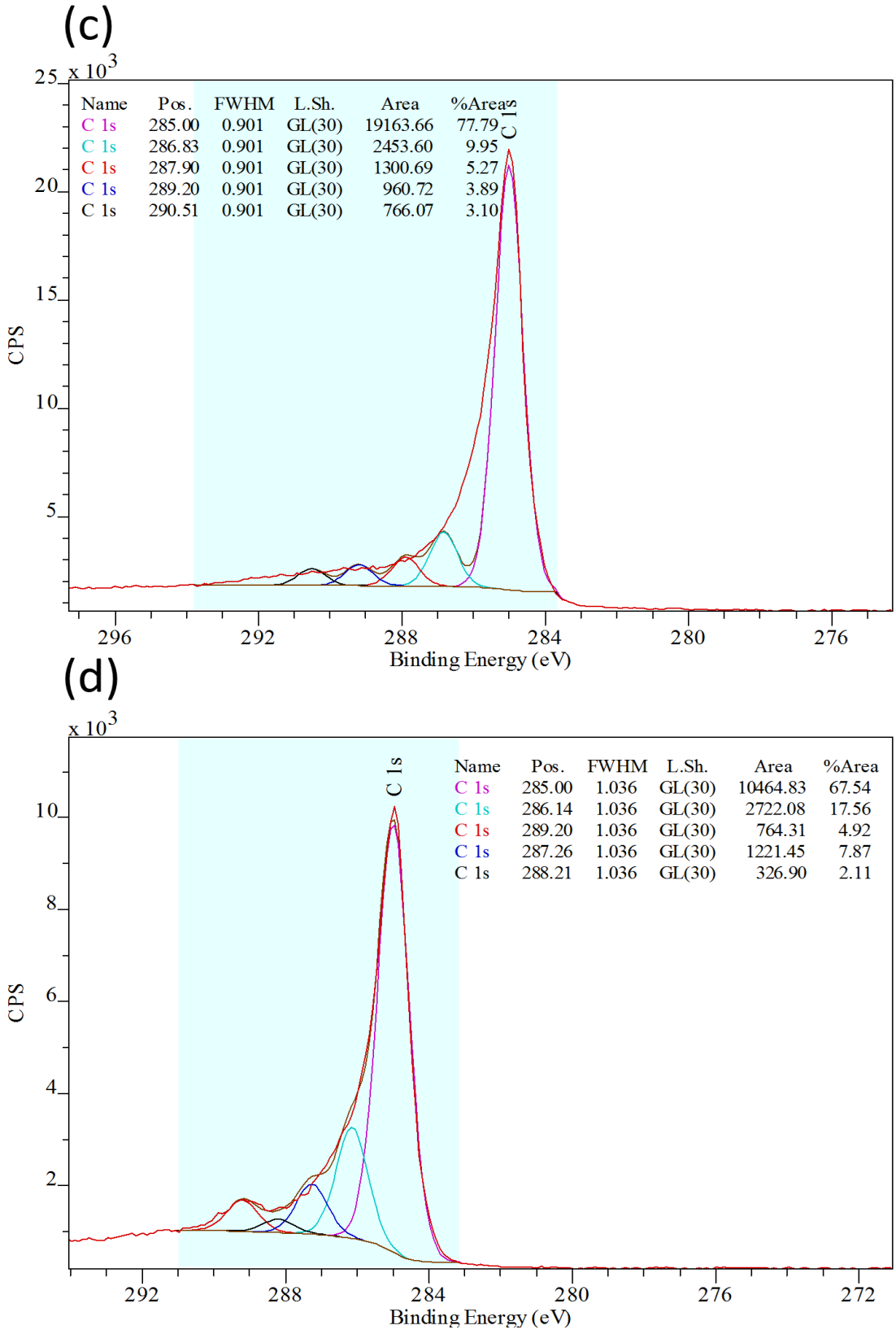

Figure 4.9 C1s core level spectra from CF surfaces activated by the 5-second Ar-APP with AAc vapour grafting for (a) 1 minute (b) 3 minutes (c) 5 minutes and (d) 10 minutes.

4.2.6 2,2,2-Trifluoroethanol (TFE) derivatization

To eliminate the concern that the peak at 289.2 eV in the C1s core level studied in this study might stand for -COOR group, a carboxylic derivatization test was also utilized to label the carboxylic acid groups on the surface.

The results (Figure 4.10) show that after TFE derivatization, a small atomic percentage around 289.2 eV was detected on the neat silicon surface (3.90%) and the percentage increased to 10.20% after the surface was activated by the 5-second Ar-APP. No peak at around 293.0 eV was observed on both neat and Ar-APP activated silicon wafers. However, after TFE derivatization of the silicon wafer surface activated by the 5-second Ar-APP with AAc vapour grafting for 10 minutes, the peak at the binding energy of 292.8 eV, which refers to CF_3 and defines –COOH over –COOR, was observed, along with a 23.41% atomic percentage at 289.0 eV. The percentage of –COOH functional groups introduced on the surface can then be evaluated (discussed in Chapter 5).

(a)

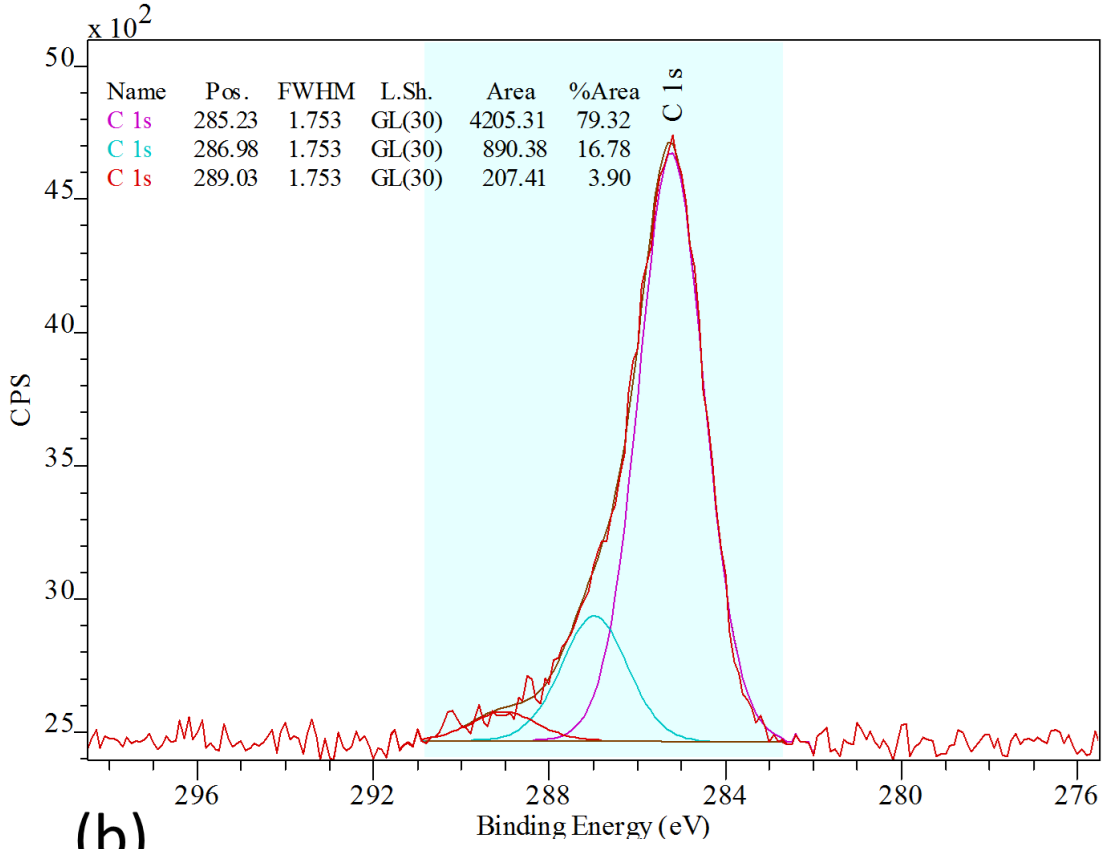
x 10^2
Name Pos. FWHM L.Sh. Area %Area
C 1s 285.23 1.753 GL(30) 4205.31 79.32
C 1s 286.98 1.753 GL(30) 890.38 16.78
C 1s 289.03 1.753 GL(30) 207.41 3.90
C 1s
CPS
Binding Energy (eV)

(b)

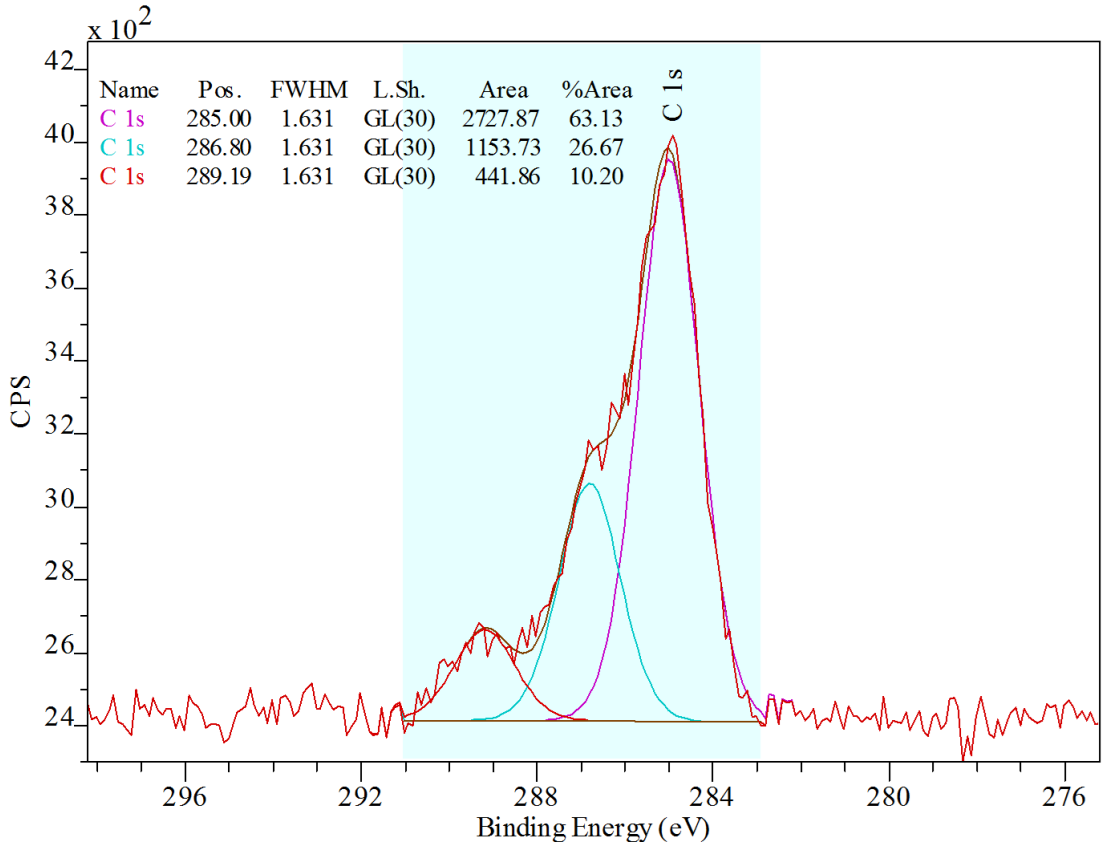
x 10^2
Name Pos. FWHM L.Sh. Area %Area
C 1s 285.00 1.631 GL(30) 2727.87 63.13
C 1s 286.80 1.631 GL(30) 1153.73 26.67
C 1s 289.19 1.631 GL(30) 441.86 10.20
C 1s
CPS
Binding Energy (eV)

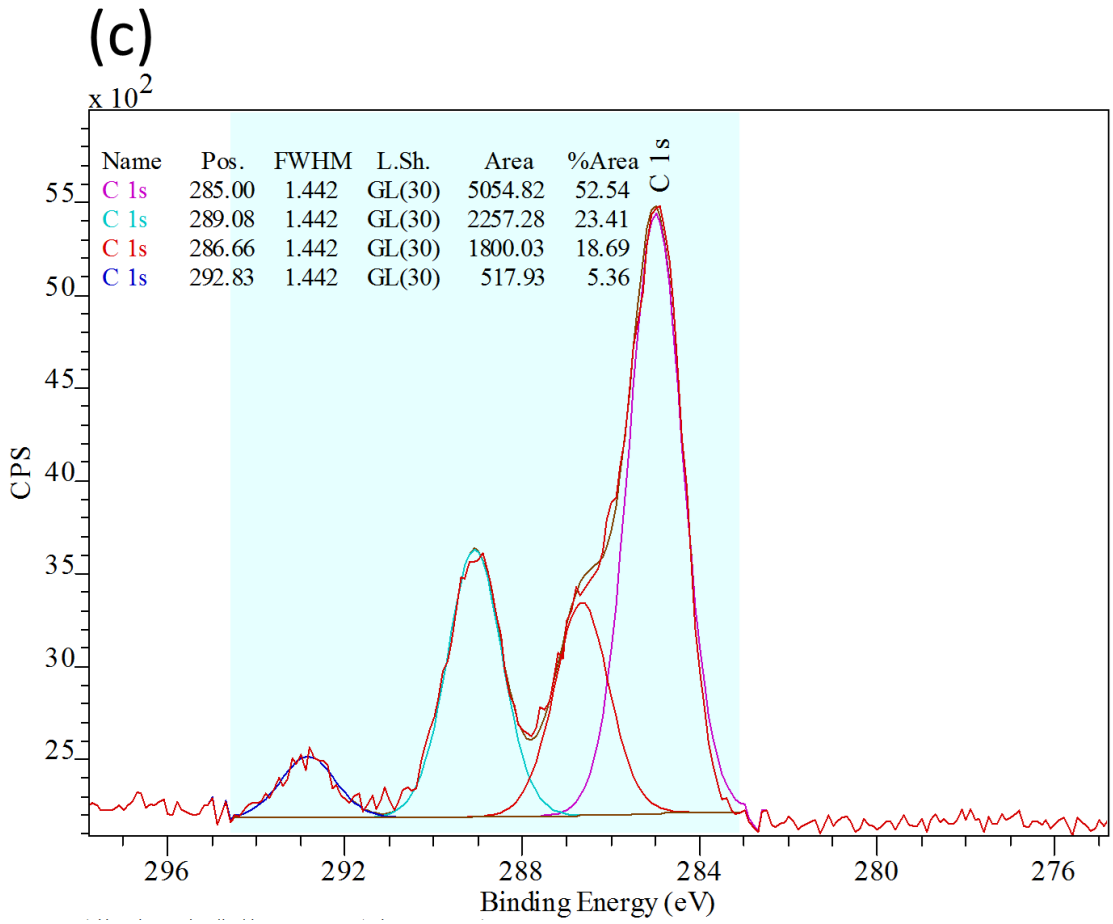

Figure 4.10 C1s core level spectra after TFE derivatization (a) neat silicon surface (b) 5-second Ar-APP activated silicon surface (c) silicon surface activated by the 5-second Ar-APP with AAc vapour grafting for 10 minutes.

4.3 Ionomer-modified self-healing epoxy resin

4.3.1 Introduction

The concept of preparing a self-healing composite in this study focuses on using the functionalized CFs and ionomer-modified epoxy resin. The idea is that the sodium carboxylate functional groups in the ionomer-modified epoxy resin cannot only react with each other for repairing crack(s) inside the matrix but also with carboxylic acid functional groups on the APP-functionalized CFs to repair the debonding and heal the

interfaces between the matrix and the CFs. The effects of the APP functionalization on both silicon wafers and CFs and the stability of the functionalized surfaces were studied and confirmed via the results of wettability and XPS. In this chapter, the healing efficiency of the ionomer network, Araldite 5052 resin containing 4-amino-sodium salicylate end-capped DGEBA, was recorded and compared to the unmodified network to examine its capability of self-healing. The interaction of functional groups between the APP-functionalized surfaces and ionomer healing agent was then studied via XPS. Finally, the interfacial healing performance was examined by observing the healing performance of a composite prepared by APP-functionalized CFs and the ionomer-modified epoxy resin.

4.3.2 Healing efficiency of ionomer-modified epoxy resin

Before embedding functionalized CFs into the ionomer-modified epoxy resin to prepare self-healing composites, the healing efficiency of the ionomer-modified epoxy resin was studied via the SENB test to evaluate the healing performance of the ionomer-modified resin. The healing efficiency comparison between unmodified and ionomer-modified systems was made to determine whether the formulation is suitable for self-healing composites.

The samples prepared with unmodified epoxy resin were made of Araldite LY 5052 epoxy resin without any addition of an ionomer healing agent, while the ionomer-

modified epoxy resin samples were prepared by using an ionomer-modified Araldite LY 5052 epoxy, which contains 7.5 wt% of ionomer healing agent (Figure 4.11).

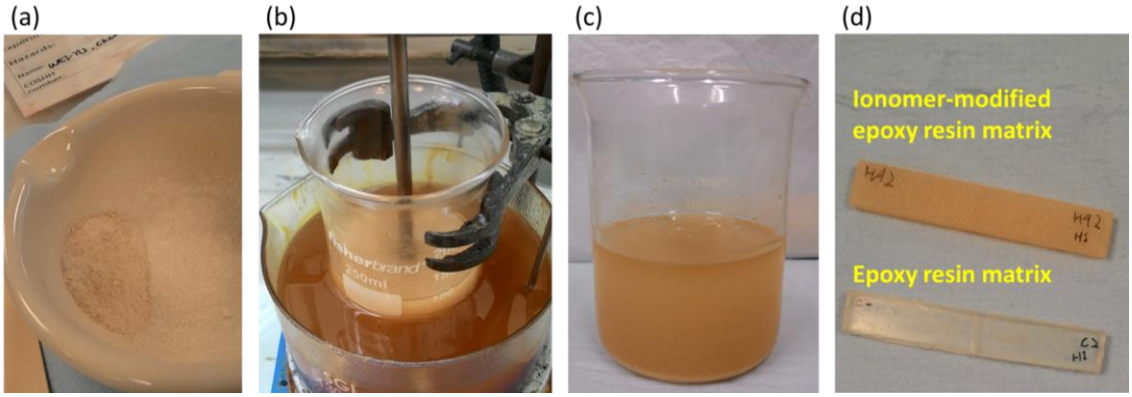

Figure 4.11 Images of (a) ionomer healing agent (b) the preparation of ionomer-modified epoxy resin by heating the mixture in an oil bath at 130°C for 3 hours (c) ionomer-modified Araldite LY 5052 epoxy resin (d) SENB samples after the 1st healing event.

The estimation of healing efficiency is described schematically in Figure 4.12. Samples were loaded to failure using the SENB test by a three-point bending machine, and the failure load (N) was recorded (101.30 N for unmodified epoxy resin sample and 91.06 N for ionomer-modified epoxy resin sample). The fractured surfaces of the tested specimens were placed and gently clamped together, then put into an oven at 120 °C for 2 h to trigger and perform healing. This healing performance was defined as the 1st healing event. The samples, which were loaded to failure before, was then loaded to failure after the 1st healing event using the method described above, and the failure load was again recorded (15.44 N for unmodified epoxy resin sample and 28.29 N for

ionomer-modified epoxy resin sample). These samples were then healed using the same healing process (2nd healing event), then loaded to failure and recorded the failure load again (0 N for unmodified epoxy resin sample and 13.49 N for ionomer-modified epoxy resin sample). Healing efficiency (%) was calculated by dividing the failure load of a sample after the 1st or 2nd healing event to that before healing.

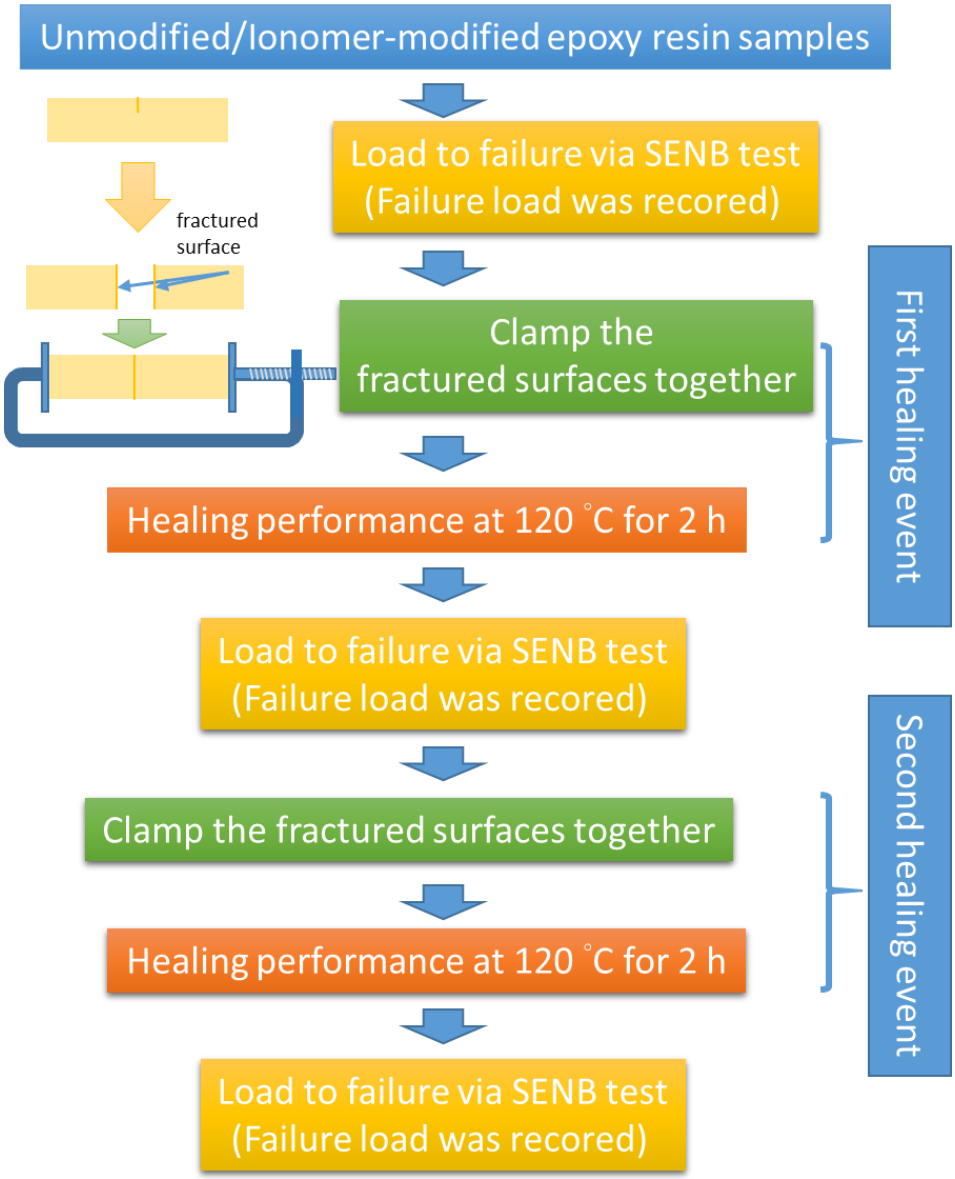

Figure 4.12 Diagram of the healing efficiency evaluation.

For the unmodified epoxy resin sample, it required a force of 101.30 N to load it to failure. However, after the 1st healing event, only a force of 15.44 N is needed to break the sample. Thus, the healing efficiency was calculated and found to be 15.24%. After the 2nd healing event, no healing performance was observed. Therefore, the healing efficiency of the unmodified epoxy resin sample was 0%.

For the ionomer-modified epoxy resin sample, a force of 91.06 N was required to break the sample. After the 1st healing event, a force of 28.29 N was sufficient to load the sample to failure. Noticeably, it still needed a load of 13.49 N to break the ionomer-modified epoxy resin sample after the 2nd healing event. These results show the healing efficiencies of the ionomer-modified epoxy resin system after first (31.07%) and second (14.81%) healing events.

Figure 4.13 represents the healing efficiency of unmodified and ionomer-modified epoxy specimens from SENB tests. The unmodified system exhibited a 15.24% healing efficiency, while the ionomer-modified system was observed with a 31.07% healing efficiency after the first healing event. After the second healing event, the unmodified system was not able to heal the fracture (0% healing efficiency), while the ionomer-modified system showed a 14.81% healing efficiency.

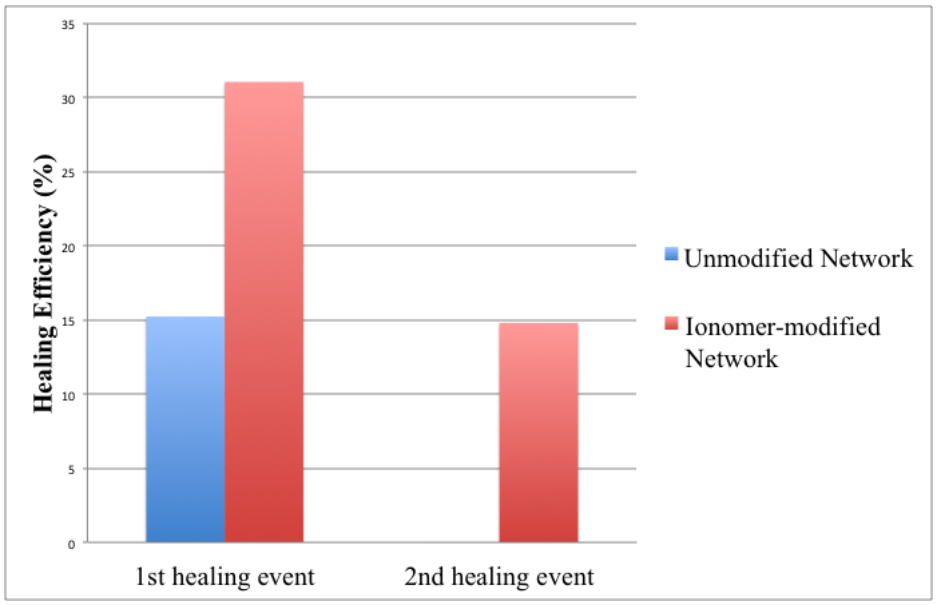

Figure 4.13 Healing efficiency of unmodified and ionomer-modified epoxy specimens.

4.3.3 Simulation of potential interface healing using ionomer adsorption

The survey spectra from neat and AAc-grafted silicon surfaces after isopropanol immersion are presented in Figure 4.14. The presence of silicon, carbon and oxygen were spotted in the survey. Unlike the XPS results of the neat silicon surface, which was cleaned by isopropanol and distilled water with the process mentioned in Chapter 3, a small atomic percentage of sodium was observed after isopropanol immersion. The peak assigned to sodium was also found on silicon specimens after immersing them in a 4-amino-sodium salicylate (7.5 wt% in isopropanol) solution.

As shown in Figure 4.15, peaks assigned to silicon, carbon and oxygen were observed from the survey of neat and AAc-grafted silicon surfaces after 4-amino-sodium

salicylate immersion. The concentration of sodium on the neat silicon surface after 4-amino-sodium salicylate immersion (0.08%, Figure 4.15 (a)) is similar to that after isopropanol immersion (0.19%, Figure 4.14 (a)). However, a higher atomic percentage of sodium (5.21%) and the presence of nitrogen were found on the AAc-grafted silicon surface after 4-amino-sodium salicylate immersion.

The spectral survey of neat and AAc-grafted silicon surfaces after ionomer immersion (Figure 4.16) exhibited a similar trend to the XPS results from 4-amino-sodium salicylate immersion. The peaks related to silicon, carbon oxygen and sodium were spotted from the survey of both neat and AAc-grafted silicon surfaces, while higher atomic ratios of sodium (5.80%) and nitrogen (1.73%) were only observed on AAc-grafted silicon surface after ionomer immersion.

To further estimate the potential of employing both the Ar-APP/AAc grafting technology and ionomer system developed in this project to self-healing composite applications, the functional group reaction between the ionomer healing agent (sodium carboxylate groups) and the Ar-APP/AAc grafted silicon surface (carboxylic acid groups) was investigated (details were described in Chapter 3.10).

Figure 4.17 shows the spectra survey of neat and AAc-grafted CF surfaces after ionomer immersion. Compared to the silicon surface, the CF surface exhibited a higher

percentage of carbon. The atomic percentage of carbon and sodium is higher on AAc-grafted CF (77.23% carbon and 2.96% sodium) than on neat CF (74.49% carbon and 0.50% sodium). Nitrogen was only detected on the AAc-grafted CF surface after ionomer immersion.

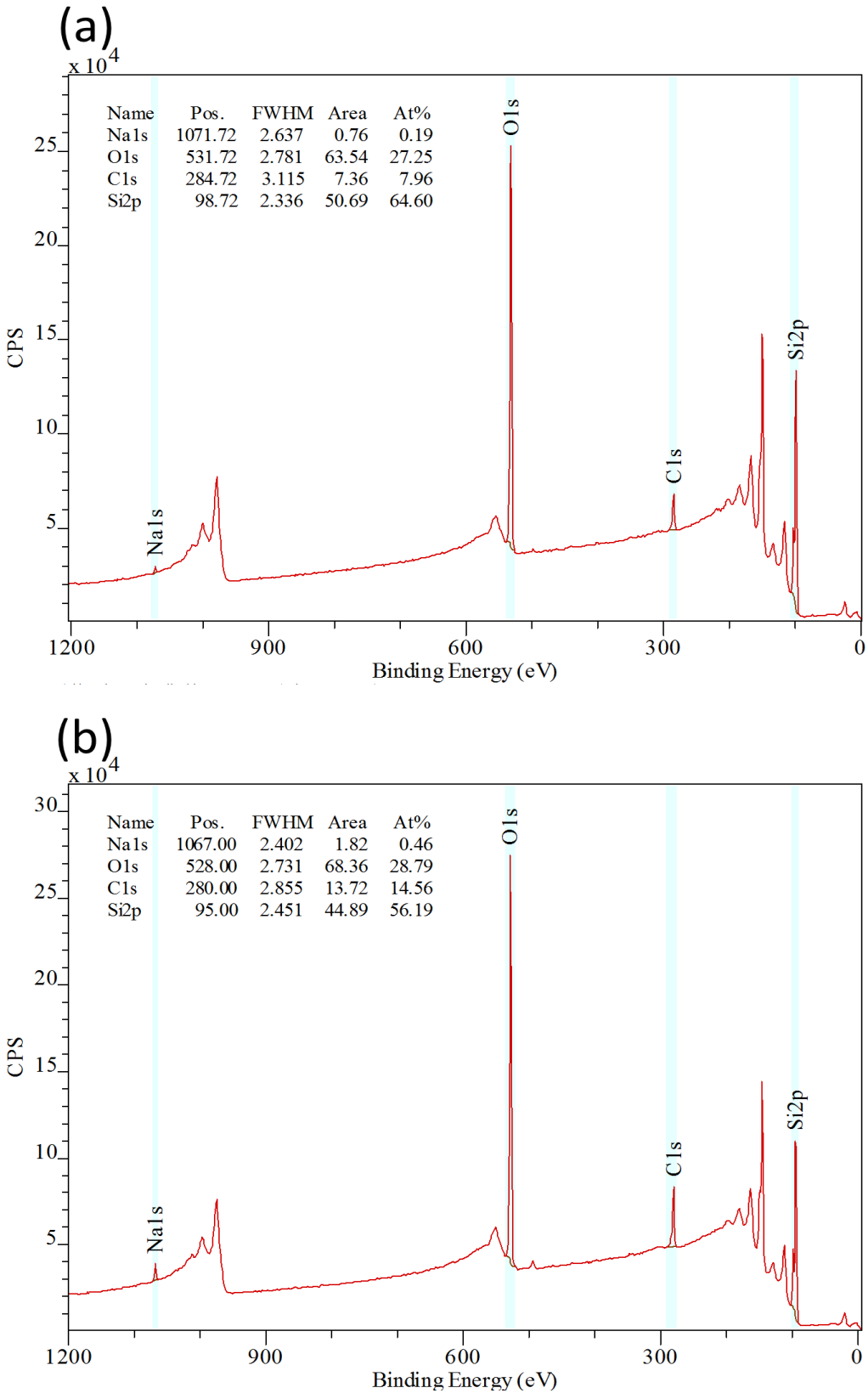

Figure 4.14 XPS survey spectra of silicon specimens after isopropanol immersion (a) neat silicon surface (b) silicon surface activated by the 5-second Ar-APP with AAc vapour grafting for 10 minutes.

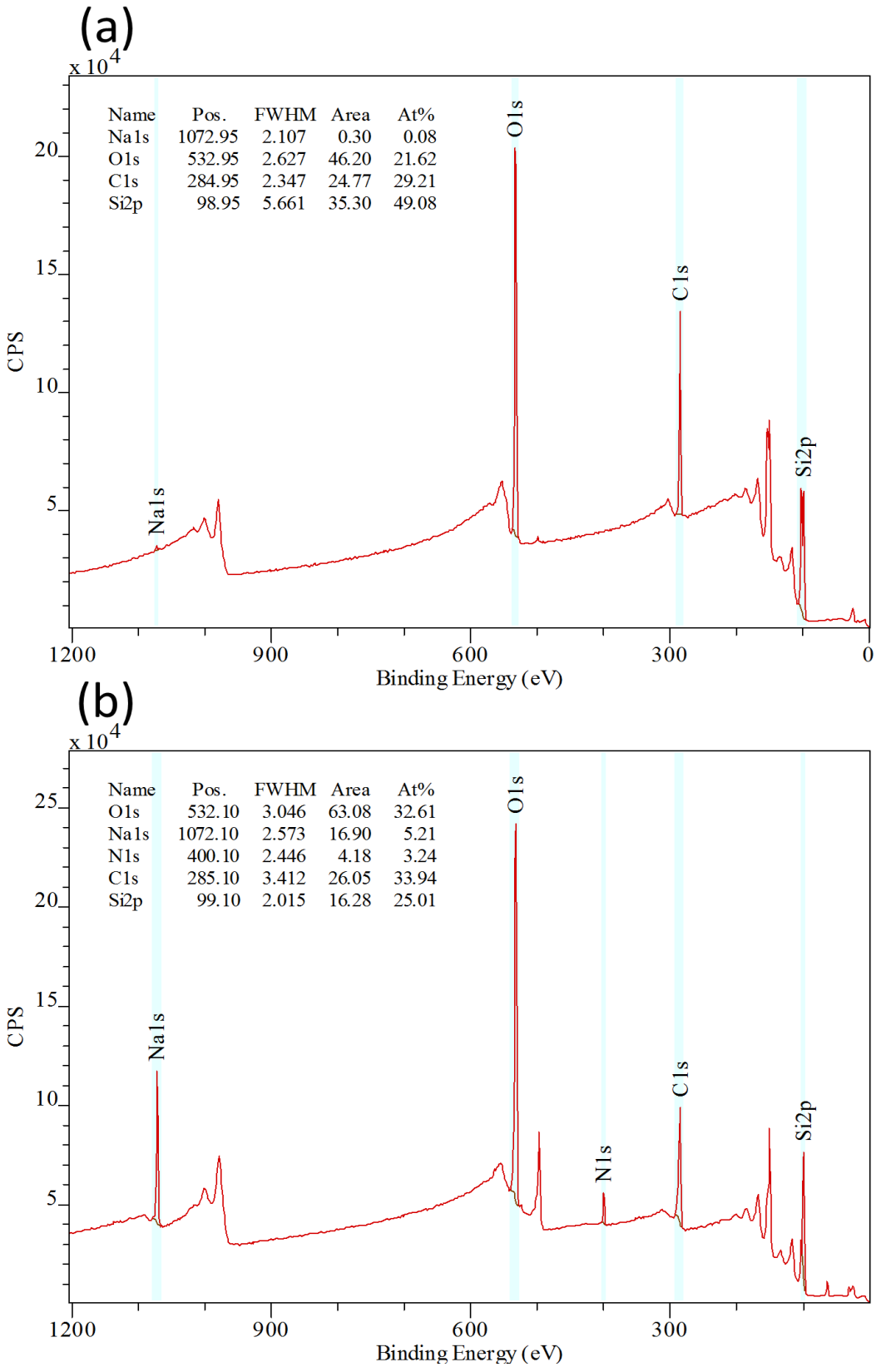

Figure 4.15 XPS survey spectra of silicon specimens after 4-amino-sodium salicylate immersion (a) neat silicon surface (b) silicon surface activated by the 5-second Ar-APP with AAc vapour grafting for 10 minutes.

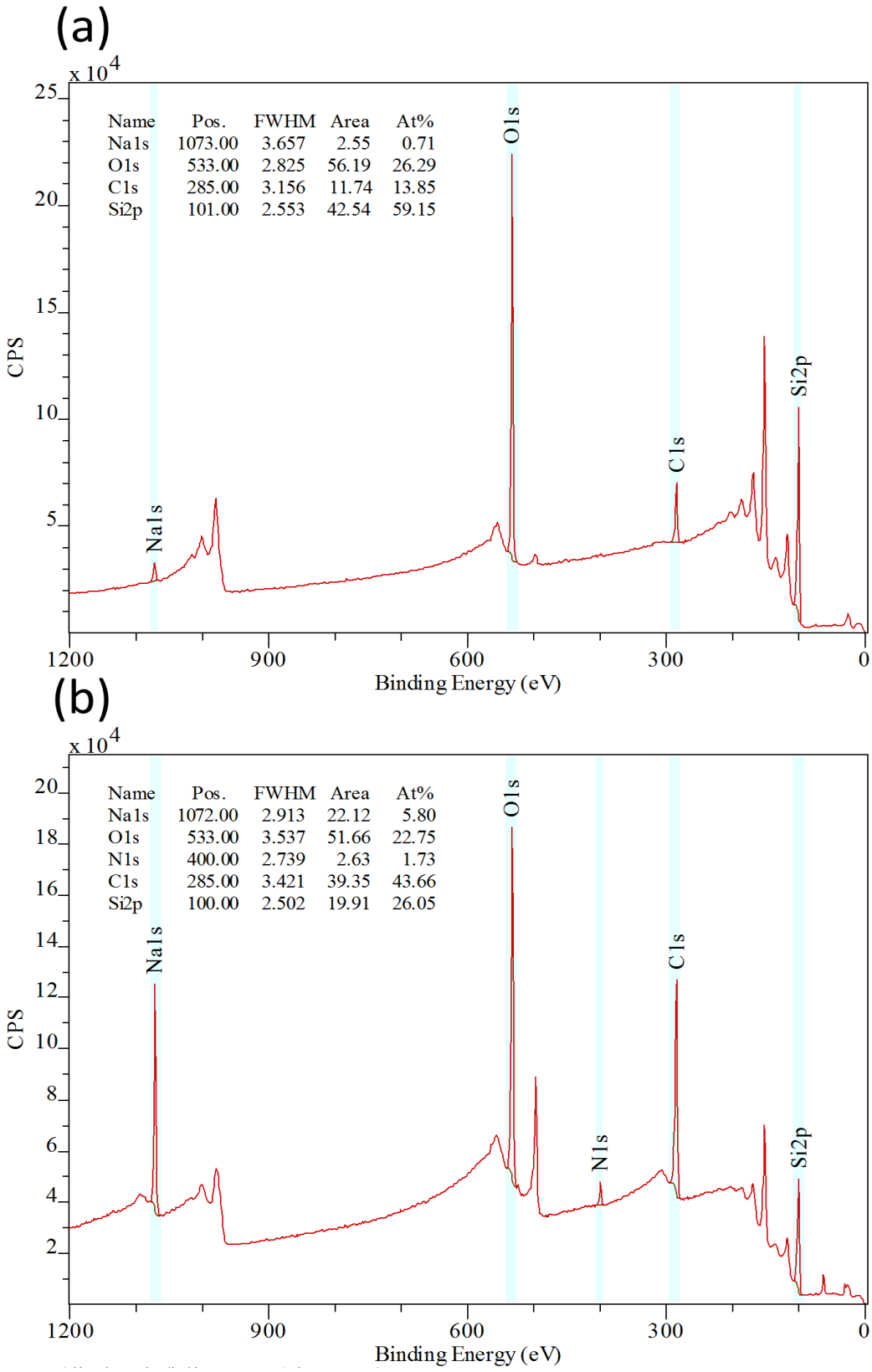

Figure 4.16 XPS survey spectra of silicon specimens after immersing in ionomer healing agent (a) neat silicon surface (b) silicon surface activated by the 5-second Ar-APP with AAc vapour grafting for 10 minutes.

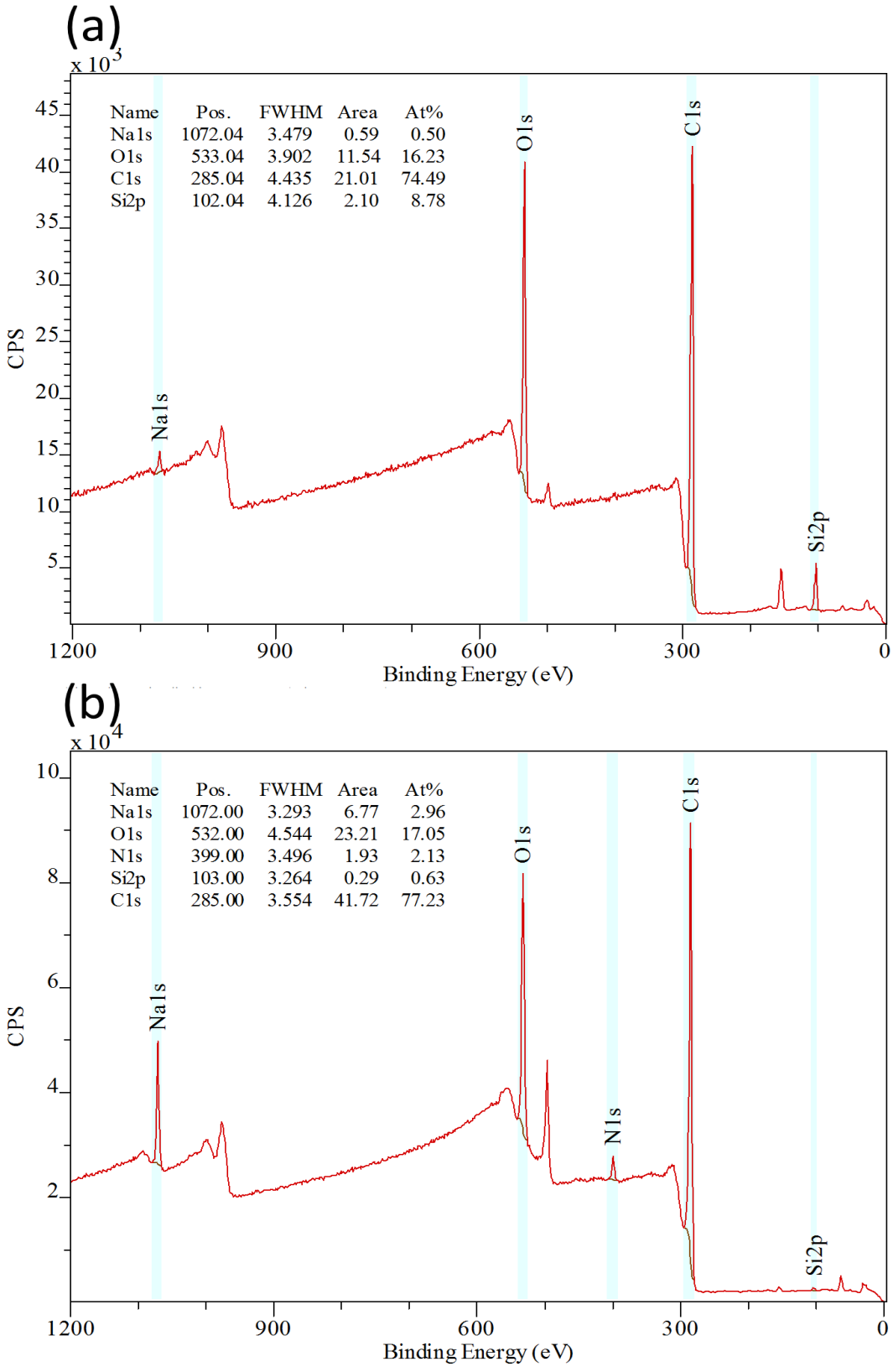

Figure 4.17 XPS survey spectra of CFs after immersing in ionomer healing agent (a) neat CF (b) CF activated by the 5-second Ar-APP with AAc vapour grafting for 10 minutes.

4.3.4 Interfacial healing performance

After the capability of functional group reactions between the APP-functionalized CFs and the ionomer healing agent and the healing efficiency of ionomer-modified epoxy resin were studied, healing performance on the interface between the APP-functionalized CF bundle and ionomer-modified epoxy resin was investigated.

It can be observed from Figure 4.18 that the crack site was healed after the 1st and 2nd healing events, suggesting the potential of interfacial healing between the APP-functionalized CF bundle and the ionomer-modified epoxy resin after the healing events.

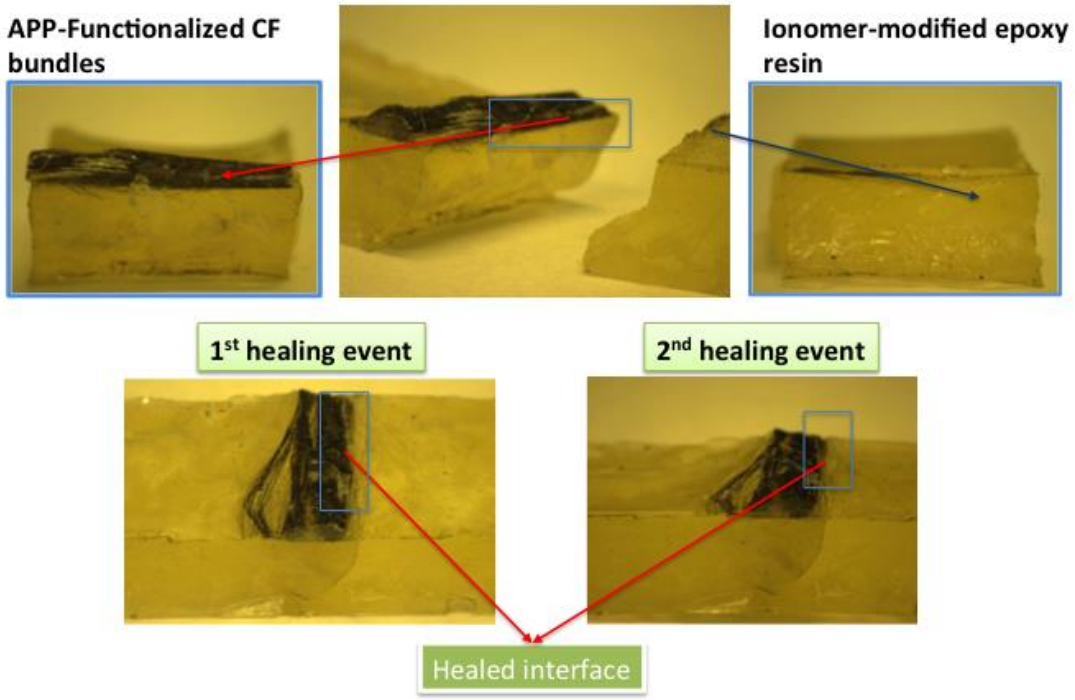

Figure 4.18 Interfacial healing performance after the 1st and 2nd healing events.

Chapter 5 Discussion

This study aims towards the development of a novel atmospheric pressure plasma process to functionalize CFs via retaining a high concentration of carboxylic acid functional groups, and further embedding functionalized CFs into an ionomer-modified epoxy resin, which was also developed in this research, to achieve a self-healing composite with improved mechanical properties. To estimate the effects of various parameters of the APP process on the surface, n-type silicon wafers were used for examinations of wettability and chemical composition via XPS. From the surface images in Figure 4.1, an observable difference can be seen on the silicon surface after Ar-APP/AAc-grafting, which suggests that AAc vapour was introduced on hydrophilic surface (Figure 4.1 (c)). This is further supported by wettability and XPS results.

5.1 Surface wettability of silicon specimens

The measurement of surface wettability is a preliminary method, prior to XPS analysis, to estimate the effect of the APP/AAc grafting functionalization, as the alternation of wettability reflects changes of the surface. A significant difference of surface wettability can be seen from Figure 4.2 and more detailed comparisons are illustrated in Figures 5.1 to 5.3. From the results of wettability, the contact angle with water was found to be the lowest after argon- or air-APP activation only. A similar result was also reported by Chen et al. [142], because of the free radicals or/and peroxide groups, which are introduced during APP activation. Argon-APP can form free radicals on the

substrate surface, which partially become peroxide groups after exposure to atmospheric gas. Air-APP offers free radicals and peroxide groups from both the APP working gas and exposing activated samples to the atmospheric gas. The free radicals or peroxide groups, which are introduced from the air-APP working gas, turn the surface hydrophilic and benefit the AAc vapour grafting. After APP activation with a subsequent AAc vapour grafting, it can be observed that the WCAs have increased. This is due to the fact that the Ar-APP /AAc vapour grafting process deposited a poly-AAc like film containing non-polar groups on the surface, which are more hydrophobic than oxygen-contained polar groups produced by the APP activation. After treatment by different activation/grafting parameters, the WCAs of silicon surfaces decreased from 56.1±0.8° (neat silicon wafer) to between 4.1±0.3° and 9.5±3.4° (Ar-APP series) or 8.2±0.2° and 16.1±0.2° (Air-APP series), suggesting a preliminary effect of the APP activation/AAc grafting process on surface functionalization.

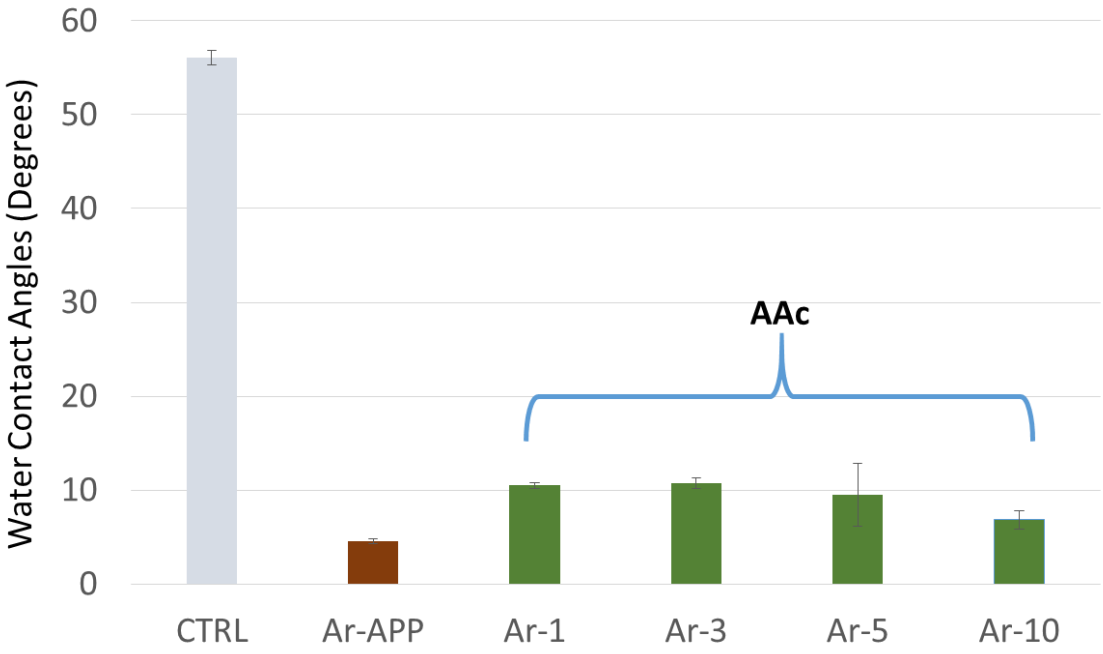

Figure 5.1 Comparison of the wettability of Ar-APP (5s) and AAc grafting.

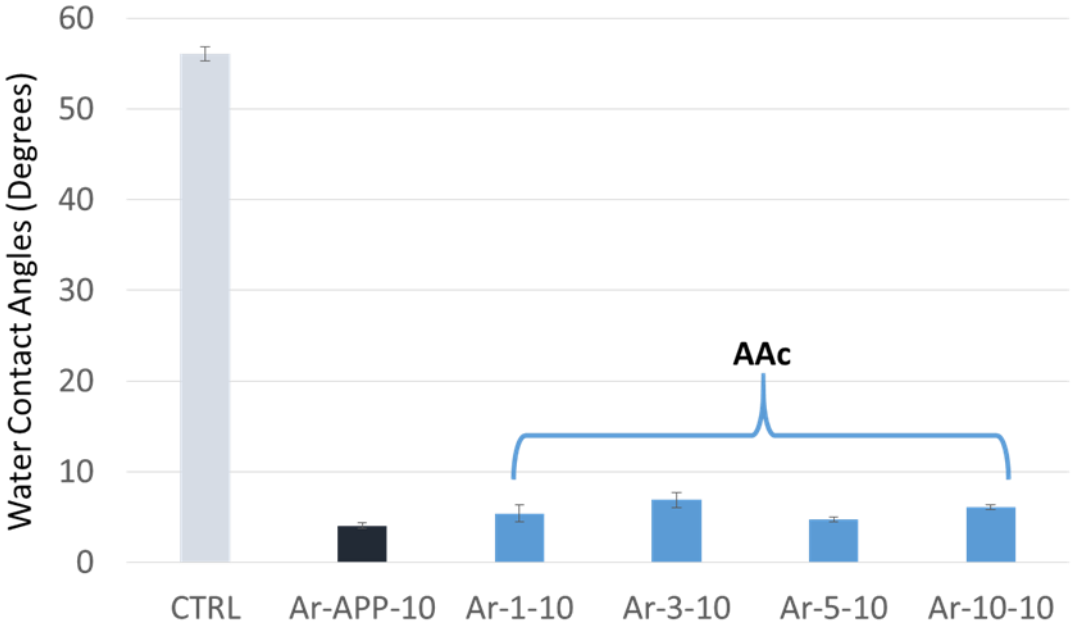

Figure 5.2 Comparison of the wettability of Ar-APP (10s) and AAc grafting.

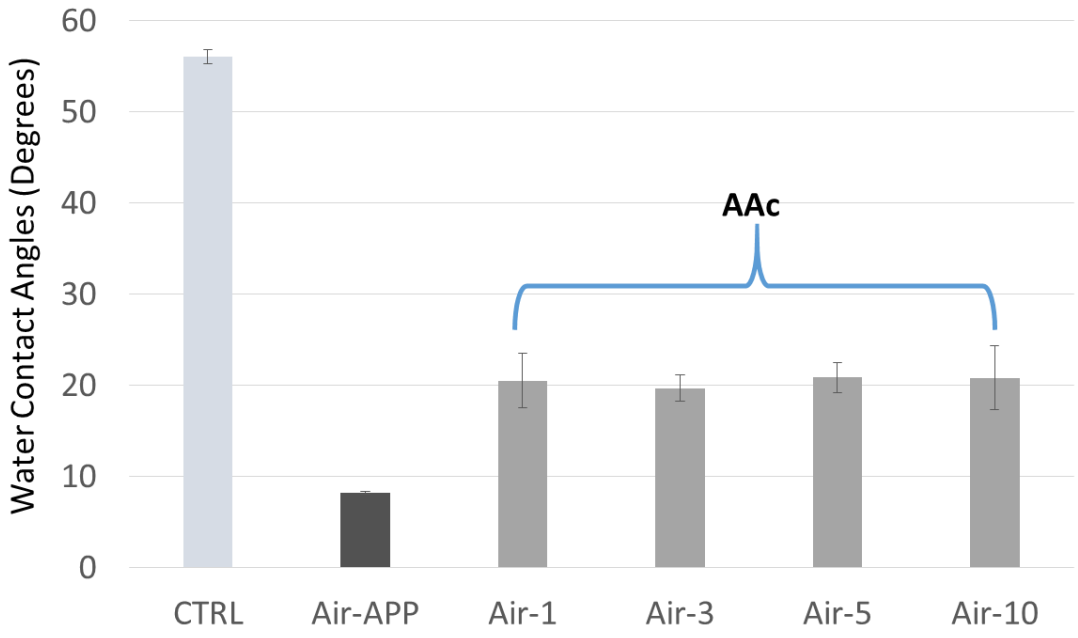

Figure 5.3 Comparison of the wettability of Air-APP (5s) and AAc grafting.

5.2 Surface stability of the functionalized silicon surfaces

To investigate the functionalized surface stability, the WCAs of the silicon specimens were also measured 2, 4 and 8 days after treatment. By observing the change of WCA on a specimen, the stability of its surface can be evaluated. From the results illustrated in Table 4.3 and Figure 5.4, the increase of WCAs on silicon was observed with a longer time after treatment, which reflects a decrease of hydrophilicity. The decline of hydrophilicity is due to the interaction between the APP process treated surface and the atmospheric compounds. Therefore, for a silicon specimen, a lower degree on decay of hydrophilicity suggests that it possesses a more stable surface. Compared to the neat silicon surface (56.1±0.8°), APP process treated surfaces were found to be more hydrophilic even 8 days after treatments (between 20.9±1.2° and 26.6±1.3°). A higher

decrease of hydrophilicity is also observed on the APP-activated silicon surface, compared to that treated with APP activation/AAc vapour grafting. This indicates the high reactivity an APP-activated surface possesses, which not only proves the effects of the APP activation on the silicon surface but also supports the assumption that it is essential to perform an AAc-grafting process on the APP-activated surface, instead of using only APP-activation on silicon specimens or CFs. Although the decrease of hydrophilicity was observed to be higher on Ar-APP involved processes, it is not significantly different compared to processes using Air-APP. Since both Ar-APP and Air-APP processes developed in this work are capable of preparing a stable surface, silicon specimens treated by these processes were further examined by XPS to evaluate their effects on depositing carboxylic acid functional group.

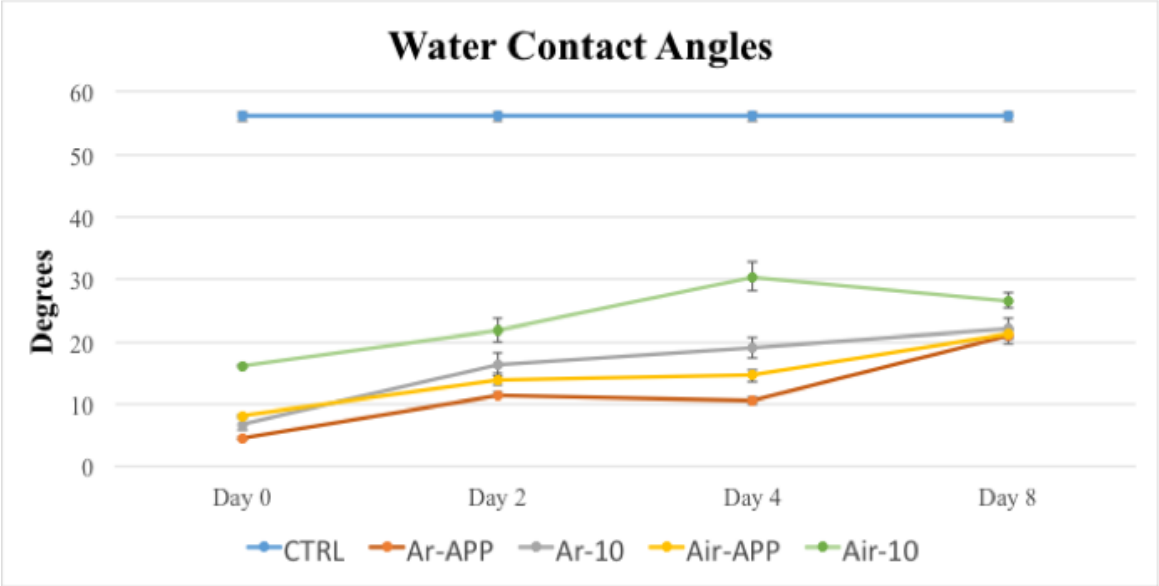

Figure 5.4 WCAs of untreated and APP process treated silicon specimens 2, 4 and 8 days after treatments.

5.3 X-ray photoelectron spectroscopy analyses of functionalized silicon surfaces

In the C1s spectrum, the peak at 285.0 eV stands for C-C and C-H, 286.5 eV for C-OH and C-O-C functional groups, 287.8 eV for O-C-O and C=O groups and 289.2 eV for COOH/COOR groups. In this study, the focus was placed on the intensity of the peak at 289.2 eV to evaluate the carboxylic acid functional groups deposited on the surface, because it not only fits into -COOH components in the C1s spectrum of poly-AAc [139] but is also absent in the C1s core level spectrum of the untreated sample. There might be a concern that the peak at 289.2 eV, which may not only refer to carboxylic acid functional groups (-COOH) but also ester groups (-COOR), is from atmospheric gas as an atmospheric pressure plasma/vapour grafting process was employed in this study. However, the synthesis of ester groups (esterification) requires the reaction of alcohols and carboxylic acids, which requires carboxylic acids to be heated up, while the grafting process presented in this work is a room temperature process without the participation of alcohol groups. To further support this point, TFE derivatization, which is a process for labelling carboxylic acid functional groups, was employed to identify the functional groups after studying XPS results of the C1s core level on neat or APP/AAc-grafted specimens.

XPS results showed that the peak at a binding energy of 289.2 eV was not observed on neat or APP activated silicon wafers but appeared on silicon wafers after APP activation and subsequent AAc vapour grafting. The concern that the peak intensity at 289.2 eV

may be due to the fragmentation of AAc during the plasma process was also considered, as for that reason the bespoke chamber was designed to prevent the precursor from fragmentation. The effect was proven as the silicon treated with AAc directly exposed to plasma glow exhibited a lower 289.2 eV peak intensity compared to silicon functionalized via the process developed in this thesis.

For APP activated silicon, after AAc vapour grafting, the carboxylic acid percentage rose from 3.65% to 19.72% (5-second Ar-APP), 8.75% to 17.33% (10-second Ar-APP) or 15.64% to 20.30% (5-second Air-APP) with the increase of grafting time (Figure 5.5). This showed the capability of this APP functionalization process for immobilizing high percentage of carboxylic acid functional groups, as the theoretical value of pure polyAAc is 33.33% [143].

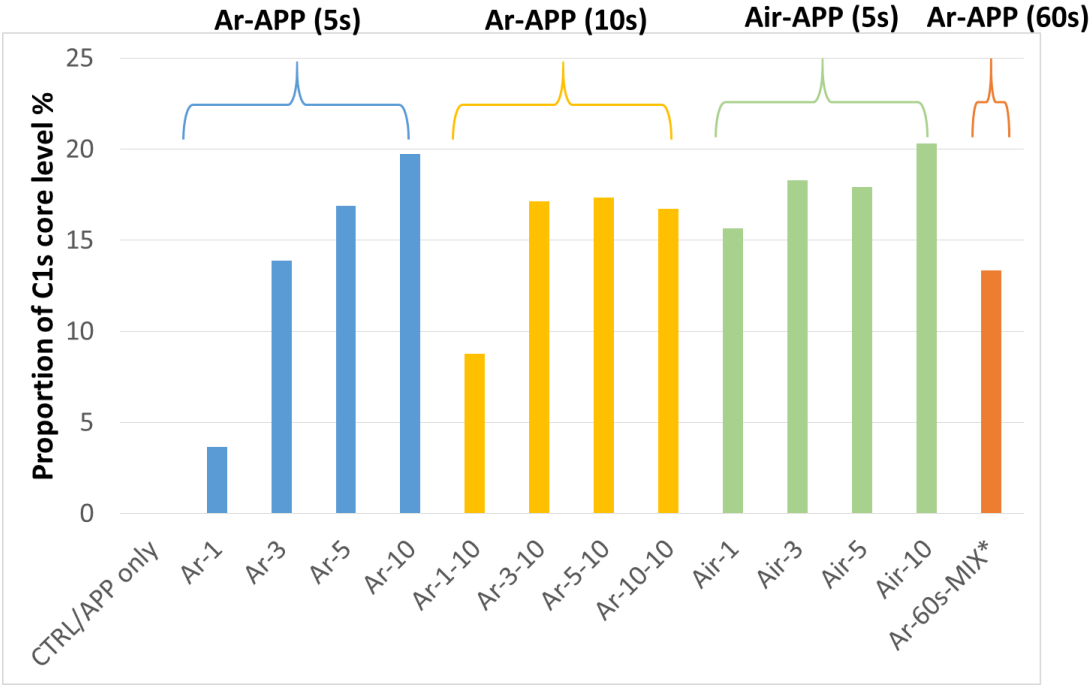

Figure 5.5 Comparison of surface carboxylic acid groups on silicon modified by APP or AAc grafting (XPS: C1s 289.2 eV).

To investigate the differences between this APP functionalization process and the conventional APP process, which exposed the precursor directly to plasma glow, a process was run to functionalize silicon wafers by exposing AAc vapour to Ar-APP. Unlike the process developed in this study, instead of running the APP nozzle for 5 or 10 seconds, it required to operate the APP nozzle for 60 seconds to deposit 13.36% carboxylic acid groups on the silicon surface.

As displayed in Figure 5.5, the Air-APP series were observed to be more efficient at introducing a higher fraction of carboxylic acid functional groups. A relatively higher plasma temperature, compared to Ar-APP, has limited their application on CFs or

polymer materials, which can not bear high temperature. On the other hand, the 5-second Ar-APP series promised a carboxylic acid concentration after a 10-minute AAc grafting (19.72%), which is higher than that of the 10-second Ar-APP (16.33%) and similar to the value of the 5-second Air-APP series with a 10-minute AAc grafting (20.30%). Therefore, the process with a 5-second Ar-APP activation with subsequent 10-minute AAc grafting was employed for the functionalization of CFs.

5.4 X-ray photoelectron spectroscopy analyses of functionalized carbon fibers

From the C1s spectra of functionalized CFs, the atomic percentage of carboxylic acid functional groups increase from 3.7% (1 min AAc grafting) to 4.92% (10 min AAc grafting). This is further supported by the change of the C1s peak pattern. For untreated CFs, due to the lack of functionality on their surfaces, the main C1s graphitic peak shows an asymmetric tailing towards high binding energy, which is referred to as conduction-band interaction and has also been observed on simple metal via XPS [144, 145]. This tailing tended to decrease with an increase degree of CF surface functionalization because the graphitic rings of CFs were altered by oxygen-contained functional groups, which broke up the extended π-electron system which contributes to the conductivity in graphite [144]. Therefore, a decreasing atomic percentage of peaks at binding energies above 291.0 eV, which corresponds to π-π* shake up satellite, after increasing the AAc grafting time from 1 minute to 10 minutes was observed from the

C1s spectra results in this study, suggesting an increased degree of surface functionalization and further supporting the results concluded from the atomic percentage of peak at 289.2 eV.

Compared to the XPS results on silicon surfaces treated under the same parameters, the percentage of carboxylic acid groups decreased on CFs activated by the 5-second Ar-APP with AAc vapour grafting. This may due to the lack of free radicals on the surface due to the conductive nature of CFs, which limits the chance of AAc to react with free radicals or peroxides during AAc vapour grafting, therefore resulting in a lower percentage of carboxylic acid functional groups on the surface.

5.5 TFE derivatization of functionalized surfaces

Figure 4.10 (a) and (b) show the C1s core level spectra from TFE derivatized neat and Ar-APP activated silicon surfaces. From the TFE derivatized neat silicon surface, peaks at binding energies of around 285.0 eV, 286.9 eV and 289.0 eV were found. The intensity of the peaks at around 285.0 eV (79.32%) and 286.9 eV (16.78%) from the derivatized neat silicon surface is similar to the neat silicon specimen, which exhibited atomic ratios of 85.84% at 285.0 eV and 14.16% at 286.9 eV. The presence of a peak at 293.0 eV, which stands for CF_3 and reflects the labelled carboxylic acid groups, was observed. This result proved the reliability of the TFE derivatization process utilized in this research as not only the process did not introduce a significant amount of additional

functional groups on the specimen but also no carboxylic acid groups, which should not exist on the neat silicon surface, was labelled and detected. However, a 3.90% atomic percentage at a binding energy of 289.0 eV, which stands for the presence of -COOR group, was observed. The peak observation at 289.0 eV on the neat surface without carboxylic acid groups has also been reported [146], which might be due to contamination (e.g., stearates) from the solvent or the glass chamber.

After the Ar-APP activated silicon surface was derivatized by TFE, increased atomic ratios at around 286.8 eV and 289.2 eV were spotted. The peak at 286.8 eV, which stands for the C-OH component, was contributed by 2,2,2-trifluoroethanol. The -COOR groups, as described in the case of the TFE-derivatized neat silicon surface, might be the contamination from the solvent or the glass jar. For the Ar-APP activated silicon surface, the presence of free radicals and peroxide groups has made the surface more hydrophilic (4.1±0.3°) than untreated silicon (56.1±0.8°), which has further retained more solvent, including 2,2,2-trifluoroethanol, on the surface after TFE derivatization. Therefore, a higher peak percentage at 286.8 eV and 289.2 eV was observed. Since AAc grafting was not performed here, it is reasonable that no peak at 293.0 eV was found.

For the 5-second Ar-APP activated/10-min AAc-grafted silicon surface, a peak at a binding energy of 292.8 eV was observed after TFE derivatization. The presence of the peak at 292.8 eV indicates the labelled carboxylic acid functional groups, which further

proves that the atmospheric pressure plasma activating/AAc vapour grafting process developed in this project is capable of introducing carboxylic acid functional groups on the specimen surface. Noticeably, a 23.41% peak intensity at 289.08 eV was also detected. In this case, it is presumed that this is contributed by not only the contamination from the solvent/reaction chamber but also by/from carboxylic acid functional groups. Although the derivatization process using TFE/di-tBuC/pyridine is one of the most promising acid labelling techniques, the labelling efficiency, which reflects the percentage of carboxylic acid functional groups this technology is able to label, varies from research to research [135] and can be influenced by the reacting time and the size of reacting chamber. The labelling efficiency has been reported as 75% or 87 ± 15% [147], and the size of the reacting chamber was not the same as used in this project. Moreover, from Figure 4.10 (b), a 10.20% intensity of the 289.19 eV peak can be observed on the carboxylic acid group free silicon surface. In the case of the Ar-APP activated/AAc-grafted silicon surface (Figure 4.10 (c)), assuming that 23.41% of the 289.08 eV peak contains 10.20% of the contamination from the solvent/reaction chamber, the rest (13.21%) may be carboxylic acid groups. In addition to the labelled 5.36%, 18.57% of carboxylic acid functional groups might be actually on the surface, which is similar to the XPS results of silicon surfaces activated by a 5-second Ar-APP with a subsequent 10-min vapour AAc grafting (19.72%), as shown in Figure 4.6 (d).

5.6 Healing efficiency of the ionomer-modified epoxy resin

For the matrix of the self-healing composite, LY 5052 epoxy resin containing 7.5 wt% ionomer healing agent was used, as a higher percentage above 7.5 wt% may cause healing efficiency falling off due to phase separation [128]. The ionomer healing agent is a 4-amino-sodium salicylate end-capped DGEBA. Before being applied as the matrix for the self-reassemble composite, the healing efficiency of this ionomer-modified epoxy resin was examined by the SENB test. Compared to the neat LY 5052 epoxy resin, the ionomer-modified network showed a higher healing efficiency after the first healing event (31.07% to 15.24%) and the trend was more obvious after the second healing event. After the second healing event, the unmodified epoxy network lost the healing function, while the ionomer-modified system still exhibited a healing efficiency of 14.81%.

The 15.24% healing efficiency monitored on the unmodified network after the first event may be due to some continued curing of the epoxy during the healing process, which is able to bind the fracture site of the specimen. However, after the first healing event, the unmodified system lost the healing ability because of the decreased concentration and availability of these reactive groups within the network.

On the other hand, the healing performance of the ionomer-modified system is achieved since ionomer healing agents diffused and entangled on the fracture site. During the

thermo-induced healing event, the ionomer healing agent lost its attractions (hydrogen bonding) with the rigid LY5052 epoxy network, and migrated to the fracture surface. After the temperature started to drop to room temperature, the sodium carboxylate groups on the 4-amino-sodium salicylate end-capped end groups of the ionomer healing agent tended to cluster together and healed the fracture. The SENB results suggest that compared to the neat LY 5052 epoxy resin network, the superior mendable system, which was made in this study through the ionomer-modification, is a potential system to be applied to the matrix for self-healing composite usage.

Although the ionomer-modified epoxy resin developed in this research has exhibited the capability of thermo-induced self-healing, the interaction between the matrix and the fibers is also an important topic to investigate. The approach of preparing a self-healing composite in this study focuses on the ionic bonding between the functional groups of the ionomer healing agent and the fibers. These functional groups are the sodium carboxylate groups, which are at the two ends of the ionomer healing agent (4-amino-sodium salicylate end-capped DGEBA), and carboxylic acid functional groups on the surface of the functionalized CFs. Therefore, this research also investigated the reaction between the Ar-APP/AAc-grafting process introduced carboxylic acid groups and the sodium carboxylate groups from the ionomer healing agent.

5.7 Simulation of potential interface healing using ionomer adsorption

Since the functional groups of the ionomer healing agent are located on the two end-capped groups of the DGEBA, which are end-capped by 4-amino-sodium salicylate, the first approach of examining the effects of the functional groups interaction was carried out by immersing neat or Ar-APP/AAc-grafted silicon specimen in isopropanol with 7.5 wt% of 4-amino-sodium salicylate. Prior to the 4-amino-sodium salicylate immersion, neat and Ar-APP/AAc-grafted silicon specimens were immersed in pure isopropanol and surface elements were identified via XPS to examine the influence of isopropanol on the immersion experiment. It is crucial to monitor the surface atomic percentage of sodium and nitrogen in the immersion experiment, as in this examination these elements only exist in 4-amino-sodium salicylate and the ionomer healing agent (4-amino-sodium salicylate end-capped DGEBA).

The survey spectra of neat and Ar-APP/AAc-grafted silicon specimens after isopropanol immersion is shown in Figure 4.14. Comparing Figure 4.14 (a) to (b), it can be observed that the atomic percentage of carbon on the Ar-APP/AAc-grafted silicon surface (14.56%) is almost double to that on the neat silicon surface (7.96%), which is because of the carboxylic acid functional groups introduced by AAc grafting. The survey spectra of the neat silicon surface after immersion is almost the same as that of the cleaned neat silicon surface, but 0.19% of sodium was observed. It may be contamination from the solvent, because unlike the cleaned silicon wafer surface, which was ultrasonically washed by isopropanol and then subsequently rinsed twice with

HPLC grade water, the neat or Ar-APP/AAc grafted silicon sample was only immersed once in isopropanol and left to dry up before XPS analysis. The elemental percentage of sodium is higher (0.46%) on the Ar-APP/AAc grafted silicon sample than the neat silicon surface (0.19%). As described before, the contamination from the solvent may have contributed to the sodium atomic ratio. This result is reasonable as the Ar-APP/AAc grafted surface is more hydrophilic than the neat silicon surface, which results in retaining more solvent on the surface, thus contains more sodium on the surface. The percentage of sodium on neat or Ar-APP/AAc-grafted silicon surface after isopropanol immersion is minor, but can be a reference for further experiments of 4-amino-sodium salicylate immersion.

Figure 4.15 illustrates the XPS survey spectra of neat and Ar-APP/AAc-grafted silicon surface after 4-amino-sodium salicylate immersion. Similar to the trend in Figure 4.14, the atomic percentage of carbon on the Ar-APP/AAc-grafted silicon surface (33.94%) is higher than that on the neat silicon surface (29.21%), due to the carboxylic acid functional group deposited via AAc-grafting. 0.08 % of sodium was found on the neat silicon surface. This percentage is not only low but also similar to the neat silicon surface immersed in only isopropanol (0.19%, Figure 4.14 (a)). Therefore, the sodium might be contributed not by the 4-amino-sodium salicylate but by the solvent. The survey spectrum of the Ar-APP/AAc-grafted silicon surface (Figure 4.15 (b)) exhibited not only a higher percentage of sodium (5.21%) but also the presence of nitrogen (3.24%). In comparison to the survey spectrum in Figure 4.14 (b), the atomic

percentage of sodium is around 10 times higher on the Ar-APP/AAc-grafted silicon surface after 4-amino-sodium salicylate immersion. Additionally, 3.24% nitrogen, which can only be contributed by the 4-aminosalicylic acid sodium salt in this examination, was observed only on the Ar-APP/AAc-grafted silicon surface. Because of the absence of carboxylic acid functional groups on the neat silicon surface, 4-amino-sodium salicylate, which was not ionically bonded to the surface, was washed out after immersion. In contrast, 4-amino-sodium salicylate was retained and observed on the Ar-APP/AAc-grafted silicon surface, which contains carboxylic acid functional groups, suggesting that functional group reactions, which play an important role in self-healing, happened between the 4-amino-sodium salicylate and the carboxylic acid groups.

To further support the hypothesis and concept of the self-healing mechanism in this study, another approach was executed to study the effects of functional groups reaction between the ionomer healing agent and the fiber for the simulation of potential interface healing. Previous results from this study have proven that carboxylic acid functional groups are capable of being ionically bonded to sodium carboxylate groups from 4-aminosalicylic acid sodium salt. However, it is still necessary to estimate the effects of the binding when carboxylic acid functional groups react with the ionomer healing agent, as the backbone of the ionomer healing agent is DGEBA, and when it comes to the mechanical aspect, it is the ionomer healing agent (4-amino-sodium salicylate end-capped DGEBA) that will be utilized. Thus, in the second approach, neat and Ar-APP/AAc-grafted silicon specimens were immersed in isopropanol containing 7.5 wt%

ionomer healing agent, then washed by isopropanol and examined by XPS.

Comparing the surface elements of the neat silicon to the Ar-APP/AAc-grafted silicon surface after ionomer immersion (Figure 4.16), much more carbon (43.66%) was observed on the AAc-grafted surface than on the neat surface (13.85%). Although this trend is similar to the survey spectra of the 4-amino-sodium salicylate immersion test (Figure 4.15), the difference in the percentage is larger after the ionomer immersion. From Figure 4.15, the percentage difference of carbon is 4.73%, as the result of 33.94% (Ar-APP/AAc-grafted silicon surface) - 29.21% (neat silicon surface), while in the case of ionomer immersion, is 29.81%, as the result of 43.66% (Ar-APP/AAc-grafted silicon surface) - 13.85% (neat silicon surface). This may be due to the retaining of the DGEBA-based ionomer healing agent, which contains a higher percent of carbon. The atomic percentage of sodium after ionomer immersion is 0.71% on the neat silicon surface and 5.80% on the Ar-APP/AAc-grafted silicon surface, which is similar to the 4-amino-sodium salicylate immersion test. Noticeably, the survey spectrum showed 1.73% of nitrogen, which was not identified on the neat silicon surface. Higher atomic ratios of carbon and sodium and the presence of nitrogen suggest that the potential of utilizing the plasma/grafting process developed in this study to manufacture a self-healing composite material.

This suggestion was further supported after estimating the effects of the functional groups reaction between the ionomer healing agent and the neat or Ar-APP/AAc-

grafted CFs, as shown in Figure 4.17. A small percentage of sodium (0.50%) was spotted on the neat CFs, which may be due to contamination, as described before. Although this phenomenon has happened on the neat silicon wafer or the CFs after every immersion test, the atomic percentage of sodium was below 1.0% in each case. The Ar-APP/AAc-grafted CFs contain more carbon (77.23%) and sodium (2.96%) than the neat CFs (74.49% carbon and 0.50% sodium) after ionomer immersion. Furthermore, nitrogen (2.13%) has been observed only on the Ar-APP/AAc-grafted CFs after ionomer immersion. The signals of both nitrogen and sodium on AAc-grafted CFs were found similar but slightly weaker than that on the AAc-grafted silicon wafer (shown in Figure 4.16). This fits the trend of the carboxylic acid functional group percentage introduced on the surface, as under the same parameter (a 5-sec Ar-APP activation with a 10-minute AAc grafting), a higher percentage of the functional group was identified on the silicon wafer surface, as described before.

Taking into account the higher atomic percentage of carbon, sodium and the presence of nitrogen, these results indicate that compared to the neat CFs, the functionalized CFs, due to the presence of carboxylic acid groups on them, are able to react with the functional (sodium carboxylate) groups from the ionomer.

5.8 Interfacial healing performance

The capability of the functional group reactions between carboxylic acid groups (from APP-functionalized CFs) and sodium carboxylate groups (from ionomer healing agent) was proven from the results of ionomer adsorption. The ability of interfacial healing between the APP-functionalized CFs and the ionomer-modified epoxy resin in a composite was further demonstrated by observing the interface of the composite before and after healing events (Figure 4.18). It can be observed that after the healing event(s), the functionalized CF/ionomer modified epoxy resin matrix interface was healed. However, in this case, the healing performance might be dominated by the healing ability of the ionomer-modified epoxy resin matrix, which has been proved via estimating the healing efficiency. Therefore, although the results from the interfacial healing performance and simulation via XPS showed a strong potential of interfacial healing between the functionalized CFs and ionomer-modified epoxy resin, further study would be required to confirm the effects.

These results indicate that the development of a novel and rapid APP process for CF functionalization, an ionomer healing system and a potential self-healing composite prepared by the APP-functionalized CFs and the ionomer-modified epoxy resin were achieved. As the carboxylic acid groups on the CFs have been reported to possess potential for improving interfacial adhesion, tensile strength and modulus when being utilized in composite material [12, 13], the preparation of a self-healing composite

material with enhanced mechanical properties can be envisaged via employing this novel Ar-APP/AAc-grafting technique and ionomer self-healing process developed in this study.

Chapter 6 Summary, Conclusions and Recommendations for Future Works

6.1 Summary and conclusions

This project aimed towards developing a novel atmospheric pressure plasma process for controlling surface functional groups on CFs, which can be applied to manufacturing self-healing composites with enhanced load carrying capacities. CFs and silicon wafers were functionalized via an APP and AAc vapour grafting to immobilize carboxylic acid functional groups on the surface, and the epoxy resin was modified by an ionomer system developed by end-capping DGEBA with 4-amino-sodium salicylate.

The study can be summarized into seven stages:

1. Design of a bespoke plasma chamber.

2. Examination of the effects of Ar- or Air-APP combined with AAc vapour grafting on the carboxylic acid functional group deposition.

3. Estimation of the effects of introducing carboxylic acid functional group on CFs via the Ar-APP/AAc grafting process.

4. Identification of carboxylic acid functional groups on the surface via TFE derivatization, which showed that –COOH are introduced without significant reorganization in –COOR.

5. Preparation of a healing agent and examination of the healing efficiency.

6. Investigation of functional groups reaction between the grafted surface and the ionomer healing agent to estimate the interface self-healing mechanism designed in this study.

7. Observation of potential interfacial healing performance between the APP-functionalized CFs and the ionomer-modified epoxy resin matrix after healing events.

The design of the chamber is based on the idea of separating the plasma activating and vapour grafting zones to prevent precursor fragmentation and further retain a higher percentage of functional groups. The idea was supported by the XPS results on silicon surfaces as an increasing atomic percentage of carboxylic acid group has been observed, compared to a conventional atmospheric pressure plasma which directly exposes the precursor to a plasma glow. Noticeably, a 19.72% carboxylic acid atomic percentage was achieved in this study, compared with the theoretical value of 33.3% [143].

The Ar-APP, compared to the Air-APP, showed a lower temperature and a higher chance to keep the bulk properties of the specimens. Therefore, it was further employed with subsequent AAc vapour grafting for functionalizing of the CFs. The result indicated that this process can introduce carboxylic acid functional groups on not only the silicon surface, which was also identified via TFE derivatization, but also on the unsized CFs.

An ionomer self-healing system using 4-amino-sodium salicylate end-capped DGEBA as healing agent has also been examined. The results indicate that the functional groups on the two end groups of the healing agent can ionically bond not only to each other to heal the crack in the matrix, but also to the carboxylic acid functional group, suggesting the potential to repair the debonding and heal the interfaces between the matrix and the fibers.

To sum up, in this work a novel, rapid process was developed, which utilizes APP activation and AAc vapour grafting in a bespoke Pyrex chamber, in order to introduce carboxylic acid functional groups on the surface. A thermo-induced ionomer self-healing system was also used and the sodium carboxylate functional groups on the healing agent proved to be able to react with the APP/AAc-grafted carboxylic acid functional groups. Combining this novel APP process with the ionomer self-healing system, this study developed a potential self-healing composite material with enhanced load carrying capacity.

6.2 Recommendations for future work

As described in the literature review (Chapter 2), the chemically inert surface of CFs leads to weak interfacial adhesion between the CFs and the matrix, which results in

debonding and poor mechanical performance of a composite. To address this issue, surface functionalization on CFs is required to optimize the interfacial adhesion between the CFs and the matrices. This thesis reported a novel and rapid approach to this problem by introducing carboxylic acid functional groups on the CFs. The immobilized carboxylic acid functional groups were observed as being capable of reacting with the ionomer-modified epoxy resin to heal the interfacial debonding.

Previous studies [12, 13] have reported that the presence of carboxylic acid functional groups on CFs improves interfacial adhesion, tensile strength and modulus when the CFs are utilized in a composite material. Therefore, it would be interesting to look into the effects of the APP-functionalization (introduction of carboxylic acid groups) and the ionomer-modification on tailoring the interfacial adhesion.

As for the demonstration of the interfacial healing and adhesion performance of the APP-functionalized CFs (introduction of carboxylic acid groups) and the ionomer-modified matrix, some studies have only been partially completed. Further work on short beam shear tests and transverse bundle tests are needed to confirm the results presented here.

6.2.1 Short beam shear test

The interfacial shear strength can be evaluated via a short beam shear test to investigate the effects of APP functionalized CFs on controlling the adhesion property in the composite. Specimens were prepared according to ASTM D2344 with dimensions of 16 mm x 16 mm x 48 mm. The dimensions of the samples were planned after taking the minimal span length of the universal tester and the access availability of the positive mould for preparing the negative mould for short beam shear tests in this work into account. The silicone mould for the short beam shear test, which was tailored for in this work, comprises an upper part (hollow) and a lower part (with a sealed bottom) (Figure 6.1 (a)). Both the upper and the lower parts had a rectangular cavity with dimensions of 8 mm x 16 mm x 48 mm.

CF bundles (60 mm in length, 3 mm in width and 1 mm in thickness) with/without functionalization were selected and put longitudinally into the middle of two silicone rubber moulds to ensure the bundle is in the central position of the specimen (Figure 6.1 (b)), followed by pouring a resin mixture gently into the cavity (Figure 6.1 (c)), then placed into a vacuum oven at room temperature for 10 minutes to avoid bubbles forming inside the resin mixture. The details of preparing the resin mixture was described in Chapter 3.7. A comparison of the interfacial shear strength between composite samples made by different parameters (Figure 6.1 (c)), including neat CF/neat epoxy resin, neat CF/ionomer-modified epoxy resin, functionalized CF/neat

epoxy resin and functionalized CF/ionomer-modified epoxy resin should be studied in the future.

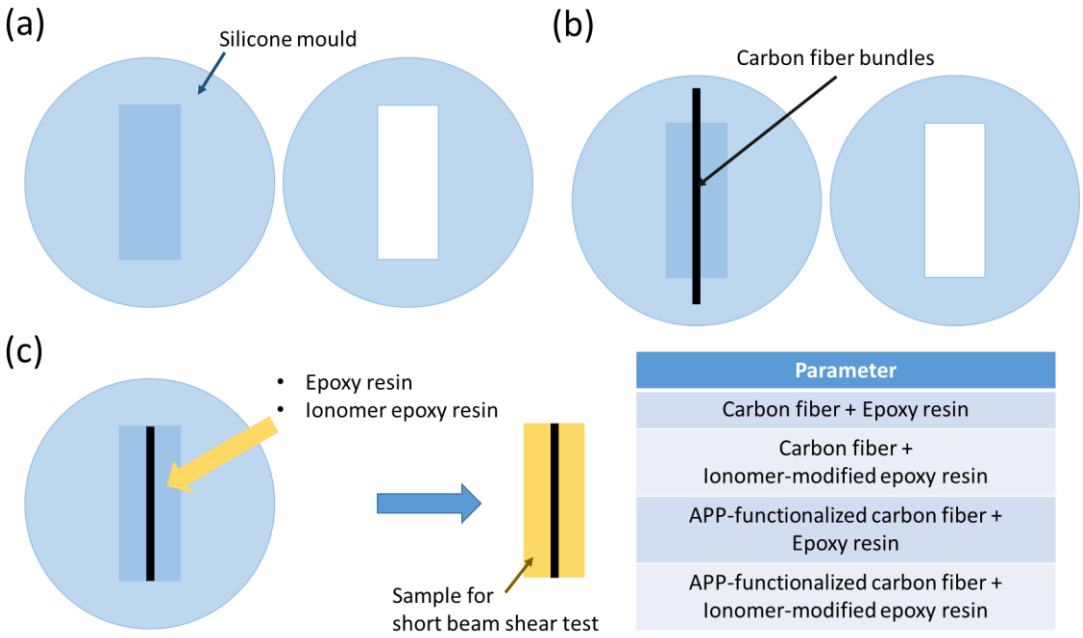

Figure 6.1 The preparation diagram for short beam shear test samples.

The interfacial shear strength of the CF composites should be recorded by a universal tester applying the ASTM D 2344 standard test for reinforced polymer specimens. Based on this standard, the loading speed should be determined to be 1 mm/min, while the span-to-thickness ratio is 4.0 to an accuracy of ±0.3 mm. During the test, it is very important to ensure: (1) The specimen is placed symmetrically on the support rollers. (2) The loading roller operates precisely with the route vertically to the centreline of the sample.

The interfacial shear strength can be calculated from:

$$ILSS = 0.75\ P/wt$$

where w refers to the width of specimen cross-section (m), P to the maximum failure load (N), t to the specimen thickness (m).

Figure 6.2 shows the images of the development of the silicone mould and the short beam shear test sample prepared by it. Both the upper and the lower parts had a rectangular cavity with dimensions 8 mm x 16 mm x 48 mm and were manufactured in round petri dishes with flat bottoms. Therefore, a plane short beam shear test sample surface was achieved.

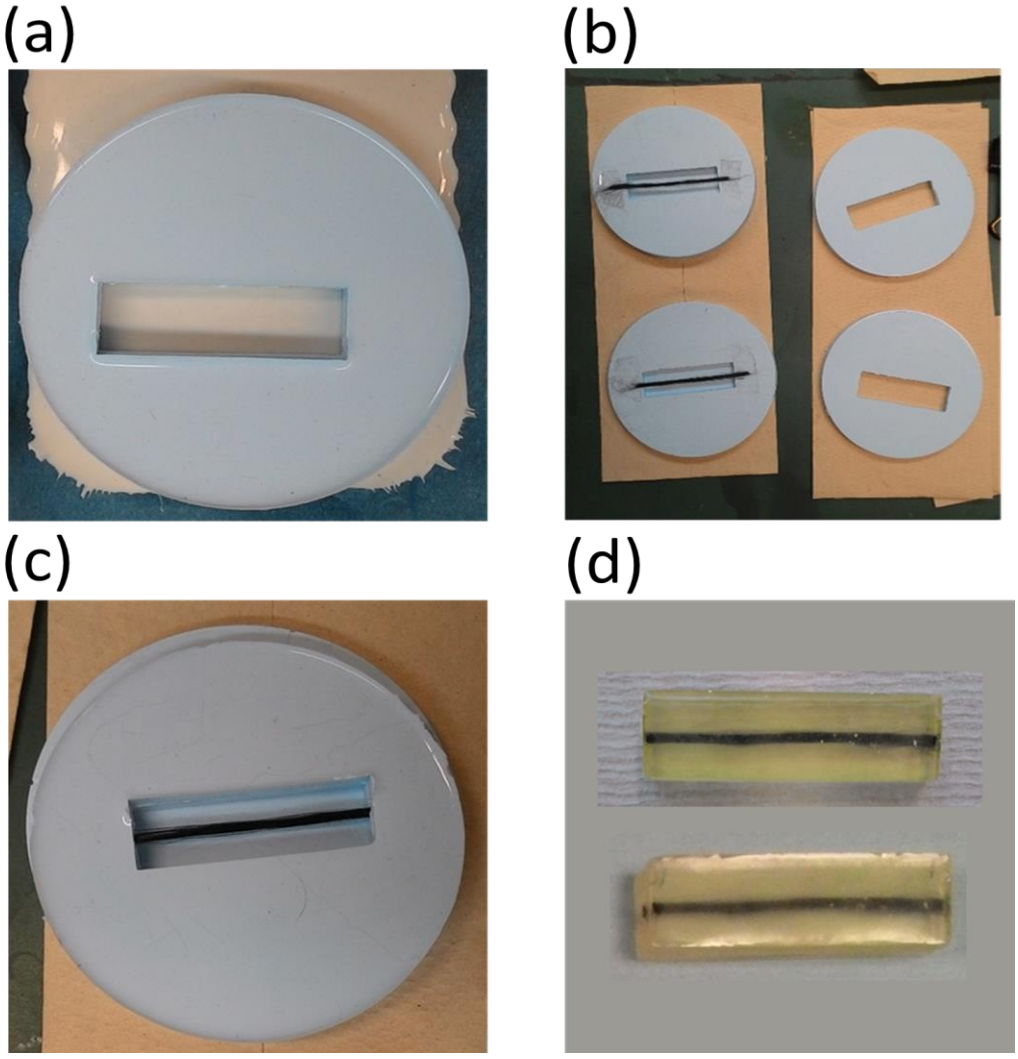

Figure 6.2 Images of (a, b, c) the development of the silicone mould and (d) the short beam shear test sample prepared by it.

The maximum load the universal tester employed in this study could offer was 500 N. However, the results of short beam shear test revealed that 500 N was not able to load the samples to failure. Therefore, the interfacial shear strength of the composites

prepared in this work were not collected and required a tester being capable to offer a higher load or a shorter span length.

6.2.2 Transverse bundle test

After the healing efficiency of the ionomer-modified network has been confirmed by the SENB test, transverse bundle tests should be utilized to demonstrate the effects of AP functionalized CFs on the interface healing with the ionomeric healing agents. Samples were prepared with dimensions of 2 mm x 25 mm x 75 mm, using four kinds of parameters (neat CF/neat epoxy resin, neat CF/ionomer modified epoxy resin, functionalized CF/neat epoxy resin and functionalized CF/ionomer modified epoxy resin) (Figure 6.3 and Table 6.1). CF bundles (2 mm in width) were placed transversely in the centre of the specimen and both ends of the sample were tabbed with glass fiber mats to prevent slipping between the grips and the specimens.

The principle is to apply uniaxial tension to the composite to create a debonding between the bundle and the matrix. By monitoring the debonding site before and after the healing process and recording the tensile strength which leads to the first debonding, not only the healing function but also whether a better interfacial shear strength has been achieved can be studied by comparing neat and modified specimens.

Tensile stress should be applied to the specimen via a universal tensometer (loading

speed: 10 mm/min) and stopped when the first debonding between the CF bundle and the matrix is observed under the microscope attached to the tensometer (Figure 6.4). The specimen with debonding should then be heated up in the vacuum oven under 120°C for 4 hours to execute thermo-induced self-healing process. The specimen should be examined under the microscope again to see whether the debonding has been fixed.

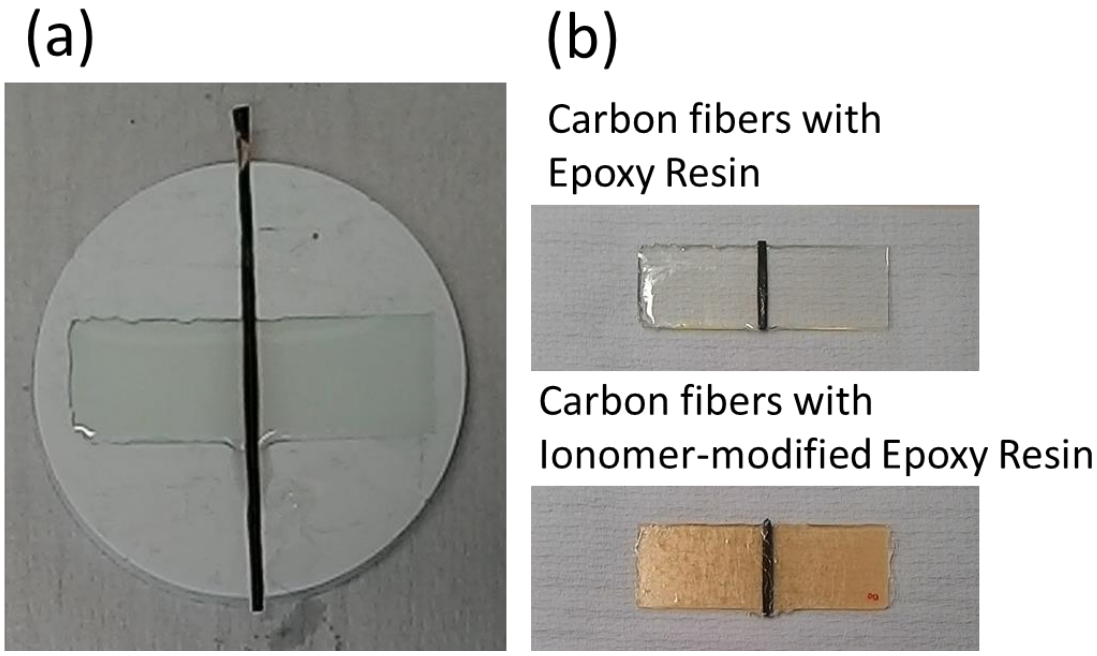

Figure 6.3 Images of (a) SENB sample preparation (b) SENB samples before surface polishing.

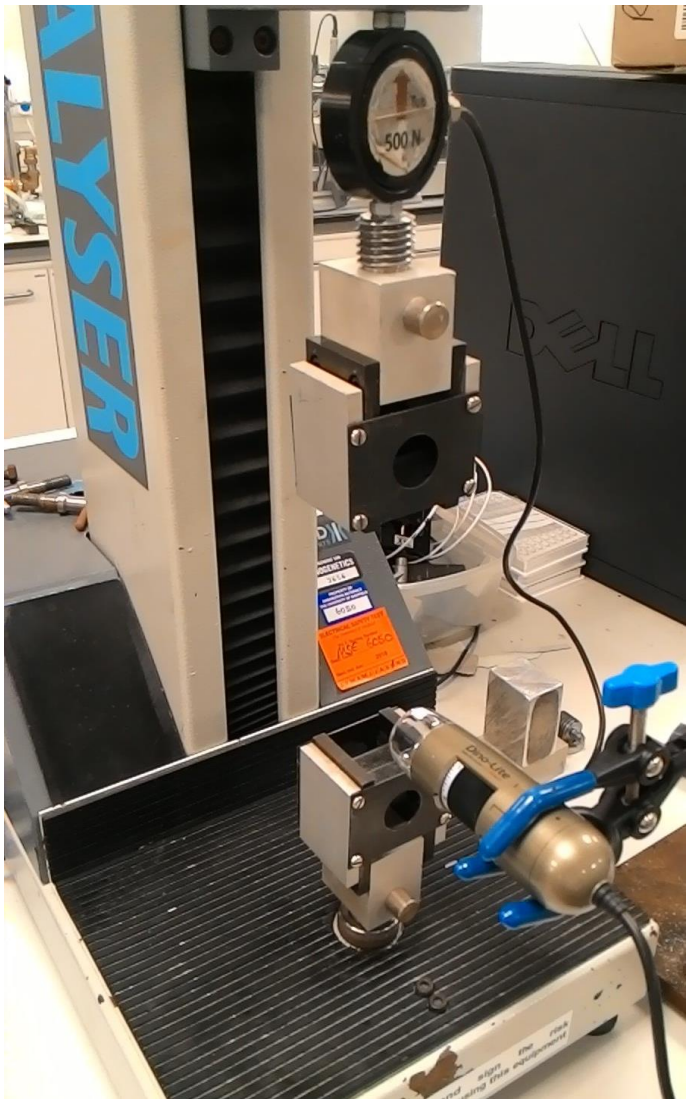

Figure 6.4 Image of the tensometer with microscope attached.

Table 6.1 Parameters of sample preparation for transverse bundle test.

Parameters
Carbon fiber + Epoxy resin
Carbon fiber + Ionomer-modified epoxy resin
APP-functionalized carbon fiber + Epoxy resin
APP-functionalized carbon fiber + Ionomer-modified epoxy resin

6.2.3 Further applications of the atmospheric pressure plasma functionalization process

The APP functionalization process presented in this work could also be applied to the functionalization of carbon nanotubes (CNTs).

CNTs have excellent mechanical properties, which make them ideal materials for reinforcing epoxy resin composites. However, because of certain characteristics of CNTs, including high aspect ratio and intrinsic van der Waals forces between CNTs, they are highly entangled bundles, which are difficult to be dispersed into a polymer matrix. Moreover, the chemically inert nature of CNTs limits their interfacial interaction with a polymer matrix. In order to solve this problem, surface functionalization of CNTs has been widely investigated.

Similar to the functionalization of CFs, the oxidation of CNTs via treatment under strongly acidic conditions was used to functionalize them [148, 149]. The introduced carboxylic acid groups react with epoxide groups from an epoxy resin matrix to form a strong bond. This improves the interfacial interaction of the CNTs with an epoxy matrix, leading to efficient dispersion of the CNTs. However, the structure of the CNTs may be damaged by this acidic functionalization process due to etching of the graphitic surface of the material [150], which is also not environmentally friendly.

Since the reason for and issues in the functionalization of CNTs share many

similarities with the functionalization of CFs, utilizing the APP process in the functionalization of CNTs would be a beneficial option.

The APP process could be utilized to functionalize polymers for hydroxyapatite deposition. Hydroxyapatite has good biocompatibility and osteoconductivity and is suitable to be coated on the surfaces of medical implants. However, the inert surface of the polymer implant material has limited the deposition of hydroxyapatite on it. The presence of carboxylic acid groups on polymer surfaces has been shown to be beneficial for the adhesion between the hydroxyapatite and the substrates. By employing the APP process for introducing carboxylic acid functional groups on polymers, it is expected to improve the efficiency and the quantity (due to a higher percentage of carboxylic acid groups on the substrate) of hydroxyapatite deposition.

Other than the deposition of hydroxyapatite, the immobilization of chitosan is also a popular method for improving surface biocompatibility. Because of the characteristics of chitosan, including its non-toxic, biocompatible and biodegradable natures, it has been applied to the preparation of cell scaffolds and drug delivery systems for cancer therapies [151]. It has been demonstrated by Chen et al. [152] that immobilized carboxylic acid groups covalently bonded with chitosan through 1-Ethyl-3-(3-dimethylaminopropyl) carbodiimide/N-hydroxysuccinimide crosslinking agents, then an improved biocompatibility was observed from the results of the 3-(4,5-dimethylthiazol-2-yl)-2,5-diphenyltetrazolium bromide (MTT) assay. In this study

[152], a 5-minute low-pressure plasma treatment and a 20-minute grafting process was applied to immobilize carboxylic acid groups, whereas by utilizing the APP process developed in this thesis, it is expected that the functionalization time for the immobilization can be shorten by a factor of 2.5.

The idea of using the APP process to shorten the functionalization time for introducing carboxylic acid functional groups can be further utilized on environmental engineering aspects.

Chen et al. [153] grafted carboxylic acid groups on bamboo charcoals to achieve the function of ammonia adsorption on them. Compared to an untreated sample, the ammonia adsorption ability of functionalized bamboo charcoal was found to improve from 61% to 98%. In that work, bamboo charcoals were treated by two low-pressure plasmas (to prepare a hydrophilic surface) and a UV grafting process to introduce carboxylic groups. By performing the APP process, functionalization of bamboo charcoals can be accomplished and made ready for further application in the sample chamber with a shorter treatment time.

The APP/AAc-grafting process possesses not only the potential for use in composite materials but also prospective applications for bioengineering, biocompatibility improvement and environmental engineering.

The APP process developed in this thesis comprised of an APP nozzle for surface activation and a grafting process for introducing functional groups. The Ar- or Air-APP activation is capable of tailoring surface wettability, which improves surface hydrophilicity. For sterilization of medical tools (e.g., scalpels), the APP activation can be applied to clean the surfaces by introducing free radicals for anti-bacterial purposes. The process also has possibilities in the textile industry. For example, by performing the APP activation in the dyeing process, the dyeing efficiency on the linen is expected to be improved due to a more hydrophilic surface of the linen. By improving the hydrophilicity of polymer materials, their surfaces would be more suitable for spin-coating (e.g., of TiO_2 on them to prepare an antibacterial function on them).

To sum up, there are many possible applications for this technology and it is recommended to carry out further studies based on the APP process developed in this work.

References

1. J.B. Donnet and R.C. Bansal, *Carbon Fibers.* Marcel Dekker, Inc., 1990.
2. W.S. Smith, *Engineered Materials Handbook-Vol. 1.* ASM International Ohio, 1987:49.
3. S.J. Park and B.J. Kim, *Roles of acidic functional groups of carbon fiber surfaces in enhancing interfacial adhesion behavior.* Materials Science and Engineering a-Structural Materials Properties Microstructure and Processing, 2005. **408**(1-2):269-273.
4. H. Dvir, J. Jopp, and M. Gottlieb, *Estimation of polymer-surface interfacial interaction strength by a contact AFM technique.* Journal of Colloid and Interface Science, 2006. **304**(1):58-66.
5. J. Harvey, C. Kozlowski, and P.M.A. Sherwood, *X-Ray Photoelectron Spectroscopic Studies of Carbon-Fiber Surfaces .6. Pilot-Plant Surface-Treatment and Epoxy-Resin Composites.* Journal of Materials Science, 1987. **22**(5):1585-1596.
6. T.R. King, D.F. Adams, and D.A. Buttry, *Anodic-Oxidation of Pitch-Precursor Carbon-Fibers in Ammonium-Sulfate Solutions - the Effect of Fiber Surface-Treatment on Composite Mechanical-Properties.* Composites, 1991. **22**(5):380-387.
7. S. Yumitori and Y. Nakanishi, *Effect of anodic oxidation of coal tar pitch-based carbon fibre on adhesion in epoxy matrix .1. Comparison between H2SO4 and NaOH solutions.* Composites Part a-Applied Science and Manufacturing, 1996. **27**(11):1051-1058.
8. A. Fukunaga and S. Ueda, *Anodic surface oxidation for pitch-based carbon fibers and the interfacial bond strengths in epoxy matrices.* Composites Science and Technology, 2000. **60**(2):249-254.
9. B.W. Chun, C.R. Davis, Q.A. He, and R.R. Gustafson, *Development of Surface-Acidity during Electrochemical Treatment of Pan-Carbon Fibers.* Carbon, 1992. **30**(2):177-187.
10. M.J. Sun, B.R. Hu, Y.S. Wu, Y. Tang, W.Q. Huang, and Y.X. Da, *The Surface of Carbon-Fibers Continuously Treated by Cold-Plasma.* Composites Science and Technology, 1989. **34**(4):353-364.

11. R.Z. Li, L. Ye, and Y.W. Mai, *Application of plasma technologies in fibre-reinforced polymer composites: A review of recent developments.* Composites Part a-Applied Science and Manufacturing, 1997. **28**(1):73-86.
12. N. Lopattananon, S.A. Hayes, and F.R. Jones, *Stress transfer function for interface assessment in composites with plasma copolymer functionalized carbon fibres.* Journal of Adhesion, 2002. **78**(4):313-350.
13. K.K.C. Ho, S. Bai, G. Knox, and A. Bismarck, *Impact of Continuous Atmospheric Pressure Plasma Polymerization of Acrylic Acid on the Interfacial Properties of Carbon Fibre - RFL Elastomer Composites.* 15th EUROPEAN CONFERENCE ON COMPOSITE MATERIALS, 2012.
14. J.W.C. Pang and I.P. Bond, *A hollow fibre reinforced polymer composite encompassing self-healing and enhanced damage visibility.* Composites Science and Technology, 2005. **65**(11-12):1791-1799.
15. R.S. Trask, G.J. Williams, and I.P. Bond, *Bioinspired self-healing of advanced composite structures using hollow glass fibres.* Journal of the Royal Society Interface, 2007. **4**(13):363-371.
16. R.S. Trask and I.P. Bond, *Biomimetic self-healing of advanced composite structures using hollow glass fibres.* Smart Materials & Structures, 2006. **15**(3):704-710.
17. S.H. Cho, H.M. Andersson, S.R. White, N.R. Sottos, and P.V. Braun, *Polydimethylsiloxane-based self-healing materials.* Advanced Materials, 2006. **18**(8):997-+.
18. J.L. Yang, M.W. Keller, J.S. Moore, S.R. White, and N.R. Sottos, *Microencapsulation of Isocyanates for Self-Healing Polymers.* Macromolecules, 2008. **41**(24):9650-9655.
19. H.P. Wang, Y.C. Yuan, M.Z. Rong, and M.Q. Zhang, *Self-Healing of Thermoplastics via Living Polymerization.* Macromolecules, 2010. **43**(2):595-598.
20. S.A. Hayes, F.R. Jones, K. Marshiya, and W. Zhang, *A self-healing thermosetting composite material.* Composites Part a-Applied Science and Manufacturing, 2007. **38**(4):1116-1120.
21. X.F. Luo, R.Q. Ou, D.E. Eberly, A. Singhal, W. Viratyaporn, and P.T. Mather, *A*

Thermoplastic/Thermoset Blend Exhibiting Thermal Mending and Reversible Adhesion. Acs Applied Materials & Interfaces, 2009. **1**(3):612-620.

22. R.J. Varley and S. van der Zwaag, *Towards an understanding of thermally activated self-healing of an ionomer system during ballistic penetration.* Acta Materialia, 2008. **56**(19):5737-5750.
23. J.A. Syrett, C.R. Becer, and D.M. Haddleton, *Self-healing and self-mendable polymers.* Polymer Chemistry, 2010. **1**(7):978-987.
24. R.J. Varley, B. Dao, C. Pillsbury, S.J. Kalista, and F.R. Jones, *Low-molecular-weight thermoplastic modifiers as effective healing agents in mendable epoxy networks.* Journal of Intelligent Material Systems and Structures, 2014. **25**(1):107-117.
25. M.M. Tang and R. Bacon, *Carbonization of Cellulose Fibers .1. Low Temperature Pyrolysis.* Carbon, 1964. **2**(3):211-&.
26. J. Liu, P.H. Wang, and R.Y. Li, *Continuous carbonization of polyacrylonitrile-based oxidized fibers: Aspects on mechanical properties and morphological structure.* Journal of Applied Polymer Science, 1994. **52**(7):945-950.
27. M.S.A. Rahaman, A.F. Ismail, and A. Mustafa, *A review of heat treatment on polyacrylonitrile fiber.* Polymer Degradation and Stability, 2007. **92**(8):1421-1432.
28. E. Fitzer, *Pan-based carbon fibers—present state and trend of the technology from the viewpoint of possibilities and limits to influence and to control the fiber properties by the process parameters.* Carbon, 1989. **27**(5):621-645.
29. S. Chand, *Carbon fibers for composites.* Journal of Materials Science, 2000. **35**(6):1303-1313.
30. F.A. Smith, T.F. Eckle, R.J. Osterholm, and R.M. Stichel, *Manufacture of coal tar and pitches*. Bituminous materials, ed. A.J. Hoiberg. Vol. 3. 1966, New York, USA: Interscience.
31. N.M.A.B.C. Report, *High Performance Synthetic Fibers for Composites.* 1992:54.
32. S. Schimmelpfennig and B. Glaser, *One Step Forward toward Characterization: Some Important Material Properties to Distinguish*

Biochars. Journal of Environmental Quality, 2012. **41**(4):1001-1013.

33. X. Huang, *Fabrication and Properties of Carbon Fibers.* Materials, 2009. **2**(4).
34. S. Kumar, D.P. Anderson, and A.S. Crasto, *Carbon-Fiber Compressive Strength and Its Dependence on Structure and Morphology.* Journal of Materials Science, 1993. **28**(2):423-439.
35. V. Tunakova and J. Gregr, *Electrical conductivity measurement of fibers and yarns*, in *7th International Conference - TEXSCI 2010*. 2010.
36. K.W. Lafdi, M.A., *Carbon fibers*. 2nd ed. Handbook of Composites, ed. S.T. Peters. 1998, London, UK: Chapman & Hall.
37. A.H. Shinohara, T. Sato, F. Saito, T. Tomioka, and Y. Arai, *A Novel Method for Measuring Direct Compressive Properties of Carbon-Fibers Using a Micromechanical Compression Tester.* Journal of Materials Science, 1993. **28**(24):6611-6616.
38. G.J. Hayes, D.D. Edie, and J.M. Kennedy, *The Recoil Compressive Strength of Pitch-Based Carbon-Fibers.* Journal of Materials Science, 1993. **28**(12):3247-3257.
39. M. Furuyama, M. Higuchi, K. Kubomura, H. Sunago, H. Jiang, and S. Kumar, *Compressive Properties of Single-Filament Carbon-Fibers.* Journal of Materials Science, 1993. **28**(6):1611-1616.
40. V.R. Mehta and S. Kumar, *Temperature-Dependent Torsional Properties of High-Performance Fibers and Their Relevance to Compressive Strength.* Journal of Materials Science, 1994. **29**(14):3658-3664.
41. S. Kumar, W.W. Adams, and T.E. Helminiak, *Uniaxial Compressive Strength of High Modulus Fibers for Composites.* Journal of Reinforced Plastics and Composites, 1988. **7**(2):108-119.
42. M. Miwa, Y. Liu, H. Tsuzuki, A. Takeno, and A. Watanabe, *Relation between axial compressive strength of reinforcing fibres and fibre diameter.* Journal of Materials Science, 1996. **31**(2):499-506.
43. E. Frank, F. Hermanutz, and R. Buchmeiser Michael, *Carbon Fibers: Precursors, Manufacturing, and Properties.* Macromolecular Materials and Engineering, 2012. **297**(6):493-501.
44. H. Patel Rasmika and G. Patel Ranjan, *Carbon fibre reinforced epoxy*

composites. Polymer International, 1993. **30**(3):301-303.

45. D. Feldman, *Some Considerations on Thermosetting Polymers as Matrices for Composites.* Progress in Polymer Science, 1990. **15**(4):603-628.
46. V. Çeçen, M. Sarikanat, H. Yildiz, and H. Tavman Ismail, *Comparison of mechanical properties of epoxy composites reinforced with stitched glass and carbon fabrics: Characterization of mechanical anisotropy in composites and investigation on the interaction between fiber and epoxy matrix.* Polymer Composites, 2008. **29**(8):840-853.
47. H.A. Maples, S. Wakefield, P. Robinson, and A. Bismarck, *High performance carbon fibre reinforced epoxy composites with controllable stiffness.* Composites Science and Technology, 2014. **105**:134-143.
48. W.H. Lee, J.G. Lee, and P.J. Reucroft, *XPS study of carbon fiber surfaces treated by thermal oxidation in a gas mixture of O-2/(O-2+N-2).* Applied Surface Science, 2001. **171**(1-2):136-142.
49. A. Fukunaga, S. Ueda, and M. Nagumo, *Air-oxidation and anodization of pitch-based carbon fibers.* Carbon, 1999. **37**(7):1081-1085.
50. R.V. Subramanian and J.J. Jakubowski, *Electropolymerization on Graphite Fibers.* Polymer Engineering and Science, 1978. **18**(7):590-600.
51. J.M. Park, Y.M. Kim, K.W. Kim, and D.J. Yoon, *Interfacial aspects of electrodeposited carbon fiber-reinforced epoxy composites using monomeric and polymeric coupling agents.* Journal of Colloid and Interface Science, 2000. **231**(1):114-128.
52. C.L. Hamermesh and P.J. Dynes, *Effect of Plasma Polymerization on Wettability of Surfaces.* Journal of Polymer Science Part C-Polymer Letters, 1975. **13**(11):663-668.
53. J.P. Bell, J. Chang, H.W. Rhee, and R. Joseph, *Application of Ductile Polymeric Coatings onto Graphite Fibers.* Polymer Composites, 1987. **8**(1):46-52.
54. W.J. Tomlinson and R.S. Barnes, *Fiber Coatings and the Mechanical-Properties of Carbon-Fiber Nylon-6 Composites.* Journal of Materials Science Letters, 1992. **11**(8):440-442.
55. R.H. Bradley, X. Ling, and I. Sutherland, *An Investigation of Carbon-Fiber Surface-Chemistry and Reactivity Based on Xps and Surface Free-Energy.* Carbon, 1993. **31**(7):1115-1120.

56. N. Dilsiz and J.P. Wightman, *Effect of acid-base properties of unsized and sized carbon fibers on fiber/epoxy matrix adhesion.* Colloids and Surfaces a-Physicochemical and Engineering Aspects, 2000. **164**(2-3):325-336.
57. Y.L. Huang and R.J. Young, *Analysis of the Fragmentation Test for Carbon-Fiber Epoxy Model Composites by Means of Raman-Spectroscopy.* Composites Science and Technology, 1994. **52**(4):505-517.
58. J.D.H. Hughes, *The Carbon-Fiber Epoxy Interface - a Review.* Composites Science and Technology, 1991. **41**(1):13-45.
59. J. Li, *The effect of surface modification with nitric acid on the mechanical and tribological properties of carbon fiber-reinforced thermoplastic polyimide composite.* Surface and Interface Analysis, 2009. **41**(9):759-763.
60. X.R. Zhang, X.Q. Pei, and Q.H. Wang, *The effect of fiber oxidation on the friction and wear behaviors of short-cut carbon fiber/polyimide composites.* Express Polymer Letters, 2007. **1**(5):318-325.
61. Z.H. Wu, C.U. Pittman, and S.D. Gardner, *Nitric-Acid Oxidation of Carbon-Fibers and the Effects of Subsequent Treatment in Refluxing Aqueous Naoh.* Carbon, 1995. **33**(5):597-605.
62. S.J. Park and B.J. Park, *Electrochemically modified PAN carbon fibers and interfacial adhesion in epoxy-resin composites.* Journal of Materials Science Letters, 1999. **18**(1):47-49.
63. S.K. Ryu, B.J. Park, and S.J. Park, *XPS analysis of carbon fiber surfaces - anodized and interfacial effects in fiber-epoxy composites.* Journal of Colloid and Interface Science, 1999. **215**(1):167-169.
64. J. Liu, Y. Tian, Y. Chen, J. Liang, L. Zhang, and H. Fong, *A surface treatment technique of electrochemical oxidation to simultaneously improve the interfacial bonding strength and the tensile strength of PAN-based carbon fibers.* Materials Chemistry and Physics, 2010. **122**(2):548-555.
65. P. Denison, F.R. Jones, A. Brown, P. Humphrey, and J. Harvey, *Scanning secondary ion mass spectroscopic studies of the micromechanics and chemical structure in the region of the interface in carbon fibre-epoxy composites.* Journal of Materials Science, 1988. **23**(6):2153-2156.
66. J. Liu, Y. Tian, Y. Chen, and J. Liang, *Interfacial and mechanical properties of carbon fibers modified by electrochemical oxidation in*

(NH4HCO3)/(NH4)2C2O4·H2O aqueous compound solution. Applied Surface Science, 2010. **256**(21):6199-6204.

67. C.U. Pittman, W. Jiang, Z.R. Yue, S. Gardner, L. Wang, H. Toghiani, and C.A.L.Y. Leon, *Surface properties of electrochemically oxidized carbon fibers.* Carbon, 1999. **37**(11):1797-1807.
68. Z.R. Yue, W. Jiang, L. Wang, S.D. Gardner, and C.U. Pittman, *Surface characterization of electrochemically oxidized carbon fibers.* Carbon, 1999. **37**(11):1785-1796.
69. Z.S. Dai, B.Y. Zhang, F.H. Shi, M. Li, Z.G. Zhang, and Y.Z. Gu, *Chemical interaction between carbon fibers and surface sizing.* Journal of Applied Polymer Science, 2012. **124**(3):2127-2132.
70. T.H. Cheng, J. Zhang, S. Yumitori, F.R. Jones, and C.W. Anderson, *Sizing resin structure and interphase formation in carbon fibre composites.* Composites, 1994. **25**(7):661-670.
71. L.-G. Tang and J.L. Kardos, *A review of methods for improving the interfacial adhesion between carbon fiber and polymer matrix.* Polymer Composites, 2004. **18**(1):100-113.
72. D.M. Blackketter, D. Upadhyaya, T.R. King, and J.A. King, *Evaluation of fiber surfaces treatment and sizing on the shear and transverse tensile strengths of carbon fiber-reinforced thermoset and thermoplastic matrix composites.* Polymer Composites, 1993. **14**(5):430-436.
73. J.J. Lesko, R.E. Swain, J.M. Cartwright, J.W. Chin, K.L. Reifsnider, D.A. Dillard, and J.P. Wightman, *Interphases Developed from Fiber Sizings and Their Chemical-Structural Relationship to Composite Compressive Performance.* The Journal of Adhesion, 1994. **45**(1-4):43-57.
74. J.Y. Liu, H.Y. Ge, J. Chen, D.Z. Wang, and H.S. Liu, *The preparation of emulsion type sizing agent for carbon fiber and the properties of carbon fiber/vinyl ester resin composites.* Journal of Applied Polymer Science, 2012. **124**(1):864-872.
75. J. Li, Q. Fan, Z.H. Chen, K.B. Huang, and Y.L. Cheng, *Effect of electropolymer sizing of carbon fiber on mechanical properties of phenolic resin composites.* Transactions of Nonferrous Metals Society of China, 2006. **16**:S457-S461.
76. S. Yumitori, D. Wang, and F.R. Jones, *The Role of Sizing Resins in Carbon-*

Fiber-Reinforced Polyethersulfone (Pes). Composites, 1994. **25**(7):698-705.

77. B. Fernandez, A. Arbelaiz, A. Valea, F. Mujika, and I. Mondragon, *A comparative study on the influence of epoxy sizings on the mechanical performance of woven carbon fiber-epoxy composites.* Polymer Composites, 2004. **25**(3):319-330.
78. T.H. Cheng, J. Zhang, S. Yumitori, F.R. Jones, and C.W. Anderson, *Sizing Resin Structure and Interphase Formation in Carbon-Fiber Composites.* Composites, 1994. **25**(7):661-670.
79. N. Dilsiz and J.P. Wightman, *Surface analysis of unsized and sized carbon fibers.* Carbon, 1999. **37**(7):1105-1114.
80. X.Z. Zhang, Y.D. Huang, T.Y. Wang, and L. Liu, *Influence of fibre surface oxidation-reduction followed by silsesquioxane coating treatment on interfacial mechanical properties of carbon fibre/polyarylacetylene composites.* Composites Part a-Applied Science and Manufacturing, 2007. **38**(3):936-944.
81. Y. Yang, C.X. Lu, X.L. Su, and X.K. Wang, *Effects of emulsion sizing with nano-SiO2 on interfacial properties of carbon fibers/epoxy composites.* Journal of Materials Science, 2007. **42**(15):6347-6352.
82. L. Tonks and I. Langmuir, *A general theory of the plasma of an arc.* Physical Review, 1929. **34**(6):0876-0922.
83. H.K. Yasuda, *Modification of Polymer Surfaces by Plasma Treatment and Plasma Polymerization.* Acs Symposium Series, 1985. **287**:89-102.
84. D.C. Schram, G.M.W. Kroesen, and J.J. Beulens, *The Physics of Plasma Polymer Deposition.* Plasma Polymerization and Plasma Interactions with Polymeric Materials, 1990. **46**:1-16.
85. N. Dilsiz, E. Ebert, W. Weisweiler, and G. Akovali, *Effect of Plasma Polymerization on Carbon Fibers Used for Fiber/Epoxy Composites.* Journal of Colloid and Interface Science, 1995. **170**(1):241-248.
86. S. Feih and P. Schwartz, *Modification of the carbon fiber/matrix interface using gas plasma treatment with acetylene and oxygen.* Journal of Adhesion Science and Technology, 1998. **12**(5):523-539.
87. N. Dilsiz, N.K. Erinc, E. Bayramli, and G. Akovali, *Surface-Energy and Mechanical-Properties of Plasma-Modified Carbon-Fibers.* Carbon, 1995.

33(6):853-858.

88. A.P. Kettle, F.R. Jones, M.R. Alexander, R.D. Short, M. Stollenwerk, J. Zabold, W. Michaeli, W. Wu, E. Jacobs, and I. Verpoest, *Experimental evaluation of the interphase region in carbon fibre composites with plasma polymerised coatings.* Composites Part a-Applied Science and Manufacturing, 1998. **29**(3):241-250.
89. D.J. Marks and F.R. Jones, *Plasma polymerised coatings for engineered interfaces for enhanced composite performance.* Composites Part a-Applied Science and Manufacturing, 2002. **33**(10):1293-1302.
90. A.P. Kettle, A.J. Beck, L. OToole, F.R. Jones, and R.D. Short, *Plasma polymerisation for molecular engineering of carbon-fibre surfaces for optimised composites.* Composites Science and Technology, 1997. **57**(8):1023-1032.
91. T.J. Swait, C. Soutis, and F.R. Jones, *Optimisation of interfacial properties for tensile strength by plasma polymerisation.* Composites Science and Technology, 2008. **68**(12):2302-2309.
92. F. Massines, C. Sarra-Bournet, F. Fanelli, N. Naudé, and N. Gherardi, *Atmospheric Pressure Low Temperature Direct Plasma Technology: Status and Challenges for Thin Film Deposition.* Plasma Processes and Polymers, 2012. **9**(11-12):1041-1073.
93. D. Merche, N. Vandencasteele, and F. Reniers, *Atmospheric plasmas for thin film deposition: A critical review.* Thin Solid Films, 2012. **520**(13):4219-4236.
94. L.J. Ward, W.C.E. Schofield, J.P.S. Badyal, A.J. Goodwin, and P.J. Merlin, *Atmospheric pressure plasma deposition of structurally well-defined polyacrylic acid films.* Chemistry of Materials, 2003. **15**(7):1466-1469.
95. K.S. Chen, S.C. Liao, S.H. Tsao, N. Inagaki, H.M. Wu, C.Y. Chou, and W.Y. Chen, *Deposition of tetramethylsilane on the glass by plasma-enhanced chemical vapor deposition and atmospheric pressure plasma treatment.* Surface & Coatings Technology, 2013. **228**:S33-S36.
96. K.S. Chen, S.C. Liao, S.W. Lin, S.H. Tsao, T.H. Ting, N. Inagaki, H.M. Wu, and W.Y. Chen, *The film deposition via atmospheric pressure plasma from ethanol and He mixing gases.* Surface & Coatings Technology, 2013.

231:408-411.

97. S.C. Liao, H.M. Wu, Y.C. Tsao, H.R. Lin, K.S. Chen, and W.Y. Chen, *Post treatment of plasma-polymerized SnOx organic-like films with poly ethylene glycol for improving CO gas sensitivity.* J Nanosci Nanotechnol, 2012. **12**(2):1280-3.
98. L.-A. O'Hare, L. O'Neill, and A.J. Goodwin, *Anti-microbial coatings by agent entrapment in coatings deposited via atmospheric pressure plasma liquid deposition.* Surface and Interface Analysis, 2006. **38**(11):1519-1524.
99. B. Nisol, A. Batan, F. Dabeux, A. Kakaroglou, I. De Graeve, G. Van Assche, B. Van Mele, H. Terryn, and F. Reniers, *Surface Characterization of Atmospheric Pressure Plasma-Deposited Allyl Methacrylate and Acrylic Acid Based Coatings.* Plasma Processes and Polymers, 2013. **10**(6):564-571.
100. S. Bai, K.K.C. Ho, G. Knox, and A. Bismarck, *Improving the adhesion between carbon fibres and an elastomer matrix using an acrylonitrile containing atmospheric plasma treatment.* Composite Interfaces, 2013. **20**(9):761-782.
101. O. Carton, D. Ben Salem, S. Bhatt, J. Pulpytel, and F. Arefi-Khonsari, *Plasma Polymerization of Acrylic Acid by Atmospheric Pressure Nitrogen Plasma Jet for Biomedical Applications.* Plasma Processes and Polymers, 2012. **9**(10):984-993.
102. D. Ben Salem, O. Carton, H. Fakhouri, J. Pulpytel, and F. Arefi-Khonsari, *Deposition of Water Stable Plasma Polymerized Acrylic Acid/MBA Organic Coatings by Atmospheric Pressure Air Plasma Jet.* Plasma Processes and Polymers, 2014. **11**(3):269-278.
103. T.F. Cooke, *High-Performance Fiber Composites with Special Emphasis on the Interface - a Review of the Literature.* Journal of Polymer Engineering, 1987. **7**(3):197-254.
104. R. Talreja, *Damage Development in Composites - Mechanisms and Modeling.* Journal of Strain Analysis for Engineering Design, 1989. **24**(4):215-222.
105. E.K. Gamstedt and R. Talreja, *Fatigue damage mechanisms in unidirectional carbon-fibre-reinforced plastics.* Journal of Materials Science, 1999. **34**(11):2535-2546.
106. R.B. Heslehurst, *Challenges in the repair of composite structures .2.* Sampe

Journal, 1997. **33**(6):16-21.

107. R.B. Heslehurst, *Challenges in the repair of composite structures .1.* Sampe Journal, 1997. **33**(5):11-16.
108. R.B. Heslehurst, *Repair of delamination damage - A simplified approach.* Materials and Process Challenges: Aging Systems, Affordability, Alternative Applications, Books 1 and 2, 1996. **41**(Bk 1-2):915-924.
109. M.D. Hager, P. Greil, C. Leyens, S. van der Zwaag, and U.S. Schubert, *Self-Healing Materials.* Advanced Materials, 2010. **22**(47):5424-5430.
110. B.J. Blaiszik, N.R. Sottos, and S.R. White, *Nanocapsules for self-healing materials.* Composites Science and Technology, 2008. **68**(3-4):978-986.
111. M.W. Keller, S.R. White, and N.R. Sottos, *A self-healing poly(dimethyl siloxane) elastomer.* Advanced Functional Materials, 2007. **17**(14):2399-2404.
112. S.R. White, N.R. Sottos, P.H. Geubelle, J.S. Moore, M.R. Kessler, S.R. Sriram, E.N. Brown, and S. Viswanathan, *Autonomic healing of polymer composites (vol 409, pg 794, 2001).* Nature, 2002. **415**(6873):817-817.
113. E.N. Brown, S.R. White, and N.R. Sottos, *Retardation and repair of fatigue cracks in a microcapsule toughened epoxy composite - Part 1: Manual infiltration.* Composites Science and Technology, 2005. **65**(15-16):2466-2473.
114. E.N. Brown, S.R. White, and N.R. Sottos, *Retardation and repair of fatigue cracks in a microcapsule toughened epoxy composite - Part II: In situ self-healing.* Composites Science and Technology, 2005. **65**(15-16):2474-2480.
115. E.N. Brown, N.R. Sottos, and S.R. White, *Fracture testing of a self-healing polymer composite.* Experimental Mechanics, 2002. **42**(4):372-379.
116. S.R. White, N.R. Sottos, P.H. Geubelle, J.S. Moore, M.R. Kessler, S.R. Sriram, E.N. Brown, and S. Viswanathan, *Autonomic healing of polymer composites.* Nature, 2001. **409**(6822):794-797.
117. B.J. Blaiszik, S.L.B. Kramer, S.C. Olugebefola, J.S. Moore, N.R. Sottos, and S.R. White, *Self-Healing Polymers and Composites.* Annual Review of Materials Research, Vol 40, 2010. **40**:179-211.
118. K.S. Toohey, N.R. Sottos, J.A. Lewis, J.S. Moore, and S.R. White, *Self-healing materials with microvascular networks.* Nature Materials, 2007. **6**(8):581-

585.

119. K.S. Toohey, N.R. Sottos, and S.R. White, *Characterization of Microvascular-Based Self-healing Coatings.* Experimental Mechanics, 2009. **49**(5):707-717.

120. J.W.C. Pang and I.P. Bond, *'Bleeding composites' - damage detection and self-repair using a biomimetic approach.* Composites Part a-Applied Science and Manufacturing, 2005. **36**(2):183-188.

121. X.X. Chen, M.A. Dam, K. Ono, A. Mal, H.B. Shen, S.R. Nutt, K. Sheran, and F. Wudl, *A thermally re-mendable cross-linked polymeric material.* Science, 2002. **295**(5560):1698-1702.

122. Naraso and F. Wudl, *Two poly (2,5-thienythiazolothiazole)s: Observation of spontaneous ordering in thin films.* Macromolecules, 2008. **41**(9):3169-3174.

123. S.J. Kalista and T.C. Ward, *Thermal characteristics of the self-healing response in poly (ethylene-co-methacrylic acid) copolymers.* Journal of the Royal Society Interface, 2007. **4**(13):405-411.

124. X.X. Chen, F. Wudl, A.K. Mal, H.B. Shen, and S.R. Nutt, *New thermally remendable highly cross-linked polymeric materials.* Macromolecules, 2003. **36**(6):1802-1807.

125. T.A. Plaisted and S. Nemat-Nasser, *Quantitative evaluation of fracture, healing and re-healing of a reversibly cross-linked polymer.* Acta Materialia, 2007. **55**(17):5684-5696.

126. J.S. Park, H.S. Kim, and H.T. Hahn, *Healing behavior of a matrix crack on a carbon fiber/mendomer composite.* Composites Science and Technology, 2009. **69**(7-8):1082-1087.

127. J.S. Park, K. Takahashi, Z.H. Guo, Y. Wang, E. Bolanos, C. Hamann-Schaffner, E. Murphy, F. Wudl, and H.T. Hahn, *Towards Development of a Self-Healing Composite using a Mendable Polymer and Resistive Heating.* Journal of Composite Materials, 2008. **42**(26):2869-2881.

128. F.R. Jones, W. Zhang, and S.A. Hayes, *Thermally Induced Self Healing of Thermosetting Resins and Matrices in Smart Composites.* Self Healing Materials: An Alternative Approach to 20 Centuries of Materials Science, 2007. **100**:69-93.

129. S.A. Hayes, W. Zhang, M. Branthwaite, and F.R. Jones, *Self-healing of damage in fibre-reinforced polymer-matrix composites.* Journal of the Royal Society Interface, 2007. **4**(13):381-387.
130. M.S.B.M. Jamil, *Self healing epoxy composites: mechanistic studies.* The University of Sheffield, Materials Science and Engineering, 2011.
131. M. Yamaguchi, S. Ono, and K. Okamoto, *Interdiffusion of dangling chains in weak gel and its application to self-repairing material.* Materials Science and Engineering B-Advanced Functional Solid-State Materials, 2009. **162**(3):189-194.
132. M. Yamaguchi, S. Ono, and M. Terano, *Self-repairing property of polymer network with dangling chains.* Materials Letters, 2007. **61**(6):1396-1399.
133. M.A.M. Rahmathullah and G.R. Palmese, *Crack-Healing Behavior of Epoxy-Amine Thermosets.* Journal of Applied Polymer Science, 2009. **113**(4):2191-2201.
134. C. Tendero, C. Tixier, P. Tristant, J. Desmaison, and P. Leprince, *Atmospheric pressure plasmas: A review.* Spectrochimica Acta Part B: Atomic Spectroscopy, 2006. **61**(1):2-30.
135. A. Chilkoti, B.D. Ratner, and D. Briggs, *Plasma-Deposited Polymeric Films Prepared from Carbonyl-Containing Volatile Precursors - Xps Chemical Derivatization and Static Sims Surface Characterization.* Chemistry of Materials, 1991. **3**(1):51-61.
136. F.R. Jones, R. Varley, J. Gotama, and M.S.B.M. Jamil, *The Effect of Molecular Weight of the Healing Agent on the Solid State Thermal Healing of Epoxy Resins*, in *3rd International Conference on Self-Healing Materials*. 2011: Bath, UK.
137. F.R. Jones, R. Varley, B. Dao, C. Pillsbury, and S.J. Kalista, *Self Assembling Healing Agents for Mendable Epoxy Networks.* 16th European Conference on Composite Materials, ECCM 16, Seville, Spain, 2014.
138. J. Ma, Q. Qi, J. Bayley, X.S. Du, M.S. Mo, and L.Q. Zhang, *Development of SENB toughness measurement for thermoset resins.* Polymer Testing, 2007. **26**(4):445-450.
139. J. Friedrich, R. Mix, R.D. Schulze, and A. Rau, *Ultra-Thin Polymer Layer Deposition by Aerosol-Dielectric Barrier Discharge (DBD) and Electrospray*

Ionization (ESI) at Atmospheric Pressure. Journal of Adhesion Science and Technology, 2010. **24**(7):1329-1350.

140. C. Kozlowski and P.M.A. Sherwood, *X-ray photoelectron spectroscopic studies of carbon fiber surfaces VIII—A comparison of type I and type II fibers and their interaction with thin resin films.* Carbon, 1987. **25**(6):751-760.
141. Y. Xie and P.M.A. Sherwood, *X-Ray Photoelectron-Spectroscopic Studies of Carbon Fiber Surfaces. Part IX: The Effect of Microwave Plasma Treatment on Carbon Fiber Surfaces.* Applied Spectroscopy, 1989. **43**(7):1153-1158.
142. W.Y. Chen, A. Matthews, F.R. Jones, and K.S. Chen, *Deposition of a stable and high concentration of carboxylic acid functional groups onto a silicon surface via a tailored remote atmospheric pressure plasma process.* Surface and Coatings Technology, 2017.
143. P. Cools, E. Sainz-García, D. Geyter Nathalie, A. Nikiforov, M. Blajan, K. Shimizu, F. Alba-Elías, C. Leys, and R. Morent, *Influence of DBD Inlet Geometry on the Homogeneity of Plasma-Polymerized Acrylic Acid Films: The Use of a Microplasma–Electrode Inlet Configuration.* Plasma Processes and Polymers, 2015. **12**(10):1153-1163.
144. C. Kozlowski and P.M.A. Sherwood, *X-ray photoelectron spectroscopic studies of carbon-fibre surfaces. Part 4.—The effect of electrochemical treatment in nitric acid.* Journal of the Chemical Society, Faraday Transactions 1: Physical Chemistry in Condensed Phases, 1984. **80**(8):2099-2107.
145. A. Proctor and P.M.A. Sherwood, *X-ray photoelectron spectroscopic studies of carbon fibre surfaces. I. carbon fibre spectra and the effects of heat treatment.* Journal of Electron Spectroscopy and Related Phenomena, 1982. **27**(1):39-56.
146. H. Sugihara and F.R. Jones, *Promoting the Adhesion of High-Performance Polymer Fibers Using Functional Plasma Polymer Coatings.* Polymer Composites, 2009. **30**(3):318-327.
147. M.R. Alexander, P.V. Wright, and B.D. Ratner, *Trifluoroethanol derivatization of carboxylic acid-containing polymers for quantitative XPS analysis.* Surface and Interface Analysis, 1996. **24**(3):217-220.

148. H. Yu, Y.G. Jin, F. Peng, H.J. Wang, and J. Yang, *Kinetically controlled side-wall functionalization of carbon nanotubes by nitric acid oxidation.* Journal of Physical Chemistry C, 2008. **112**(17):6758-6763.
149. J. Zhu, J.D. Kim, H.Q. Peng, J.L. Margrave, V.N. Khabashesku, and E.V. Barrera, *Improving the dispersion and integration of single-walled carbon nanotubes in epoxy composites through functionalization.* Nano Letters, 2003. **3**(8):1107-1113.
150. V. Datsyuk, M. Kalyva, K. Papagelis, J. Parthenios, D. Tasis, A.E. Siokou, J. Kallitsis, and C. Galiotis, *Chemical Oxidation of Multi-Walled Carbon Nanotubes*. Vol. 46. 2008. 833-840.
151. S.B. Rao and C.P. Sharma, *Use of chitosan as a biomaterial: Studies on its safety and hemostatic potential.* Journal of Biomedical Materials Research, 1997. **34**(1):21-28.
152. K.S. Chen, Y. Tsao, C.H. Tsen, C.C. Chen, and S.C. Liao, *Cold Plasma Surface Modified Electrospun Microtube Array Membrane for Chitosan Immobilization and Their Properties* International Journal of Bioengineering and Life Sciences, 2016. **10**(5):661-664.
153. K.S. Chen, W.Y. Chen, S.C. Liao, Y.T. Haung, S.C. Chen, H.R. Lin, and F.H. Lin, *Surface graft polymerization acrylic acid onto bamboo charcoal and to improve ammonia adsorption.* Desalination and Water Treatment, 2010. **17**(1-3):168-175.

Appendix - Supplementary studies using the atmospheric pressure plasma system

In order to further estimate the capabilities of the APP system, some trials using this plasma system were also carried out and published in scientific journals with the following titles:

i) Deposition of a stable and high concentration of carboxylic acid functional groups onto a silicon surface via a tailored remote atmospheric pressure plasma process.

ii) Immobilization of carboxylic acid groups on polymeric substrates by plasma-enhanced chemical vapor or atmospheric pressure plasma deposition of acetic acid.

This chapter shows the full content of these two papers, then discusses and compares the results from these papers to the work within the PhD project.

i) Published in Surface and Coatings Technology (SCT): Deposition of a stable and high concentration of carboxylic acid functional groups onto a silicon surface via a tailored remote atmospheric pressure plasma process

The content of this paper has been published in journal *Surface and Coatings Technology* (SCT), Volume 336, 25 February 2018, Pages 67-71.
https://doi.org/10.1016/j.surfcoat.2017.09.057

Surface & Coatings Technology 336 (2018) 67–71

Contents lists available at ScienceDirect

Surface & Coatings Technology

journal homepage: www.elsevier.com/locate/surfcoat

Deposition of a stable and high concentration of carboxylic acid functional groups onto a silicon surface via a tailored remote atmospheric pressure plasma process

Wei-Yu Chen[a,b,*], Allan Matthews[b], Frank R. Jones[a], Ko-Shao Chen[c,d]

[a] Department of Materials Science and Engineering, University of Sheffield, Sheffield, UK
[b] School of Materials, University of Manchester, Manchester, UK
[c] Department of Materials Engineering, Tatung University, Taipei, Taiwan
[d] College of Environment and Resources, Ming Chi University of Technology, New Taipei City, Taiwan

ARTICLE INFO

Keywords:
Remote atmospheric pressure plasma treatment
Acrylic acid
Carboxylic acid groups
Surface deposition

ABSTRACT

Processes to introduce carboxylic acid functional groups onto surfaces have been widely applied in various applications, such as molecular grafting for biosensors, biocompatibility improvement, gas filter/adsorption in environmental engineering and the enhancement of interfacial adhesion between fillers (such as carbon or glass fibre) and matrices (such as epoxy resin) in composite materials. To develop an environmental-friendly process to introduce a stable and high concentration of carboxylic acid functional groups, Acrylic Acid (AAc) was deposited onto silicon wafers using remote argon atmospheric plasma processing (APP) and vapour phase grafting in a bespoke Pyrex cylindrical chamber. The chamber stands vertically with an APP nozzle installed at the top, a sample platform downstream and an AAc vapour inlet on the chamber wall. In this way, both the effect of atmospheric gas on the process and AAc monomer fragmentation during APP can be limited. Silicon specimens were exposed to a combination of plasma gas and AAc vapour. Surface wettability was evaluated by measurement of water contact angles and chemical composition was analyzed using X-ray Photoelectron Spectroscopy (XPS). The peak at the binding energy of 289.2 eV, which fits with COOH components in the C1s spectrum of poly-AAc, was used to determine the contribution of the carboxylic acid groups depositing on the surface because it was absent in the C1s peak of untreated silicon wafers. A more stable and hydrophilic wettability and the binding energy peak at 289.2 eV from XPS show the presence of carboxylic acid groups on the surface of samples treated with AAc vapour with the remote argon-APP. A higher intensity peak at 289.2 eV was detected, compared with the surfaces activated by a conventional argon-APP in which the AAc vapour is exposed to the plasma glow, suggesting a potential, rapid and novel remote APP process for carboxylic acid functional group deposition.

1. Introduction

Surface functional modification has played an important role on tailoring surface properties such as adhesion, wettability, printability and dye uptake [1]. This study focused on controlling the wettability of the surface. By making a surface more hydrophilic, carboxylic acid functional groups can be introduced via acrylic acid (AAc) deposition. Carboxylic acid functional groups can improve the interfacial adhesion between fibres and matrices by reacting chemically with the resin and thus providing a mechanism of interfacial bridging through the formation of covalent bonds, leading to better mechanical properties for composites [2,3].

Several methods have been applied for surface functional modification, including radiation grafting of monomers, chemical modification, immobilizing biological molecules and plasma technology [4]. Among these methods, plasma technology has become popular because it provides rapid treatment and is environmentally friendly [5–7]. By introducing a different working gas or precursor, plasma processes are available to tailor the surface of most types and forms of material, such as flat specimens (e.g. silicon wafer), powder and fibres (e.g. carbon fibre).

In this study, a remote argon atmospheric pressure plasma (APP) was employed to activate a silicon surface. Comparing with vacuum plasmas, APP is a rapid treatment process and does not require a vacuum environment, which also saves on the costs of purchasing and maintaining vacuum equipment. By using argon as the working gas,

* Corresponding author at: Department of Materials Science and Engineering, University of Sheffield, Sheffield, UK.
E-mail address: wei-yu.chen@manchester.ac.uk (W.-Y. Chen).

https://doi.org/10.1016/j.surfcoat.2017.09.057
Received 18 June 2017; Received in revised form 22 September 2017; Accepted 24 September 2017
Available online 07 October 2017

APP is capable of creating free radicals and peroxides on the surface, which is beneficial for depositing AAc.

The introduction of carboxylic acid functional groups via AAc deposition has become popular for surface functional modification and has been utilized in various applications. For example, it has been applied to the surface of electrospun poly-L-lactic acid microtube array membranes to bind chitosan for superior biocompatibility in biomedical engineering [8]. This process was also employed on bamboo charcoal to improve its ammonia absorption ability, from 61% to 98%, which is beneficial for environmental engineering [9]. The introduction of carboxyl groups on a polyaniline (PAN) surface for the covalent immobilization of glucose oxidase is also reported by Z.F. Li et al. [10], for application as biosensors. For composite materials, Bismark et al. introduced AAc via an atmospheric plasma onto carbon fibres for optimum adhesion at the fibre-matrix interface [11]. Their results indicated a 60% increase in adhesion between carbon fibres and an elastomeric matrix with less than 6% of carboxylic acid groups on the surface.

However, in a conventional APP process the precursor tends to fragment in the plasma, which leads to the deposition of a low percentage of carboxylic acid. Therefore, a remote APP process comprising an argon-APP (Ar-APP) and a bespoke Pyrex chamber was developed in this study. The Pyrex chamber stands vertically with an APP nozzle installed at the top, a sample platform downstream and an AAc vapour inlet on the chamber wall. In this way, both the effect of the atmospheric gas on the process and AAc monomer fragmentation during APP can be limited. By using APP with this bespoke chamber, we aimed to develop a rapid and novel remote APP process to introduce carboxylic acid functional groups with high retention of the functionality of AAc. Prior to applying to carbon fibres for composite materials, in this paper we utilized this process on silicon wafers to examine the effects on surface characteristics.

2. Materials and methods

2.1. Materials

Silicon wafers (n-type), which were purchased from San Chih Semiconductor Co., Ltd., Taiwan, were cut into the size of 1 cm × 1 cm and used as specimens. The substrates were cleaned ultrasonically in 99.5% isopropanol solvent and distilled water for 15 min and dried in a desiccator to remove contaminants and organic matters on the surface. Acrylic acid (Aldrich Chemical Company, UK, with 99% purity.) was used as the precursor to introduce carboxylic acid functional groups on the silicon surface via the remote APP process.

2.2. Atmospheric pressure plasma process

The remote APP system employed in this study is shown on Fig. 1. It is constructed using a bespoke Pyrex glass column 30 mm in diameter,

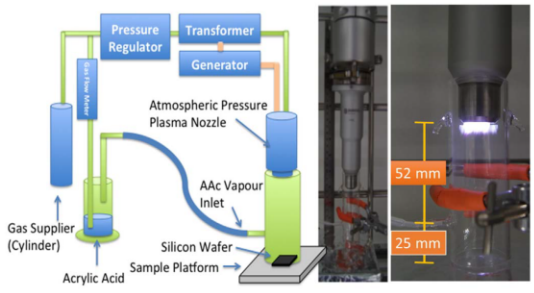

Fig. 1. Schematic diagram of the remote atmospheric plasma reactor system.

which stands vertically with an APP (OPENAIR® Plasma System, Plasmatreat GmbH) nozzle (of 5-mm diameter and 8-mm length, with DC pulsed plasma source) installed at the top, a sample platform downstream and an AAc vapour inlet, which is 52 mm from the end of the plasma nozzle and 25 mm from the sample platform, on the chamber wall. Argon (41.7 SLM, as plasma working gas) and AAc vapour (as precursor, introduced by 20 SLM argon from a bubbler) were fed into the plasma nozzle and reactor chamber, respectively, at the same time during the treatment process. The argon plasma was run at a voltage of 280.0 V and a current of 17.1 A with a 21.0 kHz power supply. The silicon wafer specimen was placed in the chamber at a distance of 77 mm from the tip of the plasma nozzle. The substrate was treated by the remote Ar-APP process (treating time: 5, 15, 30 or 60 s) to introduce a high-concentration of carboxylic acid groups on the surface. A conventional APP process, in which AAc precursor gas is in direct contact with the plasma glow, was also employed for comparison purposes. The silicon wafer placed 30 mm under the nozzle was treated by this conventional process for 30 s using the same OPENAIR® Plasma System nozzle and parameters to the remote APP process, but without the Pyrex chamber.

2.3. Water contact angle measurement

Prior to X-ray photoelectron spectroscopy (XPS) examination, the wettability of the silicon wafers treated with/without the remote plasma process were evaluated for their water contact angle as preliminary step to confirm the effect of plasma deposition. Data was an average of 5 readings with 0.03-ml sessile drop method.

2.4. X-ray photoelectron spectroscopy (XPS)

The chemical composition of the coating was obtained by XPS using AXIS Ultra DLD spectrometer. The source applied to stimulate photoemission was a monochromatic Al Kα radiation (1486.6 eV) at a power of 100 W. The C1s core spectra of the surface was fitted using Gaussian peaks, and sample charging was considered by referencing all peaks relative to the hydrocarbon peak at 285.0 eV [12].

3. Results and discussion

The water contact angles are compared in Fig. 2. Compared to the untreated Si-wafers, the water contact angle of those activated by the remote Ar-plasma decreased from 60.49 ± 1.9° (untreated) to 52.11 ± 2.0° (5 s), 41.68 ± 1.0° (15 s), 25.89 ± 1.8° (30 s) or 7.52 ± 1.4° (60 s). For those treated by the remote Ar-plasma with AAc precursor, the water contact angle decreased from 60.49 ± 1.9° to 57.51 ± 1.1° (5 s), 49.72 ± 0.4° (15 s), 48.90 ± 0.7° (30 s) or 38.11 ± 1.6° (60 s). For Si-wafers which were only exposed to AAc without the participation of the remote Ar-plasma, the contact angles with water were found to be 62.75 ± 1.5° (5 s), 55.55 ± 0.7° (15 s), 64.95 ± 1.6° (30 s) and 62.99 ± 1.6° (60 s), respectively. To understand the effect of the participation of the remote Ar-plasma on the AAc depositing process, specimens exposed to AAc vapour with and without Ar-plasma were rinsed with distilled water, dried at room temperature with air, then examined by water contact angle measurement. After water rinsing, the water contact angles for specimens treated by the remote Ar-plasma with AAc vapour were observed as 51.36 ± 2.1° (5 s), 48.30 ± 1.4° (15 s), 45.28 ± 1.8° (30 s) and 41.76 ± 1.1° (60 s). For the Si-wafer exposed to AAc vapour without the remote Ar-plasma, their contact angles with water were 57.40 ± 3.2° (5 s), 53.75 ± 2.0° (15 s), 55.77 ± 1.7° (30 s) and 53.04 ± 2.1° (60 s). Fig. 3 illustrates the difference between water contact angles of those specimens after water rinsing. (See Table 1.)

From the results of water contact angle measurements, the specimen has become hydrophilic after the remote Ar-APP treatment, which probably results from the presence of free radicals and/or peroxide

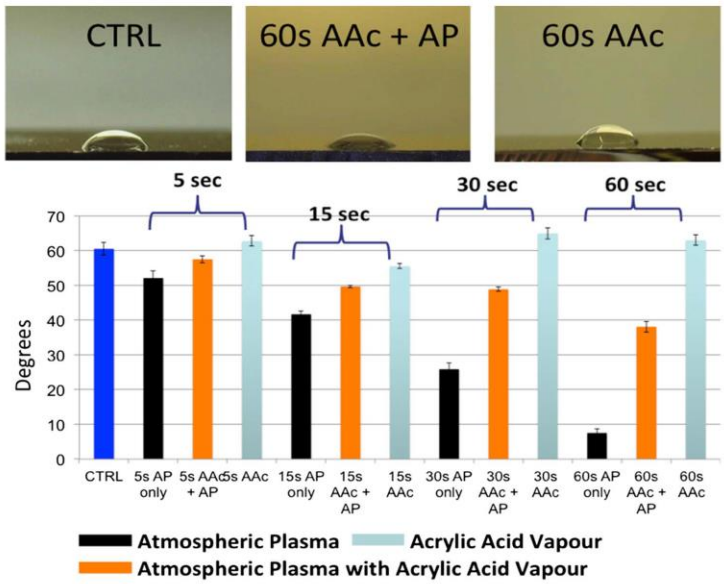

Fig. 2. Comparison of the wettability, as given by the water contact angles of substrates after plasma treatment only (AP only), plasma treatment with acrylic acid (AAc + AP), and acrylic acid vapour only (AAc).

groups formed on the surface, indicating the effect of the APP. Specimen treated by the remote Ar-APP with AAc vapour was more hydrophobic than that with remote Ar-APP treatment only. This is because of the remote Ar-APP with AAc vapour process formed a poly-AAc like film containing non-polar groups on the surface, which are more hydrophobic than oxygen-contained polar groups offered by the Ar-APP. Compared to untreated Si-wafers, those treated by the remote Ar-APP with AAc vapour were found to be more hydrophilic, suggesting the presence of polar carboxylic acid functional groups on the surface. The longer the treatment time, the more hydrophilic is the surface.

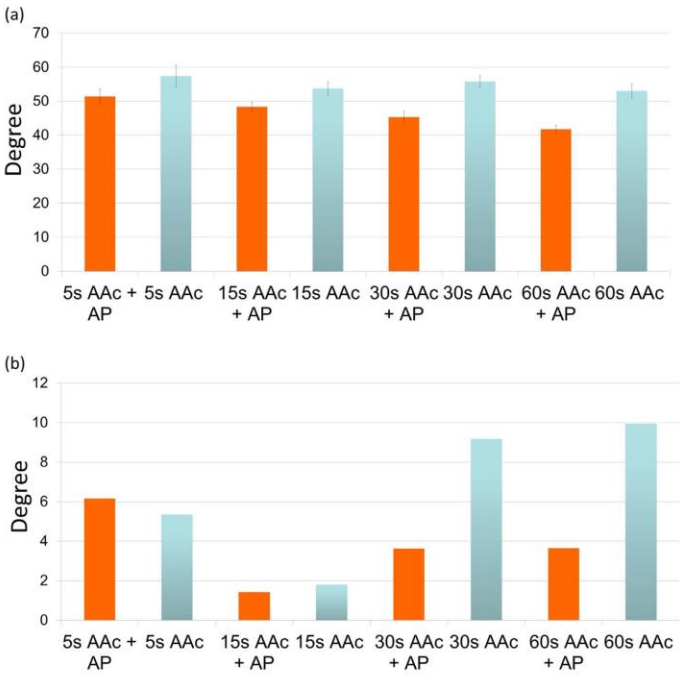

Fig. 3. (a) Water contact angles of specimens after a 10-second water rinsing (b) The difference (absolute values) of water contact angles of specimen after a 10-second water rinsing.

Table 1
Water contact angles of substrate after plasma treatment only, plasma treatment with acrylic acid, and acrylic acid vapour only. (60.49 ± 1.9° for untreated Si-wafer).

Time (sec)	Parameter		
	AP	AP + AAc	AAc only
5	52.11 ± 2.0°	57.51 ± 1.1°	62.75 ± 1.5°
15	41.68 ± 1.0°	49.72 ± 0.4°	55.55 ± 0.7°
30	25.89 ± 1.8°	48.90 ± 0.7°	64.95 ± 1.6°
60	7.52 ± 1.4°	38.11 ± 1.6°	62.99 ± 1.6°

To further investigate the effects of the participation of the remote Ar-plasma, the wettability and stability of specimens exposed to AAc vapour with and without APP treatment were studied. The stability was estimated by calculating the difference of water contact angles of specimens after water rinsing. A small difference suggests a more stable surface.

Specimens exposed to AAc vapour without APP treatment, unlike those with APP participation, exhibited a similar or even more hydrophobic surface than untreated silicon. With the same treatment time (15, 30 or 60 s), the silicon surface treated with the remote Ar-plasma and AAc vapour showed a minor difference of water contact angles after water rinsing than that exposed only to AAc vapour without APP (Fig. 3(b)). These results indicate that for a stable hydrophilic surface plasma activation is beneficial. A treatment time of 5 s was insufficient to achieve a stable surface but with 15, 30 or 60 s a surface with sufficient hydrophilicity and stability could be achieved. As the original glow affected distance is only between 5 and 15 mm from the nozzle, an adequate plasma treatment time is required to ensure that downstream plasma gas can activate the sample placed 77 mm from the nozzle.

The presence of carboxylic acid functional groups was identified by XPS through peak fitting at the C1s core level and comparing the atomic ratios with that for AAc. The peak at the binding energy of 289.2 eV was used to determine the contribution of the carboxylic acid groups deposited onto the surface because it not only fits into –COOH components in C1s spectrum of poly-AAc [13] but also was absent in the C1s peak of untreated silicon wafers. The high resolution of the C1s spectra of the Si-wafer surface treated with the remote Ar-plasma and AAc vapour for 30 s is shown in Fig. 4(b). A strong intense peak at 289.2 eV for COOH/R was calculated to be 27.6% of the total C, which compares well with the theoretical atomic ratio for the monomer of 33.3%. This indicates a high level of carboxylic acid functional groups retention on the surface (Table 2), which is supported by the results of the wettability study. The bespoke Pyrex chamber has not only confined the active species, thus concentrated their dose at the surface, but also enabled the effect of atmospheric plasma glow on the fragmentation of the precursor gas to be inhibited. This is further supported by the XPS result of the specimens treated conventionally (same OPENAIR® Plasma System nozzle and parameter to the remote APP process, 30 mm from nozzle tip to the sample) with the AAc precursor gas in direct contact with the plasma glow, where in a 30-second treatment, only 10.8% of carboxylic acid group was retained (Fig. 4(c) and Table 2).

4. Conclusions

A more stable and hydrophilic surface can be achieved with the remote Ar-APP treatment with AAc vapour. The binding energy peak at 289.2 eV from XPS shows the presence of carboxylic acid groups. A higher intensity peak at 289.2 eV was detected (27.6%), compared with the surfaces activated by a conventional APP, in which the plasma glow is in direct in contact with the AAc precursor (10.8%). This demonstrates a potential, rapid and novel remote APP technique for the retention of a high concentration of carboxylic acid functional groups in the deposit.

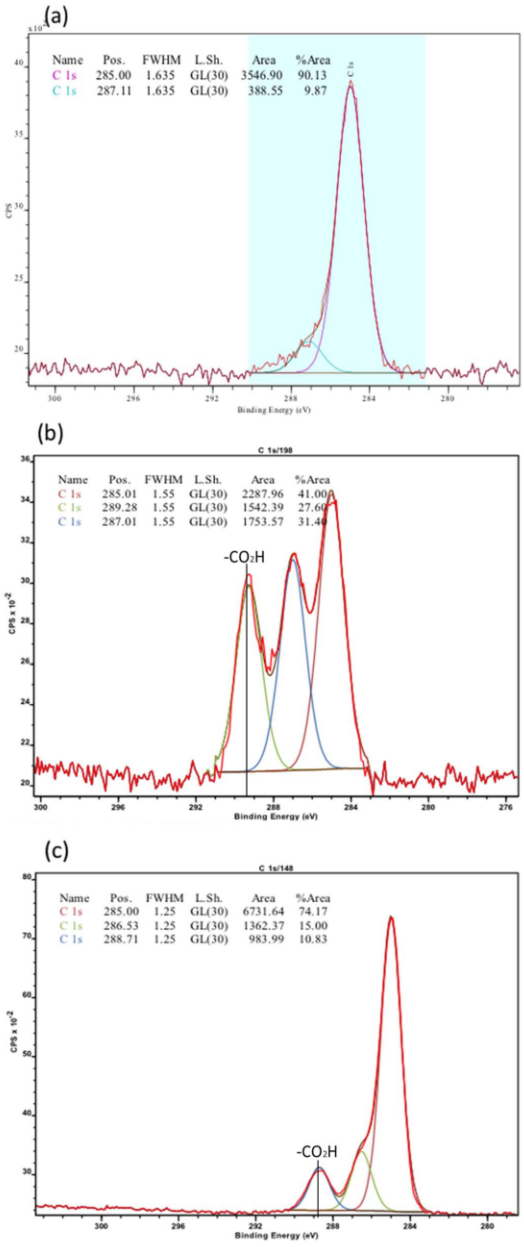

Fig. 4. The C1s core level from silicon surface (a) untreated (b) treated by the remote Ar-APP with AAc for 30 s (c) treated by the conventional Ar-APP process for 30 s.

Acknowledgements

Support under ERC Grant number 320879 (“IMPUNEP”) is gratefully acknowledged.

Table 2
Comparison of the peak intensity at 289.2 eV in C1s spectrum.

Specimen	Si-Wafer	APP	Poly-AAc (Theoretical)	Conventional APP Process[a]	Remote APP Process[b]
COOH/COOR (%) (289.2 eV)	0	0	33.3	10.8	27.6

[a] Conventional APP Process: Mixing plasma glow with AAc precursor.
[b] Remote APP Process: The process developed in this study separating plasma glow with AAc precursor.

References

[1] E.M. Liston, L. Martinu, M.R. Wertheimer, Plasma surface modification of polymers for improved adhesion - a critical-review, J. Adhes. Sci. Technol. 7 (1993) 1091–1127.
[2] A.P. Kettle, A.J. Beck, L. OToole, F.R. Jones, R.D. Short, Plasma polymerisation for molecular engineering of carbon-fibre surfaces for optimised composites, Compos. Sci. Technol. 57 (1997) 1023–1032.
[3] N. Lopattananon, S.A. Hayes, F.R. Jones, Stress transfer function for interface assessment in composites with plasma copolymer functionalized carbon fibres, J. Adhes. 78 (2002) 313–350.
[4] K.S. Chen, S.C. Liao, S.W. Lin, T.S. Hung, S.H. Tsao, H.M. Wu, N. Inagaki, W.Y. Chen, Improvement of thermoplastic polyurethane nonwoven hydrophilicity by atmospheric pressure plasma treatment with He and N-2 mixed gases, Jpn. J. Appl. Phys. 51 (2012).
[5] A.P. Kettle, F.R. Jones, M.R. Alexander, R.D. Short, M. Stollenwerk, J. Zabold, W. Michaeli, W. Wu, E. Jacobs, I. Verpoest, Experimental evaluation of the interphase region in carbon fibre composites with plasma polymerised coatings, J. Community Appl. Soc. Psychol. 29 (1998) 241–250.
[6] N. Lopattananon, A.P. Kettle, D. Tripathi, A.J. Beck, E. Duval, R.M. France, R.D. Short, F.R. Jones, Interface molecular engineering of carbon-fiber composites, J. Community Appl. Soc. Psychol. 30 (1999) 49–57.
[7] D.J. Marks, F.R. Jones, Plasma polymerised coatings for engineered interfaces for enhanced composite performance, J. Community Appl. Soc. Psychol. 33 (2002) 1293–1302.
[8] K.S. Chen, Y. Tsao, C.H. Tsen, C.C. Chen, S.C. Liao, Cold plasma surface modified electrospun microtube array membrane for chitosan immobilization and their properties, international journal of chemical, molecular, nuclear, materials and metallurgical, Engineering 10 (2016) 661–664.
[9] K.S. Chen, W.Y. Chen, S.C. Liao, Y.T. Haung, S.C. Chen, H.R. Lin, F.H. Lin, Surface graft polymerization acrylic acid onto bamboo charcoal and to improve ammonia adsorption, Desalin. Water Treat. 17 (2010) 168–175.
[10] Z.F. Li, E.T. Kang, K.G. Neoh, K.L. Tan, Covalent immobilization of glucose oxidase on the surface of polyaniline films graft copolymerized with acrylic acid, Biomaterials 19 (1998) 45–53.
[11] S. Bai, K.K.C. Ho, G. Knox, A. Bismarck, Impact of Continuous Atmospheric Pressure Plasma Polymerization of Acrylic Acid on the Interfacial Properties of Carbon Fibre - RFL Elastomer Composites, 15th European Conference on Composite Materials, (2012).
[12] L.J. Ward, W.C.E. Schofield, J.P.S. Badyal, A.J. Goodwin, P.J. Merlin, Atmospheric pressure plasma deposition of structurally well-defined polyacrylic acid films, Chem. Mater. 15 (2003) 1466–1469.
[13] J. Friedrich, R. Mix, R.D. Schulze, A. Rau, Ultra-thin polymer layer deposition by aerosol-dielectric barrier discharge (DBD) and electrospray ionization (ESI) at atmospheric pressure, J. Adhes. Sci. Technol. 24 (2010) 1329–1350.

ii) Published in Thin Solid Films (TSF): Immobilization of Carboxylic Acid Groups on Polymeric Substrates by Plasma-enhanced Chemical Vapor or Atmospheric Pressure Plasma Deposition of Acetic Acid

The content of this chapter has been published in journal *Thin Solid Films* (TSF), Volume 666, 30 November 2018, Pages 54-60.

https://doi.org/10.1016/j.tsf.2018.07.051

Thin Solid Films 666 (2018) 54–60

Contents lists available at ScienceDirect

Thin Solid Films

journal homepage: www.elsevier.com/locate/tsf

Immobilization of carboxylic acid groups on polymeric substrates by plasma-enhanced chemical vapor or atmospheric pressure plasma deposition of acetic acid

Wei-Yu Chen[a,b,*], Allan Matthews[b], Frank R. Jones[a], Ko-Shao Chen[c,d]

[a] Department of Materials Science and Engineering, University of Sheffield, Sheffield, UK
[b] School of Materials, University of Manchester, Manchester, UK
[c] Department of Materials Engineering, Tatung University, Taipei, Taiwan
[d] College of Environment and Resources, Ming Chi University of Technology, New Taipei City, Taiwan

ARTICLE INFO

Keywords:
Low-pressure plasma-enhanced chemical vapor deposition
Atmospheric pressure plasma
Carboxylic acid groups
Acetic acid
Hydrophilic

ABSTRACT

Low-pressure plasma-enhanced chemical vapor deposition (PECVD) is a process that activates the precursor in the plasma state to deposit films on the surface. Introducing carboxylic acid functional groups via PECVD has been widely applied in various applications, such as the enhancement of interfacial adhesion between fillers and matrices in composite materials, molecular grafting for biosensors and biocompatibility improvement. To develop a compatible surface for cell adhesion, polymeric substrates, poly (lactic acid) (PLA) and polyethylene terephthalate (PET), were modified by a low-pressure acetic acid plasma to improve surface hydrophilicity and biocompatibility. The acetic acid plasma deposited film maintained stability on a hydrophilic surface for long-term aging. If the acetic acid film can be deposited by process using atmospheric pressure plasma (APP), a more rapid, economic and power-saving method can be achieved. In this study, a remote APP system using a bespoke Pyrex APP chamber was utilized to deposit acetic acid film onto the surfaces of polymeric substrates. The wettability, stability of hydrophilicity and surface elemental composition of the APP-deposited film were reported and compared with that prepared via low-pressure acetic acid plasma. The plasma functionalized PET showed good stability and a long-term hydrophilicity. Although the plasma processes are able to tailor the PLA surface into hydrophilic with the presence of carboxylic acid functional group, the surface is not stable due to hydrolytic degradation of PLA structure and lost its hydrophilicity after 3 days.

1. Introduction

Comparing to natural extracellular protein components, thermoplastic polymers such as poly (lactic acid) (PLA) and polyethylene terephthalate (PET) are suitable materials for tissue engineering scaffold due to their advantages of good mechanical strength, ductility and ability to be manufactured into desired shapes easily. However, because of the hydrophobicity and the lack of reactive side-chain groups on the PLA and PET surfaces, their surface interaction with cell is limited, which results in poor cell attachment.

Therefore, surface modifications, including immobilizing biomolecule coatings via physical adsorption or chemical surface treatment, have been made to improve cell adhesion and biocompatibility [1–5]. Although the presence of biomolecules, such as protein or collagen, on the surface has exhibited an enhanced biocompatibility, the physically adsorbed biomolecule coating tends to be removed easily with altering of pH value or increased shear stress. In comparison with these modifications, plasma process is a reliable, and environmentally friendly method, and has been consequently proven highly successful as a means of developing functional interfaces for cell culture [6–8].

Functionalized surfaces with carboxylic acid groups on have been reported being capable of binding with amino groups from collagen or protein, which retain these biomolecules and lead to an improved surface biocompatibility [9]. Therefore, plasma processes were employed with acetic acid as precursor to introduce carboxylic acid functional group on the thermoplastic polymers.

This study presents the approach of utilizing an atmospheric pressure plasma and a low-pressure plasma-enhanced chemical vapor deposition (PECVD) method, with acetic acid as precursor, for introducing carboxylic acid functional groups on the PLA and PET surfaces to improve the hydrophilic quality and biocompatibility. The investigation of hydrophilicity and surface elements were carried out by water contact

* Corresponding author at: Oxford Rd, Manchester M13 9PL, UK.
E-mail address: wei-yu.chen@manchester.ac.uk (W.-Y. Chen).

https://doi.org/10.1016/j.tsf.2018.07.051
Received 24 April 2018; Received in revised form 21 June 2018; Accepted 4 July 2018
Available online 10 August 2018
0040-6090/

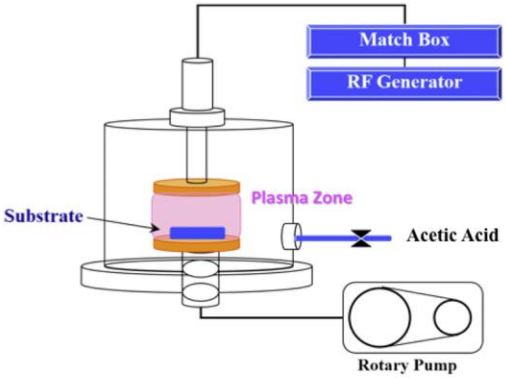

Fig. 1. Schematic of the low-pressure acetic acid plasma system.

angle measurement and XPS, respectively.

2. Materials and methods

2.1. Materials

Poly (lactic acid) (PLA) and polyethylene terephthalate (PET) were obtained from the Industrial Technology Research Institute and cut into a suitable size of about $1 \times 1\,cm^2$. Acetic acid (CH_3COOH), 95%, Mw = 60, was purchased from Aldrich Chemical Company, and applied as precursor in the plasma processes to introduce carboxylic acid groups. The specimens were ultrasonically cleaned in 99.5% isopropanol solvent and distilled water for 15 min and dried in a desiccator to remove contaminants and organic matters on the surface.

2.2. Low-pressure plasma-enhanced chemical vapor deposition of acetic acid

The substrates were put into the chamber on the lower electrode of the RF plasma instrument (Fig. 1). After the chamber was vacuumed to less than 30 mtorr, acetic acid precursor was introduced and adjusted at a constant pressure of 100 mtorr. Once the pressure has become stable, a plasma glow discharge treatment was performed for 10 min with 30 W input power from the RF generator.

Table 1
Parameters of APP and low-pressure plasma treatment(s).

Abbreviation	Substrate	Argon plasma treatment time	Acetic acid vapour grafting time
PET	PET	0 Second	0 min
PET-APP	PET	5 Seconds	0 min
PET-AA-5	PET	5 Seconds	5 min
PET-AA-10	PET	5 Seconds	10 min
PLA	PLA	0 Second	0 min
PLA-APP	PLA	5 Seconds	0 min
PLA-AA-5	PLA	5 Seconds	5 min
PLA-AA-10	PLA	5 Seconds	10 min

Abbreviation	Substrate	Low-pressure AA plasma treatment time
PET-VA-AA-10	PET	10 min
PLA-VA-AA-10	PLA	10 min

Table 2
Water contact angles of substrate without treatment (neat), after plasma treatment only, and plasma treatment with acetic acid.

	PET	PLA
CTRL (neat)	85.2 ± 2.0	78.1 ± 2.3
APP activation	28.9 ± 1.7	26.9 ± 0.6
APP/5-min AA-grafting	42.8 ± 1.5	62.4 + 1.2
APP/10-min AA-grafting	41.5 ± 1.4	60.8 + 2.4
AA low-pressure plasma polymerization (10 min)	15.7 ± 0.7	18.9 ± 0.4

2.3. Atmospheric pressure plasma functionalization

The atmospheric pressure plasma (APP) system utilized in this study (Fig. 2) was built with a DC pulsed plasma generator, a plasma nozzle (OPENAIR® Plasma System, Plasmatreat GmbH, Germany) and a tailored Pyrex chamber. The chamber is 250 mm in length, 50 mm in outer diameter, and 46 mm in inner diameter, with a pair of 8 mm Pyrex glass rods in the middle of glass column separately to act as rails for the mobile specimen holder, which provides the platform for APP treatment of specimen. The Pyrex chamber has two inlets on top of it, one

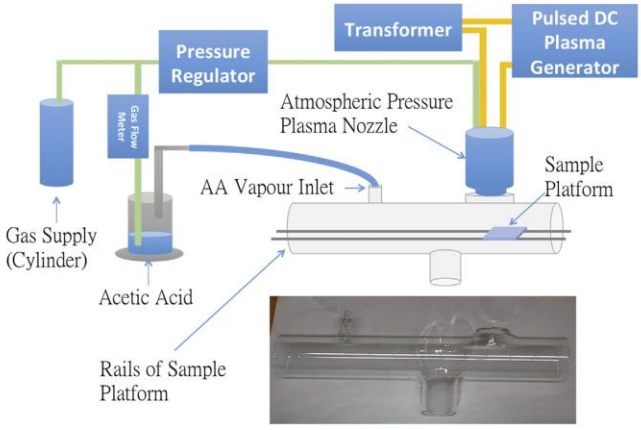

Fig. 2. Schematic diagram of atmospheric pressure plasma setup.

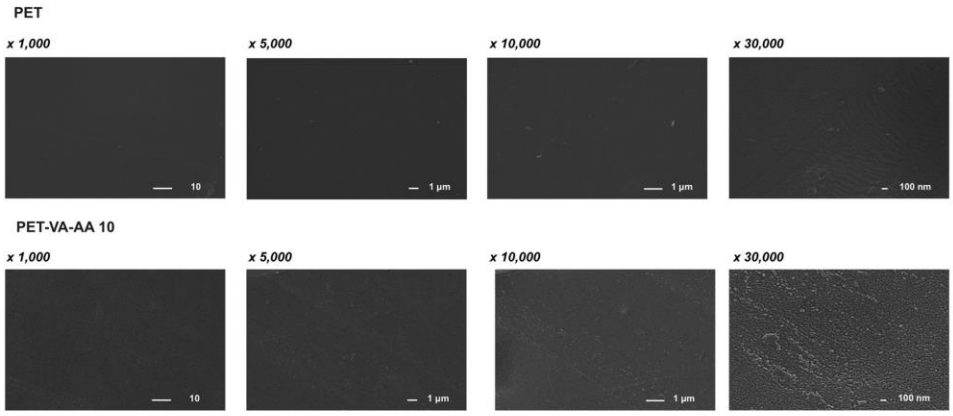

Fig. 3. SEM images of PET surface before/after acetic acid low-pressure plasma-enhanced chemical vapor deposition.

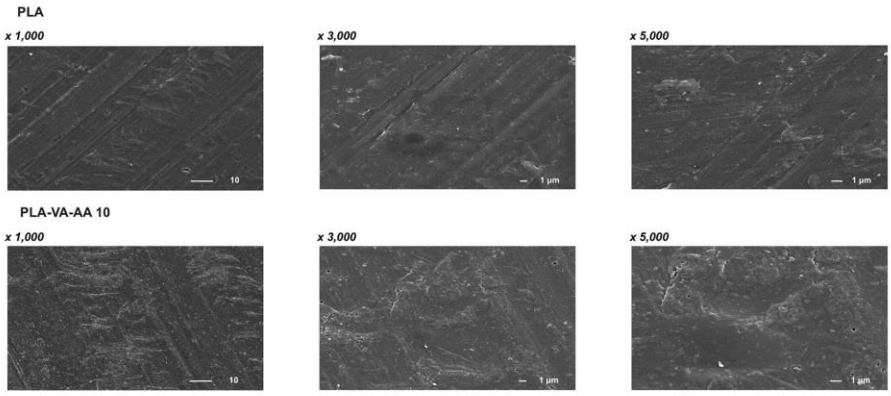

Fig. 4. SEM images of PLA surface before/after acetic acid low-pressure plasma-enhanced chemical vapor deposition.

for APP nozzle, which offers surface activation, another for inletting acetic acid precursor for grafting, and an outlet on the bottom of it for releasing gases. It has been reported by Chen et al. that comparing with a conventional APP process, which exposed precursor directly to plasma glow, this design retains a higher percentage of functional groups by separating the plasma glow and the precursor, which prevents the precursor monomer from fragmentation [10].

PET and PLA specimens were mounted on the sample platform, first activated by the argon-APP (280.0 V, 17.1A with a 21.0 kHz power supply), then shifted downstream the precursor inlet for AA vapour grafting (Grafting time: 5 or 10 min) to introduce carboxylic acid functional group. The flow rate for argon working gas and AA vapour precursor are 47.1 SLM and 30.0 SLM, respectively. Specimens were kept 10 mm from the plasma nozzle and 15 mm from the precursor inlet.

2.4. Surface characteristics

The wettability of the PET and PLA treated with/without the plasma processes were measured for their water contact angle to preliminarily confirm the effect of plasma functionalization prior to X-ray photoelectron spectroscopy analysis. Data recorded was an average of 5 readings with the 0.03-ml sessile drop method. The morphology of the PET and PLA before/after low-pressure plasma-enhanced chemical vapor deposition of acetic acid was observed by scanning electron microscope (SEM) studies. The chemical composition of PET and PLA surfaces was obtained via X-ray photoelectron spectroscopy (XPS) utilizing AXIS Ultra DLD spectrometer. The source applied to stimulate photoemission was a monochromatic Al Kα radiation (1486.6 eV) at a power of 100 W. The pass energies used for survey scans and high resolution scans were 160 eV and 20 eV, respectively. The acquisition time to obtain the C1s core spectra was 5 min. The C1s core spectra of the surface was fitted using Gaussian peaks via CasaXPS software, and sample charging was considered by referencing all peaks relative to the hydrocarbon peak at 285.0 eV [11].

3. Results and discussion

Table 1 illustrates the parameters of polymer specimen treatment(s) and the abbreviation of them.

The measurement of surface wettability reflects the surface energy, which promises a preliminary method to identify not only the effects of surface functionalization but also the stability of the coating.

The results of surface wettability are summarized in Table 2.

The contact angle with water was found to be dramatically decreased on both PET and PLA specimens after Ar-APP activation, which

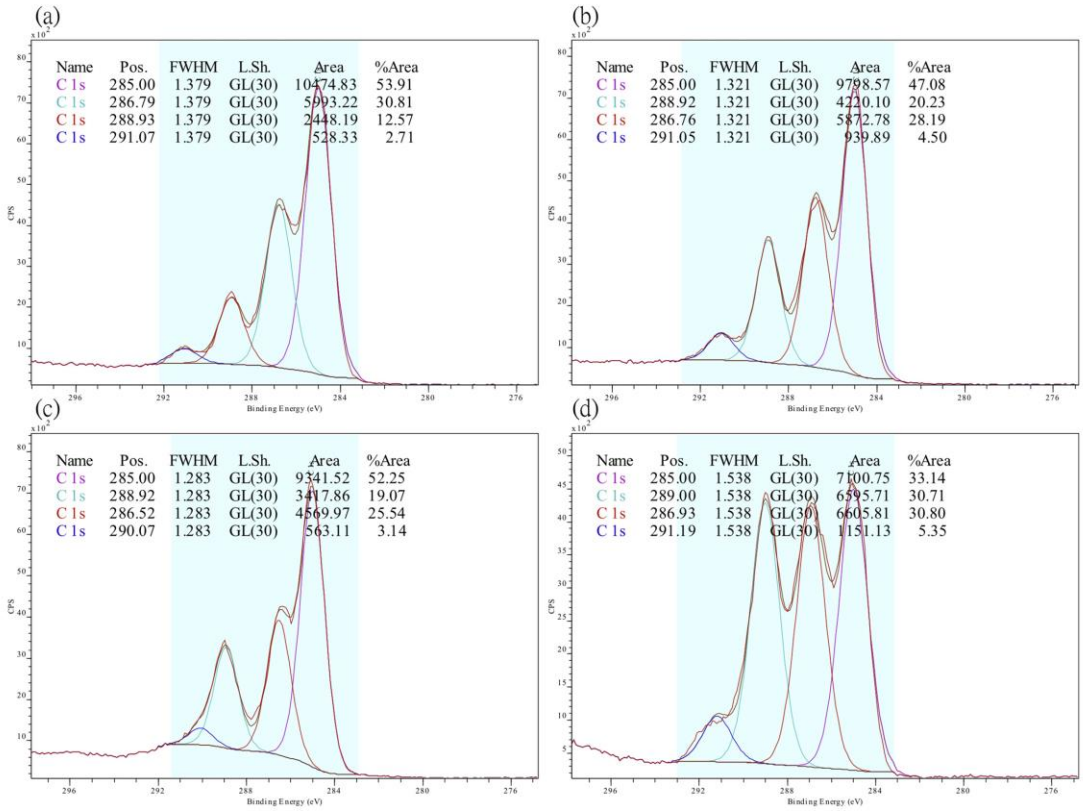

Fig. 5. The C1s core level of (a) PET (b) PET-AA-5 (c) PET-AA-10 and (d) PET-VA-AA-10.

is due to the presence of free radicals and peroxides. After AA-grafting for 5 or 10 min, the water contact angle of the polymer (PET and PLA) surface increased, which is due to the carboxylic acid groups introduced on the surface via AA-grafting. Similar results were reported by Chen et al., as the process formed a poly-AA like film, which contains more non-polar groups, such as $-CH_3-$ and $-CH_2-$, than the Ar-APP activated surface, which comprises mainly oxygen-containing polar groups [10]. However, compared to the neat specimens, the AA-grafted surfaces were still more hydrophilic due to the carboxylic acid groups from the poly-AA like films deposited on them. The same trend was also observed on acetic acid low-pressure plasma treated specimens, where a decrease of water contact angle was found on both PET and PLA specimens after the plasma treatment. The results preliminarily suggest the modification of the polymer surfaces, which is supported by the difference between the morphology of PET and PLA surfaces before and after acetic acid low-pressure plasma-enhanced chemical vapor deposition (Figs. 3 and 4).

To further investigate the percentage of carboxylic acid functional groups on the surfaces, XPS analysis was executed. The peak at a binding energy around 289.2 eV in C1s core level has been utilized to determine the contribution of the carboxylic acid groups deposited onto the surface as it fits into −COOH components in C1s spectrum of acetic acid [12].

Studies have reported that pristine PET and PLA specimens showed peaks around 289.2 eV, which represents the ester compound from their structure. Similar surface elements were identified in this study, showing an atomic ratio on ester of 12.6% for neat PET surface (Fig. 5(a)) and 15.7% for neat PLA surface (Fig. 6(a)), respectively.

Therefore, the atomic ratio of carboxylic acid group was calculated by subtracting 12.6% (for PET specimen) or 15.7% (for PLA specimen) from the measured peak intensity at 289.2 eV (Figs. 5 and 6). The atomic ratio of carboxylic acid compound contributed via APP and low-pressure plasma processes are illustrated in Table 3 and compared in Fig. 7.

For 5-second Ar-APP activated PET surface, after the subsequent AA vapour grafting, the atomic ratio of carboxylic acid group was observed as 7.7% (5 min grafting) and 6.5% (10 min grafting). Similar result was found on 5-second Ar-APP activated PLA surface, which exhibited atomic ratio of 6.9% (5 min grafting) and 5.8% (10 min grafting). For acetic acid low-pressure plasma treated specimens, the carboxylic acid ratio was found with 18.1% on PET surface, however, 0% on PLA surface. This phenomenon was further found related to the PLA surface stability.

To estimate the stability of the functionalized surface, wettability was measured 3 days after the treatment and compared in Fig. 8.

It can be observed that both APP and low-pressure plasma treated PET and PLA surfaces turned hydrophobic with the increasing amount of days. After a 5-second Ar-APP with a subsequent 5-minute AA-grafting, the contact angle with water upraised from 42.8 ± 1.5 degrees (day 0) to 50.1 ± 0.8 degrees (day 3) on PET surface, and 62.4 ± 1.2 degrees (day 0) to 61.6 ± 1.0 degrees (day 3) on PLA surface.

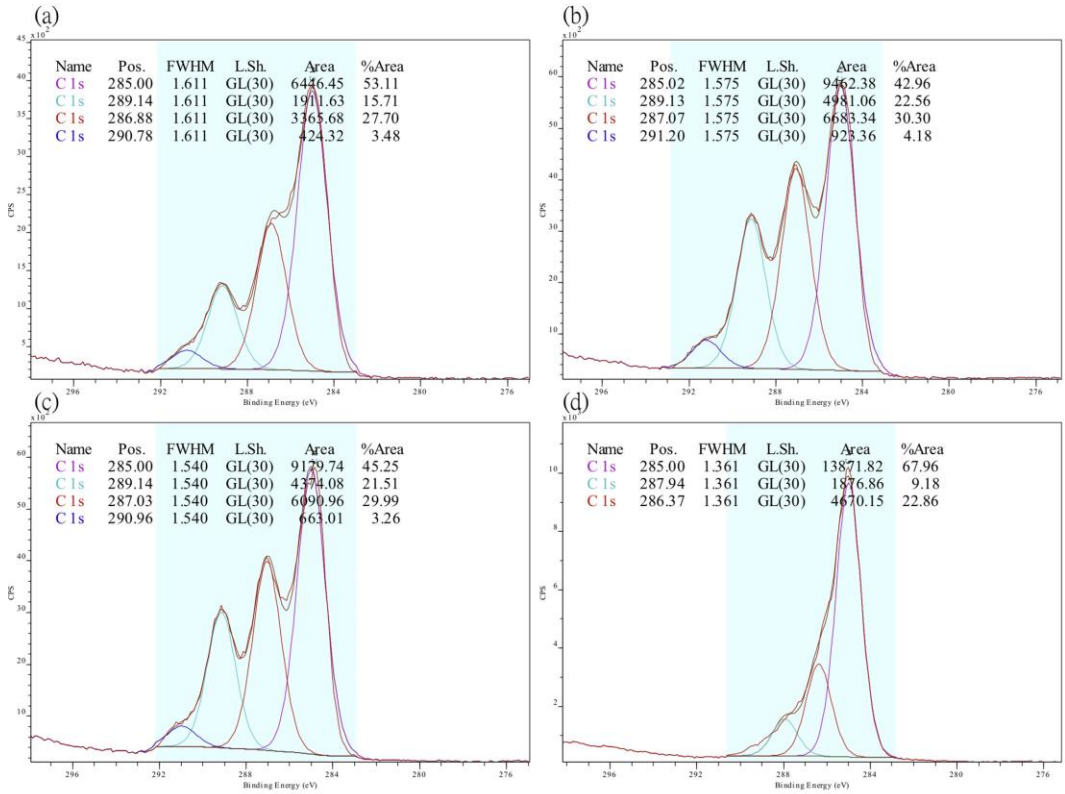

Fig. 6. The C1s core level of (a) PLA (b) PLA-AA-5 (c) PLA-AA-10 and (d) PLA-VA-AA-10.

Table 3
Comparison of the atomic ratio of carboxylic acid groups measured from the C1s spectra.

Specimen	PET-AA-5	PET-AA-10	PET-VA-AA-10	PLA-AA-5	PLA-AA-10	PLA-VA-AA-10
COOR (%)	7.7	6.5	18.1	6.9	5.8	0

For 5-second Ar-APP activated surfaces, after a 10-minute subsequent AA-grafting, the water contact angle increased from 41.5 ± 1.4 degrees (day 0) to 43.7 ± 1.4 degrees (day 3) on PET surface, and 60.8 ± 2.4 degrees (day 0) to 78.2 ± 0.4° at day 3 on PLA surface.

In the case of AA low-pressure plasma functionalization, the contact angle with water of functionalized PET increased from 15.7 ± 0.7° (day 0) to 19.4 ± 0.4° (day 3). However, for PLA surface, the water contact angle increase from 18.9 ± 0.4° (day 0) to 64.1 ± 0.3° (day 3), which is similar to the neat PLA surface, on day 3. This has further supported the XPS result of acetic acid low-pressure plasma modified PLA surface, as the result of the absence of carboxylic acid compound. In contrast, the acetic acid low-pressure plasma functionalized PET surface exhibited a more stable wettability, which is contributed by the immobilized carboxylic acid group.

The results of stability and XPS studies on the functionalized PLA specimen (PLA-VA-AA-10) further suggest that due to its aliphatic compound dominated structure, the PLA surface tends to be hydrolytically degraded [13], which results in different surface wettability for PLA and PET after they were both treated by the same plasma process. This nature of the PLA surface further explains that although the plasma processes had deposited carboxylic acid group on the surface (which was suggested by the more hydrophilic surface and the presence of carboxyl group on the APP/AA-grafted surface), after 3 days the surface lost its hydrophilicity and carboxyl functional groups. On the other hand, the aromatic compound (benzene) in the structure of PET is more stable than the aliphatic compound which dominates the structure of PLA. Therefore, a more hydrophilic and stable surface after functionalization was observed on the PET surface. Whilst a low-pressure plasma process offers the possibility of depositing a higher percentage of carboxylic acid on PET with excellent stability, APP promises a more rapid process for preparing a carboxylic acid immobilized surface for PET and PLA, as the low-pressure process utilizes the plasma glow discharge for 10 min, while the APP process only requires a 5-second plasma treatment.

4. Conclusions

Previous studies have shown that the hydrophobicity and lack of reactive side-chain groups of the PET and PLA surfaces cause poor surface-cell interaction and limited cell attachment to them. This study presented an approach of utilizing an atmospheric pressure plasma process or low-pressure plasma polymerization to achieve a stable and hydrophilic surface on PET or PLA by introducing carboxylic acid

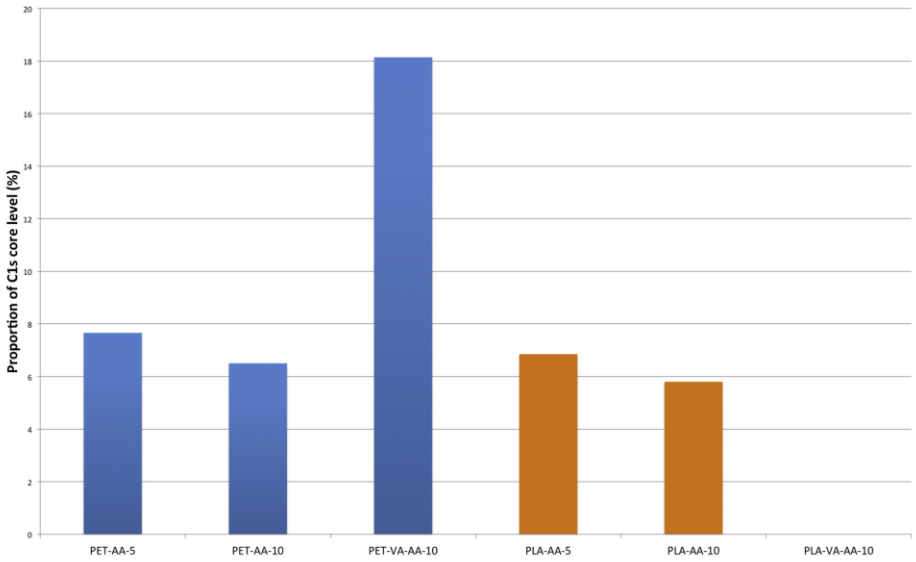

Fig. 7. Comparison of the increased atomic ratio of carboxylic acid groups after functionalization from the C1s spectra. The value was calculated by subtracting the ester atomic ratio of raw substrate from the measured peak intensity at 289.2 eV on the functionalized surface.

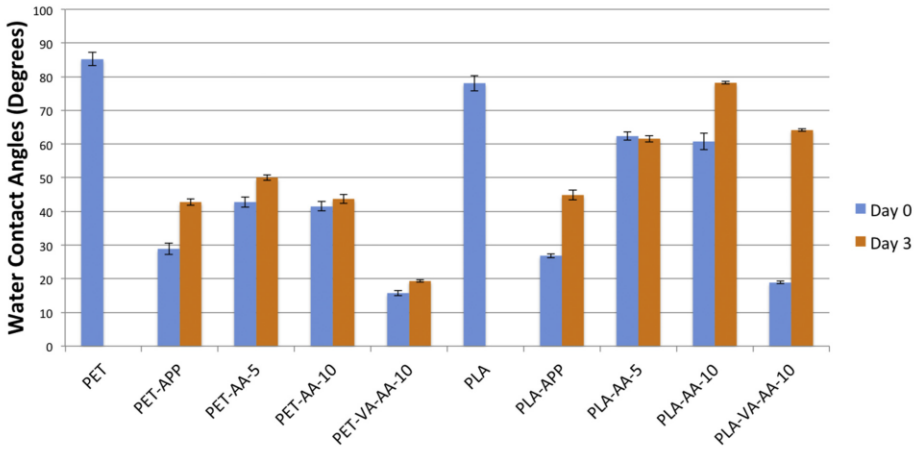

Fig. 8. Comparison of surface stability from hydrophilicity difference between plasma modified PET and PLA substrates after 3 days.

groups. The low-pressure plasma polymerization is capable of depositing a higher percentage of carboxylic acid groups on PET, while the atmospheric pressure plasma process offers a rapid method to introduce carboxylic acid compound on both PET and PLA, demonstrating novel, effective techniques to functionalize polymer surface for further applications.

Acknowledgements

Support under ERC Grant number 320879 (“IMPUNEP”) is gratefully acknowledged.

References

[1] P. Cerrai, M. Tricoli, L. Lelli, G.D. Guerra, R.S. Delguerra, M.G. Cascone, P. Giusti, Block-copolymers of L-lactide and poly(ethylene glycol) for biomedical applications, J Mater Sci-Mater M 5 (1994) 308–313.
[2] P.A. Dimilla, J.A. Stone, J.A. Quinn, S.M. Albelda, D.A. Lauffenburger, Maximal migration of human smooth-muscle cells on fibronectin and type-IV collagen occurs at an intermediate attachment strength, J. Cell Biol. 122 (1993) 729–737.
[3] R. Fukai, P.H.R. Dakwa, W. Chen, Strategies toward biocompatible artificial implants: grafting of functionalized poly(ethylene glycol)s to poly(ethylene terephthalate) surfaces, J Polym Sci Pol Chem 42 (2004) 5389–5400.
[4] W.M. Stevels, M.J.K. Ankone, P.J. Dijkstra, J. Feijen, Stereocomplex formation in Aba triblock copolymers of poly(lactide)(A) and poly(ethylene-glycol)(B), Macromol Chem Physic 196 (1995) 3687–3694.

[5] S.G. Wang, W.J. Cui, J.Z. Bei, Bulk and surface modifications of polylactide, Anal. Bioanal. Chem. 381 (2005) 547–556.
[6] R.L. Clough, High-energy radiation and polymers: a review of commercial processes and emerging applications, Nucl Instrum Meth B 185 (2001) 8–33.
[7] E.S. You, H.S. Jang, W.S. Ahn, M.I. Kang, M.G. Jun, Y.C. Kim, H.J. Chun, In vitro biocompatibility of surface-modified poly(DL-lactide-co-glycolide) scaffolds with hydrophilic monomers, J. Ind. Eng. Chem. 13 (2007) 219–224.
[8] W. Chen, C. Jie-Rong, L. Ru, Studies on surface modification of poly(tetrafluoroethylene) film by remote and direct Ar plasma, Appl. Surf. Sci. 254 (2008) 2882–2888.
[9] S.D. Lee, G.H. Hsiue, P.C.T. Chang, C.Y. Kao, Plasma-induced grafted polymerization of acrylic acid and subsequent grafting of collagen onto polymer film as biomaterials, Biomaterials 17 (1996) 1599–1608.
[10] W.Y. Chen, A. Matthews, F.R. Jones, K.S. Chen, Deposition of a stable and high concentration of carboxylic acid functional groups onto a silicon surface via a tailored remote atmospheric pressure plasma process, Surf Coat Tech 336 (2018) 67–71.
[11] L.J. Ward, W.C.E. Schofield, J.P.S. Badyal, A.J. Goodwin, P.J. Merlin, Atmospheric pressure plasma deposition of structurally well-defined polyacrylic acid films, Chem. Mater. 15 (2003) 1466–1469.
[12] A.N. Debrito, M.P. Keane, N. Correia, S. Svensson, U. Gelius, B.J. Lindberg, Experimental and theoretical Xps study of model molecules for poly(methyl methacrylate), Surf. Interface Anal. 17 (1991) 94–104.
[13] M.A. Elsawy, K.H. Kim, J.W. Park, A. Deep, Hydrolytic degradation of polylactic acid (PLA) and its composites, Renew. Sust. Energ. Rev. 79 (2017) 1346–1352.

iii) Further discussion on the context of the Appendix papers in relation to the thesis

As mentioned in Chapter 6, the PhD project comprised seven main stages. When the progress had reached stage 2, which suggested the potential of depositing a high concentration of carboxylic acid functional groups on the surface via the plasma system (plasma nozzle and tailored chamber), it attracted the author's interest to further investigate the effect of introducing carboxylic acid functional group under various parameters, including chamber dimension, distance between the plasma glow and the precursor, and the selection of precursor. Although the aim of the PhD thesis was to develop a novel atmospheric pressure plasma process for controlling surface functional groups on carbon fibers, which can be applied to manufacturing a self-healing composite with enhanced load carrying capacity, the process of depositing a carboxylic acid group on the surface is also an important topic to be examined due to the wide applications it promises, including biocompatibility improvement, biosensors, environmental engineering and composites (described in the Introduction chapter).

The first paper assessed the effect of a remote atmospheric pressure plasma system using the same plasma nozzle as in this thesis but in a different bespoke Pyrex chamber. Compared to the chamber utilized in this PhD thesis, the chamber employed in the first paper exhibited a higher atomic percentage of carboxylic acid functional groups (19.72% from the thesis, while 27.6% from this paper), which is close to the

theoretical value of AAc (33.3%). In the first paper, the longer distance between the plasma nozzle and the specimen, compared to the thesis plasma system, also shows the potential of protecting specimen bulk properties. However, the shape and dimensions of the chamber in the first paper limited its application on fibers or specimens with a larger area. To sum up, both the APP/grafting system in the thesis and the remote APP process in the first paper promise rapid and novel methods for introducing higher concentrations, compared to the conventional AP process described previously, of carboxylic acid functional group via AAc deposition on the specimen surface.

After the effects and capability of an APP process with AAc on carboxylic acid deposition were studied, the focus shifted to achieving similar results using other kinds of precursors and the comparison between this APP system and a low-pressure plasma PECVD system. Therefore, in the second paper, acetic acid was utilized as precursor to introduce carboxylic acid functional groups on polymer materials. The APP parameter, chamber setup and vapour grafting in the second paper followed the setting employed in this PhD project. Although in the case of using acetic acid as precursor, low-pressure plasma exhibited a higher percentage of carboxylic acid groups on the surface (18.5%) than the APP/acetic acid grafting treatment (7.7%), the APP process only required a 5-second plasma operation and saved time on evacuating the chamber, while the low-pressure plasma process ran the plasma for 10 minutes.

The effect of APP and low-pressure plasma processes on carboxylic acid functional group deposition is illustrated in Table A.1. These results further suggest that the APP/vapour grafting process designed in the PhD project promises advantages such as saving time on plasma operation, the capability of depositing carboxylic acid functional groups on not only silicon and carbon fibers but also on polymer materials. This also indicated that the parameter and setup of the APP activation/vapour grafting process developed in this PhD project is not limited to using AAc but also available in acetic acid, which widens the selection of precursors and broadens the application of this APP system.

Table A.1 The effect of APP and low-pressure plasma treatments on carboxylic acid functional groups deposition.

	Precursor	Specimen	Plasma operating time (second)	Atomic percentage of carboxylic acid group (%)
APP activation/vapour grafting	Acrylic acid	Silicon	5	19.72
APP activation/vapour grafting	Acrylic acid	Carbon fiber	5	4.92
Remote APP	Acrylic acid	Silicon	30	27.6
APP activation/vapour grafting	Acetic acid	PET	5	7.7
APP activation/vapour grafting	Acetic acid	PLA	5	6.9
Low-pressure plasma	Acetic acid	PET	600	18.5